INFORMATION TO USERS

This manuscript has been reproduced from the microfilm master. UMI films the text directly from the original or copy submitted. Thus, some thesis and dissertation copies are in typewriter face, while others may be from any type of computer printer.

The quality of this reproduction is dependent upon the quality of the copy submitted. Broken or indistinct print, colored or poor quality illustrations and photographs, print bleedthrough, substandard margins, and improper alignment can adversely affect reproduction.

In the unlikely event that the author did not send UMI a complete manuscript and there are missing pages, these will be noted. Also, if unauthorized copyright material had to be removed, a note will indicate the deletion.

Oversize materials (e.g., maps, drawings, charts) are reproduced by sectioning the original, beginning at the upper left-hand corner and continuing from left to right in equal sections with small overlaps. Each original is also photographed in one exposure and is included in reduced form at the back of the book.

Photographs included in the original manuscript have been reproduced xerographically in this copy. Higher quality 6" x 9" black and white photographic prints are available for any photographs or illustrations appearing in this copy for an additional charge. Contact UMI directly to order.

UMI

A Bell & Howell Information Company
300 North Zeeb Road, Ann Arbor MI 48106-1346 USA
313/761-4700 800/521-0600

Interactions of Atmospheric Particulate and Trace Gases with Clouds at Cheeka Peak, WA

by

Tristine Marie Samberg

A dissertation submitted in partial fulfillment
of the requirements for the degree of

Doctor of Philosophy

University of Washington

1997

Approved by _____
Co-chairperson of Supervisory Committee

_____
Co-chairperson of Supervisory Committee

Program Authorized
to Offer Degree Chemistry

Date 6/4/97

In presenting this dissertation in partial fulfillment of the requirements for the Doctoral degree at the University of Washington, I agree that the Library shall make its copies freely available for inspection. I further agree that extensive copying of this dissertation is allowable only for scholarly purposes, consistent with "fair use" as prescribed in the U.S. Copyright Law. Requests for copying or reproduction of this dissertation may be referred to University Microfilms, 1490 Eisenhower Place, P.O. Box 975, Ann Arbor, MI 48106, to whom the author has granted "the right to reproduce and sell (a) copies of the manuscript in microform and /or (b) printed copies of the manuscript made from microform."

Signature Justine Marie Sanberg

Date 6/6/97

University of Washington

Abstract

Interactions of Atmospheric Particulate and Trace Gases with Clouds at Cheeka Peak, WA

by Tristine Marie Samberg

Chairperson of the Supervisory Committee: Professor William H. Zoller
Department of Chemistry
Co-chairperson: Professor Dean A. Hegg
Department of Atmospheric Sciences

Measurements of various aerosol, trace gas, and cloud water constituents were made during two intensive observation periods at the Cheeka Peak Observatory (CPO) on the Washington state coast. These measurements were a part of the second and third Cloud and Aerosol Chemistry Experiments (CAChE 2 and CAChE 3) conducted from April 19 to May 18, 1994 and August 30 to September 23, 1994, respectively. Gas phase hydrogen peroxide was measured continuously during these two time periods. Cloud water samples were analyzed for major ion constituents and aqueous hydrogen peroxide. The cloud water samples collected during CAChE 2 represented bulk collection, whereas the cloud water samples collected during CAChE 3 were segregated into two size fractions, with mean droplet diameter of approximately 12 μm and 13 μm. Major ion concentrations (e.g., Na^+, NH_4^+, H^+, NO_3^-, $SO_4^=$, etc.) were higher than previously observed at Cheeka Peak, but comparable to other West coast locations. Despite the small difference in collected droplet size, size dependence was observed for several species. Seasalt ions and NO_3^- were more concentrated in the larger drops, whereas peroxide was more concentrated in the smaller drops. Size dependence was not observed for MSA, non seasalt sulfate (nss-$SO_4^=$), and NH_4^+, and was only weakly observed for H^+.

Cloud-free gas phase H_2O_2 and organic peroxide average concentrations were on the order of a few hundred pptv and did not vary much by wind sector; slightly higher

concentrations were observed from the continental sector. In general, these concentrations were lower than those measured at east coast sites. Average cloudwater H_2O_2 concentrations for both CAChE experiments were approximately 35 μM and indicated conditions at Cheeka Peak were never oxidant-limited.. Evidence for sulfate production via H_2O_2 oxidation was observed but was not conclusive.

Finally, a preliminary comparison was made between predictions of a size-resolved cloud chemical model and limited observations of size-resolved cloud chemistry for cases upon which the model was initialized. Some agreement was obtained and discrepancies could be attributed to an unrealistic treatment of particulate nitrate in the model.

TABLE OF CONTENTS

LIST OF FIGURES

LIST OF TABLES

ACKNOWLEDGEMENTS

I would have never made it through without the constant help, guidance, encouragement and support of four terrific people: Dr. Dean Hegg, my dissertation co-advisor, who never turned me away or said he was too busy; Drs. Michelle Shulman and Susan Harder, comrades from the very start of my graduate career who never gave up on me and pushed me to finish even after they graduated; and my wonderful husband, Michael Hablewitz, whose love and support were unflappable amidst the rantings and tears.

CHAPTER 1 - INTRODUCTION

Clouds are complex systems comprised of multiple phases: gas, aqueous, and particulate. Four main processes control the composition of cloud drops: 1) nucleation scavenging of pre-existing soluble aerosol particles, 2) absorption of soluble interstitial gases via Henry's law equilibrium, 3) chemical reactions, like oxidation of SO_2, that add to the acidity of the cloud drop, and 4) microphysical evolution of the system (Fuzzi *et al.*, 1988). In addition, other processes, like scavenging of interstitial unactivated aerosol via diffusion and oxidation of moderately soluble NO_x species, contribute to chemical composition of cloud drops.

The measurement of clouds present unique challenges because they require a multi-disciplinary approach that involves chemistry, meteorology, aerosol physics (Iribarne and Cho, 1989). Detecting the subtle chemical changes in cloud can be facilitated by well-characterized Lagrangian studies; however truly Lagrangian studies are difficult to achieve (Kelly *et al.*, 1989). In addition, several modeling (e.g., Twohy *et al.*, 1989; Hegg and Larson, 1990;, Pandis and Seinfeld, 1990) and field results (e.g., Noone *et al.*, 1988 and 1992; Munger *et al.*, 1989; Ogren *et al.*, 1989) have demonstrated that cloud droplets do not possess a uniform chemical composition. Not only do cloud droplets of different sizes have different compositions, droplet of the same size can likely have different compositions. For these reasons, clouds present analytical and characterization challenges.

Regardless of their difficulty in characterization, clouds are of great interest to atmospheric scientists because they perform many interrelated functions. Chemical transformations are more likely to occur in cloud droplets (and aerosol particles) than in the gas phase due to greater collision frequency. Particularly important is the oxidation of SO_2 to $SO_4^=$ in the aqueous phase. Lelieveld and Heintzenberg (1992) estimate that 80 to 90% of this transformation occurs in clouds. As a result, clouds play an important role in the cycling of trace gases, especially soluble ones like SO_2, NH_3 and H_2O_2. Chemical and

physical processes within the cloud also result in an aerosol following cloud evaporation that is likely to be much different than when it entered the cloud (Fuzzi *et al.*, 1992). Repeated cycling of aerosol through non-precipitating clouds can change the aerosol size distribution (Hoppel *et al.*, 1990), which results in better CCN and larger particles that are more efficient light scatterers (Lelieveld and Heintzenberg, 1992; Hegg *et al.*, 1992). Recent evidence has suggested that clouds also absorb short-wavelength radiation, contradicting conventional wisdom that has assumed clouds only scatter incoming solar radiation (Levi, 1995). Chemical processing within clouds could then potentially effect the amount of this radiation absorption. All of these cloud processes can potentially effect climate forcing and present additional challenge to climate modelers who try to incorporate the complex effects of clouds on climate into their cloud models.

Studies in marine environments are important because they serve as comparatively simple systems in contrast to more perturbed continental scenarios. This research is exploratory in nature and investigates some of the basic processes that lead to the transformation of trace gas and aerosol species in marine clouds. The goal of this study was to characterize the chemical properties of marine clouds, with special emphasis on oxidative capacity and processes in the marine environment that until now has been largely unstudied. This was accomplished through a combination of field measurement and model studies using the field results for initialization.

CHAPTER 2 - CLOUD IONIC CHEMISTRY AT CHEEKA PEAK

2.1 INTRODUCTION

Clouds are multiphase systems that influence the transformation and transport of all soluble species found in the atmosphere. The formation of clouds depends on the presence of aerosol particles known as cloud condensation nuclei; supersaturations in excess of several hundred percent would be required for clouds to condense from water alone (Prupaccher and Klett, 1978). The condensation of atmospheric water vapor onto aerosol particles, called nucleation scavenging, determines the initial composition of the newly formed cloud droplet. The chemical properties of the droplet are subsequently altered by three main processes during the evolution of the cloud: (1) scavenging of soluble gases (e.g. ammonia and nitric acid) and particles; (2) chemical reactions within the aqueous phase, such as the oxidation of SO_2 to $SO_4^=$; and (3) microphysical evolution of the system, e.g. changing drop size distribution or entrainment of air outside the cloud system (Fuzzi *et al.*, 1988 and references therein).

Cloud droplets do not possess a uniform chemical composition. A cloud droplet population can be chemically heterogeneous for several reasons: the CCN on which droplets form are heterogeneous, different size drops grow and dilute at different rates, and rates of diffusion of gases and unactivated aerosol particles to cloud droplets are variable (Ogren and Charlson, 1992). Variations in cloud droplet chemistry with size have been predicted in cloud models (Twohy *et al.*, 1989; Hegg and Larson, 1990; Pandis and Seinfeld, 1990) and observed in experimental measurements (Noone *et al.*, 1988 and 1992; Munger *et al.*, 1989; Ogren *et al.*, 1989; Collett *et al.*, 1993 and 1994; Vong *et al.*, 1997). These experimental studies suggest that small drops are activated on submicron aerosol while large drops are activated on supermicron, mechanically generated aerosol. The size dependence of species influenced by gas phase processes can be enriched in either small drops (Munger *et al.*, 1989) or large drops (this study) depending on initial conditions.

Measurements of several cloud events were made at the Cheeka Peak Observatory during the spring and summer of 1994. Measurements of clouds at this site are important for two reasons. First, coastal stratiform clouds are a major feature of the Pacific Northwest weather pattern. Second, Cheeka Peak is a "background" site, meaning that concentrations measured here represent mid-latitude Northern Hemisphere average concentrations influenced mainly by natural emissions (Vong, 1990).

The impetus for investigating cloud chemistry has historically risen from its role as a precursor to acid rain and the interception of cloud droplets by forest canopies. This important pathway for deposition of pollutants from acidic cloud has been studied in Los Angeles (Jacob *et al.*, 1985), the northeastern U.S. (c.f. Husain *et al.*, 1991) and Europe (c.f. Dollard et al., 1983 and Fuzzi *et al.*, 1988). Although the scope of this study did not include quantification of these effects, the goals of this study were:

- to determine the variability of chemical concentration in clouds at Cheeka Peak,
- to investigate size dependent cloud droplet chemistry, and
- to identify the factors that control the cloud water composition in remote marine stratiform clouds.

Ultimately, this information provides a reference point for comparison to other polluted urban areas and is intimately associated with the effects listed above.

2.2. EXPERIMENTAL

2.2.a Site Description

Cloud water samples for the Cloud and Aerosol Chemistry Experiment (CAChE - 3) were collected from August 10 to September 19, 1994 at the Cheeka Peak Observatory (CPO) in conjunction with Rick Vong from Oregon State University. Cheeka Peak Observatory is a remote site, located on the northwest corner of the Olympic peninsula (48°N, 125°W). The station is 3 km inland from the Pacific Ocean on the western edge of a ridge at 480 m elevation. The terrain to the west drops to a coastal plain in 1 km, allowing an unobstructed exposure to the Pacific Ocean within the westerly quadrant (270

± 60°). Within the westerly quadrant, the maximum overland trajectory to the site is 5 km. The surrounding area has been logged within the past 20 years and is covered with small conifers. As a result, local sources of aerosols are assumed negligible during the short overland transport from the coast to the sampling site.

2.2.b Field Measurements

Prevailing westerly (on-shore) winds dominated the transport of atmospheric constituents during cloud events. Bulk cloudwater was collected on a 10 m tower using a modified version of an active cloud water sampler described by Pade *et al.*, 1987. Cloud droplet collection into two size fractions is achieved by impaction on two stages of rods, 1.02 cm diameter (top stage) and 0.167 cm diameter (bottom stage). A high volume intake passed air by the rods at 250 L/sec, rather than the ambient wind speed; hence the term "active sampler." The sampler inlet was oriented such that the effects of ambient wind speed were negligible. Complete removal of the larger size fraction by the first set of rods was not possible, so each stage received "ambient" cloud exposure. The top set of rods collected drops >12 μm whereas the lower stage of rods collected drops > 5 μm. However, the ambient drop size distribution and collection efficiencies of the rods resulted in a real difference in size collection between the two fractions of only about 1 μm, where the large rods collected droplets with an average size of 13 μm and the small rods collected droplets with an average size of 12 μm. A description of the cloudwater collector and characterization of its performance is in Vong *et al.*, 1996.

Collected drops drained down the rods and were collected in pre-cleaned polyethylene or polypropylene 60 mL bottles. The collection bottles were acid washed in 1 N HNO_3 and repeatedly rinsed with distilled, deionized water until the conductivity of the last rinse was within 10% of 1 μS/cm.

Other chemical and cloud microphysical parameters were measured continuously (by the OSU research team) from a boom extending upwind of the tower and ~3 m crosswind from the cloudwater collector. These parameters included: O_3 concentration (Dasibi Model 1003PC), aerosol number concentration (TSI Model 3760), temperature,

net radiation, three dimensional winds (sonic anemometer, ATI SWS-211-3K) and liquid water content, cloud drop volume mean diameter, and number of droplets (forward scattering spectrometer, PMS FSSP-100).

2.2.c Description of Cloud Events Sampled

Table 2.1 presents a summary of the twenty CAChE 3 cloud events that were sampled. Samples were generally collected at one-hour intervals during each cloud event. The samples were collected in pairs (with the exception of event 16), representing the two size fractions collected. The events are numbered chronologically until Event 16. Events 17-20 were analyzed later than Events 1-16 and were appended to the data set. Air mass trajectories for the twenty events are given in Appendix A. Cloud events were also sampled during CAChE 2 (April – May 1994) but were not segregated by size and are therefore only tabulated in Section 2.4.a for comparison purposes.

2.2d Sample Analysis

During the cloud event, the collection bottles were refrigerated at 4°C. Immediately following the cloud event, the cloud water was aliquoted into 2 mL pre-cleaned vials inside a Class 100 clean bench for each pH, anion, cation, and organic acid analysis. Not all samples had enough volume for the four aliquots. The sample pH was determined in the field (Orion 720A pH meter equipped with a Ross 8115sc combination electrode) within 4 hours of collection. The pH meter was calibrated regularly with pH buffers and a standard sulfuric acid solution. The manufacturer's reported accuracy for the electrode is ±0.03pH.

The remaining aliquoted vials were stored at 4°C until analysis. Major anions (Cl^-, NO_3^-, $SO_4^=$) were determined by ion chromatography with a Dionex 2000I using an AS4A separator column and AMMS-I anion micromembrane suppressor. The eluant was 1.44 mM Na_2CO_3/1.36mM $NaHCO_3$. Major cations (Na^+, NH_4^+, K^+, Mg^{+2}, Ca^{+2}) were also determined by ion chromatography using a CS12 separator column, CSRS-I cation micromembrane suppressor and 20 mM MSA eluant.

Table 2.1 Summary of sampled CAChE 3 cloud events

Event Number	Local Date	Duration (Local Time)	Sample ID's	Air Mass Origin
1	8/12/94	06:55-11:22	TI 18 - TI 27	stagnant boundary layer
2	8/14/94	06:50-12:50	TI 34 - TI 41	stagnant boundary layer
3	8/14/94	19:00-24:00	TI 44 - TI 51	stagnant boundary layer
4	8/15/94	06:28-09:40	TI 52 - TI 57	stagnant boundary layer
5	8/17/94	20:40-02:23	TI 62 - TI 71	marine boundary layer
6	8/18/94	06:46-11:38	TI 72 - TI 83	stagnant boundary layer
7	8/22/94	12:35-22:22	VI 10 -VI 23	marine boundary layer
8	8/29/94	06:35-09:35	VI 36 - VI 41	marine boundary layer
9	8/31/94	07:15-16:25	VI 42 - VI 59	modified MBL
10	9/03/94	20:20-00:15	XI 06 - XI 11	modified MBL
11	9/06/94	07:44-12:10	XI 16 - XI 23	marine boundary layer
12	9/07/94	20:52-22:32	XI 26 - XI 29	southerly boundary layer
13	9/08/94	03:55-07:30	XI 30 - XI 37	southerly boundary layer
14	9/13/94	03:44-17:10	XI 50 - XI 69	marine boundary layer
15	9/15/94	09:30-11:20	YI 00 - YI 03	marine boundary layer
16	9/17/94	19:07-16:06	YI 04 - YI 44	modified MBL
17	8/11/94	18:50-01:15	TI 04 - TI 17	stagnant boundary layer
18	8/21/94	21:37-00:36	VI 02 - VI 07	marine boundary layer
19	9/08/94	20:04-23:04	XI 38- XI 43	southerly boundary layer
20	9/14/94	16:20-19:17	XI 74 - XI 79	marine boundary layer

Aliquots for organics analysis were preserved with 40 μL of chloroform. The preserved samples were analyzed by Mike Hamilton at NOAA/Pacific Marine Environmental Laboratory (PMEL) by ion chromatography using an AS4 separator column, AMMS-II micromembrane suppressor, and 12.5 mM NaOH eluant.

Anion standards were made weekly while cation standards were made daily. The variability of NH_4^+ concentration with time necessitated daily preparations of the cation standard. Multiple standards were analyzed daily to encompass the range of concentrations found in the samples. All calibration curves were linear over the range of

concentrations measured, with the exception of NH_4^+. A second order polynomial was fit to the NH_4^+ calibrations as these were nonlinear even over a small range of concentrations. Standard performance over the duration of analysis was also monitored. Standard performance is a measure of instrument stability and precision. Standard performance will also be used as a surrogate for sample error because replicate analyses were not possible given limited sample. Tables 2.2 and 2.3 show a summary of standard performance.

2.3 DATA ANALYSIS METHODOLOGY

2.3a Characterization of sample contamination and use of blank correction

Most environmental sampling is subject to contamination. Contamination from a variety of sources (including sampling apparatus, handling, storage, and analysis) inadvertently introduces the analyte of interest to the sample, leading to an erroneously high measured value. Contamination can also cause erroneously low results, but this type is not considered significant in this sampling scheme. This discussion focuses on contamination errors incurred in the field from sampling and handling. Although laboratory processing can contribute some error to the overall measurement process, rigorous determination of blanks during lab handling and analysis (laboratory blanks) indicate that error in this step was not significant.

Several types of blanks were collected in the field. These included carboy blanks, cloudwater bottle blanks, and cloudwater collector rinse blanks. Deionized water was transported from OSU and stored in carboys at Cheeka Peak because a water purification system was not available on site. Therefore, water used for various cleaning activities came from these carboys. Blanks were collected periodically from these carboys and stored identically to the samples (4°C). The carboy blanks also indicated any contamination resulting from storage or transport. The cloudwater collection bottles were stored in deionized water. Before the bottles were placed in the collector, their contents were emptied. This storage water was also analyzed as a blank to determine if the polyethylene bottles represented a source of contamination. Finally, a spray bottle filled

Table 2.2. Reproducibility of CAChE 3 anion standards during duration of analysis

Date Measured	Cl Conc [ppm]	Cl Pk Height[mm]	Cl Pk Ht/Conc	NO3 Conc [ppm]	NO3 Peak Height	NO3 Pk Ht/Conc	SO4 Conc [ppm]	SO4 Peak Height	SO4 Pk Ht/Conc
50uL sample loop									
4/25/95	1.033	49.3	47.73	1.030	358784	348334	1.035	231816	223977
4/25/95	1.033	50.6	48.98	1.030	353457	343162	1.035	231043	223230
4/27/95	1.033	50.1	48.50	1.030	352318	342056	1.035	237228	229206
4/27/95	1.033	51.8	50.15	1.030	358277	347842	1.035	233043	225162
4/28/95	1.033	52.0	50.34	1.030	346896	336792	1.035	238360	230300
5/2/95	1.033	50.9	49.27	1.030	358063	347634	1.035	226377	218722
5/4/95	1.033	50.7	49.08	1.030	327816	318268	1.035	228528	220800
5/8/95	1.033	49.5	47.92	1.030	319003	309712	1.035	221992	214485
5/8/95	1.033	50.7	49.08	1.030	325184	315713	1.035	222005	214498
		Average:	49.01			334390			222264
		Standard Deviation:	0.88			15452			5707
		Percent Standard Deviation:	1.80%			4.62%			2.57%
		Standard Error:	0.29			5151			1902
		Percent Std Error:	0.60%			1.54%			0.86%
300uL sample loop									
5/9/95	1.033	158.2	153.15	1.030	283019	274776	1.035	208464	201414
5/9/95	1.033	158.1	153.05	1.030	279893	271741	1.035	207601	200581
5/12/95	1.033	162.0	156.82	1.030	275440	267417	1.035	209056	201986
5/17/95	1.033	163.5	158.28	1.030	277013	268945	1.035	210583	203462
6/1/95	1.033	157.1	152.08	1.030	283583	275323	1.035	212716	205523
		Average:	154.68			271640			202593
		Standard Deviation:	2.71			3482			1946
		Percent Standard Deviation:	1.75%			1.28%			0.96%
		Standard Error:	1.21			1557			870
		Percent Std Error:	0.78%			0.57%			0.43%
**Overall (weighted average) Percent Std Deviation:			1.78%			3.43%			1.99%
Overall (weighted average) Percent Std Error:			0.67%			1.19%			0.70%

Table 2.3. Reproducibility of CAChE 3 cation standards during duration of analysis.

	Na		NH4		K		Mg		Ca	
Date	Conc [ppm]	PkHt/[conc]	Conc [ppm]	PkHt/[conc]	Conc [ppm]	PkHt/[conc]	Conc [ppm]	PkHt/[conc]	Conc [ppm]	PkHt/[conc]
1/19/95	0.3010	1308244	0.5963	705127	0.8034	467493	0.3988	1041931	0.9086	514874
1/19/95	0.3010	1305599	0.5963	704342	0.8034	472376	0.3988	1052746	0.9086	515462
1/23/95	0.3010	1312111	0.5963	709001	0.8034	485131	0.3988	1049754	0.9086	513767
1/23/95	0.3010	1313128	0.5963	705881	0.8034	483435	0.3988	1050705	0.9086	514309
1/25/95	0.3010	1310031	0.5963	697357	0.8034	487730	0.3988	1068413	0.9086	526369
1/27/95	0.1505	1326475	0.2981	828822	0.4017	490988	0.1994	1082096	0.4543	542780
1/27/95	0.1505	1300851	0.2981	820111	0.4017	484620	0.1994	1063340	0.4543	541744
2/1/95	0.3010	1293939	0.5963	696975	0.8034	494603	0.3988	1055318	0.9086	526360
2/1/95	0.3010	1287799	0.5963	694716	0.8034	489077	0.3988	1044215	0.9086	521793
2/3/95	0.3010	1282406	0.5963	689631	0.8034	477107	0.3988	1035594	0.9086	508016
2/13/95	0.3010	1216158	0.5963	669799	0.8034	447011	0.3988	1011898	0.9086	508792
2/13/95	0.3010	1228173	0.5963	673813	0.8034	454167	0.3988	1001437	0.9086	501648
2/14/95	0.3010	1249897	0.5963	675300	0.8034	468840	0.3988	1016126	0.9086	510407
2/20/95	0.3010	1278788	0.5963	684311	0.8034	473995	0.3988	1009471	0.9086	505573
2/21/95	0.3010	1267188	0.5963	684331	0.8034	471201	0.3988	1002370	0.9086	499179
Average:		1285386		709301		476518		1039028		516738
Standard Deviation:		32445		48356		13550		25288		13023
**% Standard Deviation:		2.52%		6.82%		2.84%		2.43%		2.52%
Standard Error:		8377		12485		3498		6529		3362
Percent Std Error:		0.65%		1.76%		0.73%		0.63%		0.65%

Table 2.4. CAChE 3 carboy blank concentrations. All concentrations are reported in ppb. When the analyte concentration was below the detection limit, a randomly generated number between 0 and the DL was used. These values are shown in the outlined cells. Detection limits are: $Cl^- = 4.0$ ppb, $NO_3^- = 5.5$ ppb, $SO_4^{=} = 4.0$ ppb, $Na^+ = 0.8$ ppb, $NH_4^+ = 0.6$ ppb, $K^+ = 5.6$ ppb, $Mg^{+2} = 0.2$ ppb, $Ca^{+2} = 2.1$ ppb.

CARBOY BLANKS

SAMPLE ID	Cl	NO3	SO4	Na	NH4	K	Mg	Ca	
QI 01	12.99	3.48	0.04	6.93	224.93	7.49	2.39	10.24	used for all samples with prefix "T" and "V"
QI 17	12.51	2.48	0.66	4.93	39.13	5.75	2.33	9.76	
QI 35	11.81	4.23	3.21	36.92	76.45	84.41	3.61	16.55	
QI 40	12.72	0.36	0.86	1.41	17.26	8.96	2.70	11.52	
QI 47	10.26	3.74	0.83	9.96	81.25	24.02	2.79	16.59	
average	12.06	2.86	1.12	12.03	87.81	26.13	2.76	12.93	
std dev	0.98	1.37	1.09	12.75	72.56	29.86	0.46	3.03	
QI 75	12.60	191.66	3.11	botched	90.23	11.91	2.43	11.23	used with samples XI48-XI79
QI 85	11.68	355.59	3.02	14.85	164.97	28.42	3.19	16.24	used with samples YI00-YI32
QI 95	193.71	4.31	2.57	29.49	214.63	53.48	3.39	17.04	used with samples YI34-YI44

Table 2.5. CAChE 3 cloud water bottle blank concentrations. Table 2.4 caption also applies.

CLOUD WATER BOTTLES

SAMPLE ID	Cl	NO3	SO4	Na	NH4	K	Mg	Ca	
QI 18	81.84	1.05	3.95	140.22	279.27	120.70	4.80	36.32	used for all samples with *prefix "T" and "V"*
QI 21	12.23	3.52	0.66	5.43	13.07	4.06	2.42	9.44	
QI 23	12.92	2.93	1.19	5.54	56.95	6.62	2.30	9.72	
QI 52	22.11	3.83	1.74	2.72	83.18	15.27	3.03	12.33	
QI 53				75.50	73.65	96.81	7.24	25.90	
average	32.27	2.83	1.89	45.88	101.23	48.69	3.96	18.74	
std dev	33.35	1.25	1.45	54.59	92.21	49.76	1.87	10.67	
QI 54	10.48	4.21	0.25	2.38	63.42	11.68	2.32	12.86	used with samples XI00-XI47
QI 57	18.49	4.35	3.11	8.80	25.11	21.40	3.04	10.94	
QI 59	11.12	3.91	0.50	1.23	15.15	7.73	2.40	10.86	
QI 61	8.92	2.20	0.04	2.12	14.15	7.48	2.58	11.43	
average	12.25	3.67	0.98	3.63	29.46	12.07	2.58	11.52	
std dev	4.26	1.00	1.44	3.48	23.18	6.51	0.32	0.93	
QI 78	7.78	474.81	12.37	5.88	131.98	14.91	3.84	14.11	used with samples XI48-XI79
QI 79	47.14	1255.06	60.74	10.27	137.36	20.87	3.67	16.06	
average	27.46	864.94	36.56	8.08	134.67	17.89	3.76	15.09	
std dev	27.83	551.72	34.20	3.10	3.80	4.22	0.12	1.38	
QI 86	74.09	1336.91	29.23	20.25	90.81	35.61	4.05	14.67	used with samples YI00-YI32
QI 89	2.43	748.42	1.86	77.90	471.71	93.32	9.20	55.62	
average	38.26	1042.67	15.55	49.08	281.26	64.47	6.62	35.14	
std dev	50.67	416.13	19.35	40.76	269.34	40.81	3.64	28.96	
QI 98	15.87	42.03	0.89	580.04	700.40	575.51	15.10	75.73	used with samples YI34-YI44
QI 99	10.97	1.87	2.02	225.93	186.02	251.68	6.42	27.61	
average	13.42	21.95	1.45	402.98	443.21	413.59	10.76	51.67	
std dev	3.46	28.39	0.80	250.39	363.72	228.98	6.14	34.02	

Table 2.6. CAChE 3 second rinse blank concentrations. Table 2.4 caption also applies.

2ND RINSE BLANKS

				Large rods					
SAMPLE ID	Cl	NO3	SO4	Na	NH4	K	Mg	Ca	
QI 04	167.03	85.82	54.25	91.83	177.29	18.23	14.55	22.04	use for all samples with prefix "TI" and "VI"
QI 10	66.38	156.98	59.52	20.87	190.87	11.32	5.41	17.70	
QI 14	36.24	2.80	15.12	42.17	43.18	7.60	4.86	11.84	
QI 28	173.51	1.10	42.80	94.60	23.29	16.47	13.47	15.17	
QI 32	65.13	0.32	41.04	17.61	40.69	18.39	6.85	13.79	
QI 38	61.79	2.31	23.80	23.91	33.07	22.75	7.25	14.67	
average	95.01	41.56	39.42	48.50	84.73	15.79	8.73	15.87	
std dev	59.36	65.82	17.16	35.68	77.39	5.45	4.20	3.58	
QI 44	162.02	0.13	35.65	97.51	165.92	54.29	17.08	21.31	use with samples XI00-XI47
QI 68	64.16	203.34	20.18	25.47	14.32	30.74	6.99	17.08	
QI 72	22.46	671.47	12.83	13.67	230.52	25.19	6.08	15.37	use with samples XI48-XI79
QI 82	35.93	531.34	1.02	19.53	122.98	26.73	6.58	19.16	use with samples YI00-YI32
QI 92	216.50	82.75	21.81	34.97	202.10	27.62	6.33	21.57	use with samples YI34-YI44

				Small rods					
SAMPLE ID	Cl	NO3	SO4	Na	NH4	K	Mg	Ca	
QI 05	449.05	177.23	130.00	284.11	54.28	26.08	34.79	25.92	use for all samples with prefix "TI" and "VI"
QI 11	69.93	306.22	211.22	80.34	121.54	17.46	14.21	24.47	
QI 15	167.45	32.26	71.73	100.40	29.31	12.30	12.30	15.00	
QI 29	862.89	182.97	226.36	527.48	28.94	35.30	59.64	28.22	
QI 33	290.36	107.20	161.00	199.10	32.77	23.27	25.50	24.47	
QI 39	367.70	170.53	168.00	310.15	6.24	24.44	33.37	26.94	
average	367.90	162.74	161.72	250.26	45.52	23.15	29.97	24.17	
std dev	278.05	90.97	56.64	164.64	40.25	7.84	17.30	4.72	
QI 45	665.08	67.00	136.01	393.05	44.39	46.38	42.49	26.40	use with samples XI00-XI47
QI 69	199.88	360.06	101.38	136.27	61.48	29.96	15.98	18.34	
QI 73	49.34	1.87	25.30	25.74	145.76	20.43	6.41	13.91	use with samples XI48-XI79
small rods broken									use with samples YI00-YI32
QI 93	464.43	87.22	71.86	192.26	126.57	31.74	21.88	27.81	use with samples YI34-YI44

with carboy water was used to clean the cloudwater collector. This blank was carried through the entire sample collection and handling process. The cloudwater collector was rinsed periodically throughout the sampling campaign. During these periodic rinsings, the collector was rinsed twice, and the second rinse was collected for analysis. Blank values are reported in Tables 2.4 - 2.6.

A few trends in blank values are evident. Carboy blanks and cloudwater bottle blanks are low until blanks QI75 and QI78. At this point we ran out of sample bottles and had to wash previously used bottles in the field. Bottle blank nitrate values are high because the first step involved a nitric acid rinse. The carboy spigot may have been contaminated at this point. In general, NH_4^+ blanks are high and variable, regardless of the type of blank. The second rinse blanks were higher than the other blanks and best represent the overall blank. The second rinse blanks from the small rods had higher blanks than the large rods. The small rods collectively had more surface area than the large rods and are therefore more subject to contamination. Because there were several high blank values, I felt it was best to confine them to a single batch, rather than attempt to discard some high values as outliers and apply an overall average to the entire sample population. Based on notes taken, time of sample collection, and knowledge of the different cloudwater bottle batches, I was able to match blanks to their corresponding samples.

Knowing which type of blank to subtract from the sample or whether to subtract a blank at all is not always a clear-cut decision. The second rinse blank appears to be the likely candidate but it is similar to an equipment blank. An equipment blank is used primarily as a qualitative check for contamination rather than a quantitative value (Lewis, 1988). I chose to interpret the second rinse as a quantitative blank the sampler would yield if it were sampling a pure water cloud. This is probably a reasonable assumption because we were never able to rinse the collector to the purity of the carboy water used to clean it. The second rinse blank values were therefore subtracted from the sample values.

Even though the blanks were high, they had little impact on concentrations determined after various quality checks (Section 2.3b) because the sample values were much higher. I examined the sample-to-blank concentration ratios to determine how

influential the blanks were. For Cl^-, the blank never exceeded the sample and the majority of samples (>80%) exceeded the blank by at least five times. The majority of NO_3^- samples (25 of 32) that had ratios less than five were due to one high blank value. The $SO_4^=$ values were outstanding, with all but four samples exceeding the blank concentration by ten times. Most Na^+ samples that had ratios less than five also were due to one high blank value. The NH_4^+ blanks were high and variable, but surprisingly the blank exceeded the sample concentration in only six cases. However, all NH_4^+ values are suspect because of consistently high and variable blank values. The K^+, Mg^{+2}, and Ca^{+2} blank values were low and not variable in most cases. Although the sample-to-blank ratios were often less than five, the blanks are known with such precision that the sample concentrations are considered valid. A comparison of uncorrected and blank corrected average values is given below (n=180):

Table 2.7. Comparison of concentrations averages [μeq/L], before and after blank subtraction

	Cl^-	$NO_3^=$	$SO_4^=$	Na^+	NH_4^+	K^+	Mg^{+2}	Ca^{+2}
uncorr'd	205.52	48.23	123.37	195.17	32.34	5.96	43.30	11.07
blank corr'd	200.01	45.28	121.84	189.96	27.17	5.33	41.96	10.10
% change	-2.7	-6.1	-1.2	-2.7	-16.0	-10.5	-3.1	-8.8

As expected, the largest change due to blank correction is the NH_4^+ average concentration. The differences become even smaller when the samples are subjected to further quality control criteria described in Section 2.3b.

2.3b Quality control through criteria selection

Average concentrations calculated from the various constituents only have meaning if they are quality checked to remove samples that were influenced by sampling, handling, or analysis errors not constrained by blank analysis. To accomplish this, the data were subjected to charge balance and seasalt ratio criteria on a sample-by-sample basis. Data that did not satisfy the criteria were considered outliers and excluded from subsequent data analysis.

Sampling errors include bottles with spurious blanks, spurious contamination on the surface of the cloudwater collector, and placement and removal of collection bottles from cloud water collector. These were discussed in Section 2.3a and were accounted for mostly through blank subtraction. Handling errors can be introduced while aliquoting samples for various analyses, during long term storage of the samples, and sample handling during ion chromatographic analysis. Analysis errors can be due to poor instrument performance, operator error, and accidental calculation errors. Any combination of these errors could cause deviations from expected results for the variables below.

Charge Balance

An ionic balance, i.e. Σcations = Σanions, must be established for the soluble species in cloud water. Positive charge results from the major ions Na^+, NH_4^+, K^+, Mg^{+2}, Ca^{+2} and H^+, but organic cations can contribute. Negative charge results mainly from Cl^-, NO_3^-, and $SO_4^=$, but organic anions like methanesulfonic, formic, and acetic acids also contribute. An arbitrary criterion chosen for this data set was $0.65 < \Sigma anions/\Sigma cations < 1.35$. Prior to applying the criterion, the average ratio was 0.978 for 180 samples (see Figure 2.1). After applying the criterion, 24 samples were eliminated and the average ratio was 0.979 (n=156).

The ratio for the "big" droplets that failed typically fell below 0.65, the lower limit of the range. Conversely, the "small" droplets failed the high criteria. The big drops that failed had unusually high NH_4^+ concentrations and came mainly from a single event. The small droplets that failed also came mostly from a single event, but the cause of failure is unknown.

Nominal Sea Salt Ratios

Examination of nominal ratios of ions derived only from seasalt also serves to check individual samples for collection anomalies and/or contamination due to sample handling. These seasalt ions are Na^+, Cl^-, and Mg^{+2}. The use of these ratios assumes there are no other sources and that there is no Cl^- deficit in either the cloud water or pre-cloud aerosol. The composition of sea salt particles in clean atmospheres is also based on the

assumption that the composition is the same as that of seawater. From Miller *et al.* (1972), the compositions are as follows:

Species	Percent by Weight
Na	30.61
Cl	55.04
Mg	3.69

Nominal ratios of ions can be calculated based on the mass percent of each ion in seawater. For example, the ratio of Cl to Mg is determined from the following expression:

$$Cl/Mg\left(ueq/L/ueq/L\right) = \frac{55.04g}{3.69g} \times \frac{\text{mol } Cl^- / 35.453g}{\text{mol } Mg^{+2} / 24.3g} \times \frac{1eq/mol}{2eq/mol} = 5.11 \qquad (1)$$

Analogous calculations were made for Mg/Na and Cl/Na, where Mg/Na = 0.227 and Cl/Na = 1.165.

Figures 2.2 - 2.4 show the trends in the three ratios. The x-axis and Sample Number correspond roughly to the sample ID labels and are in chronological order. A few trends are evident from the three ratio graphs. First, the Cl^- measurements appear to be biased low because both the Cl/Na and Cl/Mg ratios are consistently low. One explanation is that the Cl^- standard was biased low. Susan Harder (personal communication, University of Washington, Department of Chemistry, March 1996) also measured anions using the same ion chromatograph during the same time. She prepared diluted standards from purchased 1000ppm standards while I prepared my own 1000ppm standards from dried salts. A comparison of our 1ppm and 2ppm standards and peak heights are given in Table 2.8.

Table 2.8 Comparison of Cl^- standards

Tris		Susan	
Analysis Date	Pk Ht / conc	Analysis Date	Pk Ht / conc
5/9/95	307.4	4/13/95	289.3
5/9/95	327.5	4/13/95	303.9
5/9/95	309.1	4/13/95	316.2
5/9/95	308.5	4/13/95	297.6
5/12/95	314.1	4/13/95	282.1
5/12/95	312.4	4/13/95	295.8
5/12/95	303.7	4/14/95	325.2
5/12/95	302.9	4/14/95	298.3
5/12/95	315.7	4/14/95	293.9
5/12/95	321.3	4/14/95	300.2
5/15/95	302.2	4/15/95	323.6
5/15/95	310.4	4/15/95	300.3
5/17/95	306.2	4/15/95	299.9
5/17/95	329.6	4/17/95	318.8
5/19/95	300.0	4/17/95	295.2
6/1/95	300.7	4/17/95	296.7
average	310.74		302.32
stddev	9.05		12.29

Using a two sample t-test, $P(T<2.207) = 0.0182$ for the null hypothesis that the means are the same. The data support a difference at greater than a 95% confidence level ($t=2.207$, $df=26$, $P < 0.02$), with my standards slightly higher than Susan's. This suggests that my standards are not biased low and the low ratios might be reflective of a real signal.

The Cl/Na and Cl/Mg values have more variability than the Mg/Na values. This is probably due both to greater chemical lability of Cl^- in the atmosphere and difficulty in measuring Cl^- reproducibly on the IC. The Cl^- peak was never completely resolved from the water dip and this could account for some of the variability. Presumably, standards measured under identical conditions as the samples could account for this. However, system fluctuations could create greater variability.

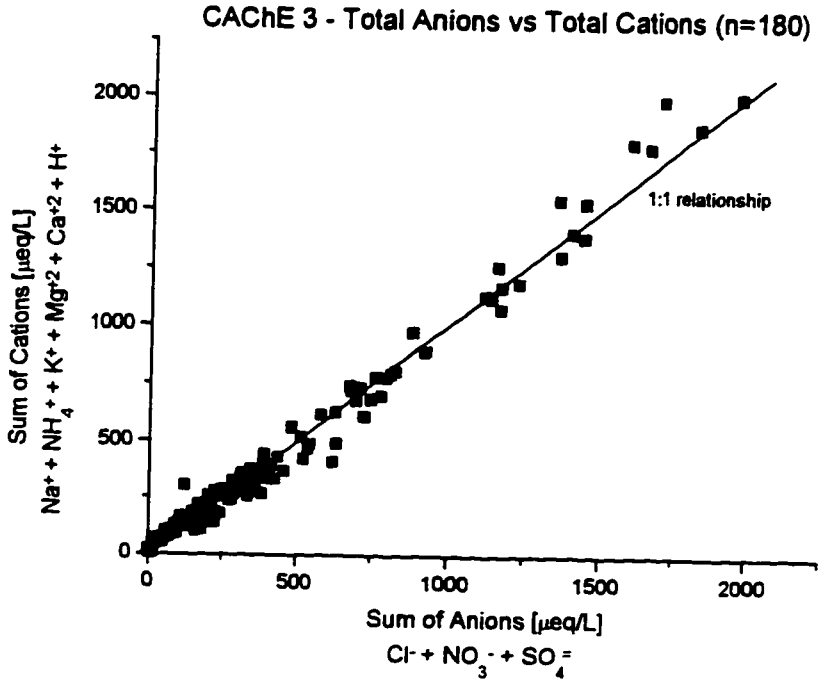

Figure 2.1. Charge balance for all CAChE 3 blank corrected samples.

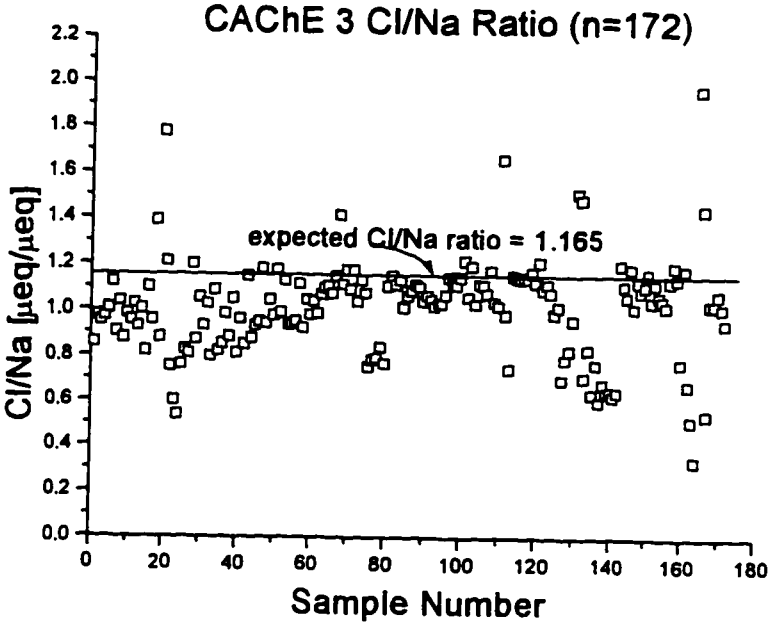

Figure 2.2. Cl/Na seasalt ratio for CAChE 3 blank corrected samples.

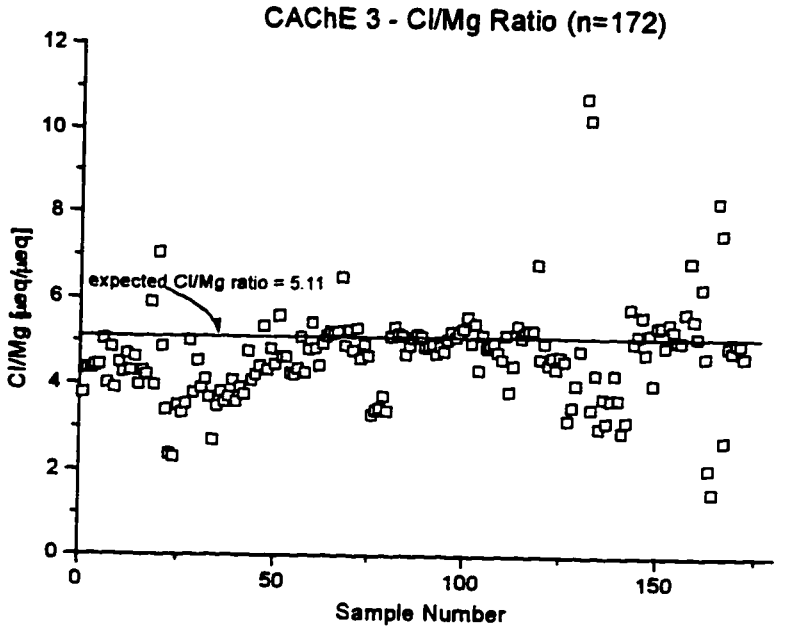

Figure 2.3. Cl/Mg seasalt ratio for CAChE 3 blank corrected samples.

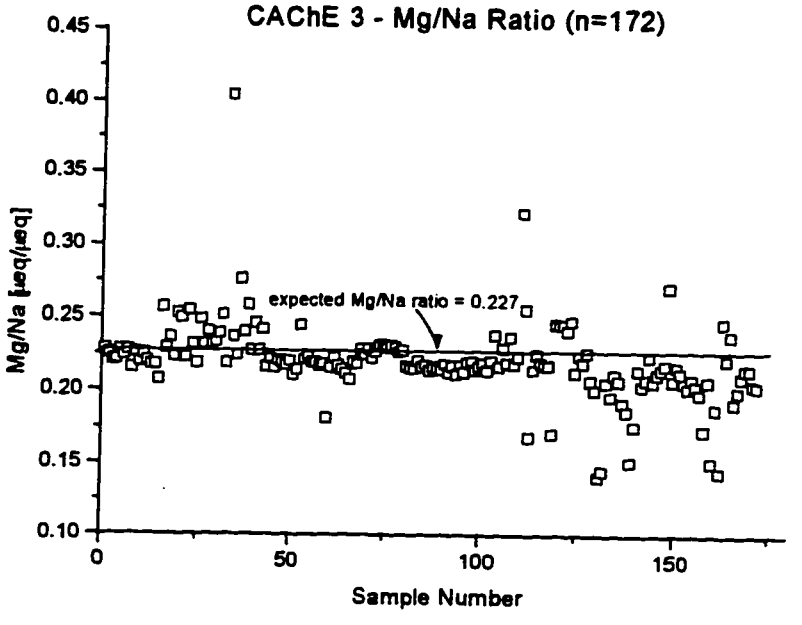

Figure 2.4. Mg/Na seasalt ratio for CAChE 3 blank corrected samples.

The Mg/Na values demonstrate the least variability and might be considered the best criterion for judging anomalies. However, using this ratio alone cannot account for possible sample contamination because anions and cations were measured from separate aliquots. It could be possible that the cation aliquot was not contaminated during sampling handling, but the anion aliquot was. Examining only cation ratios would not reveal this. Therefore, all three ratios will be used as criteria.

Although the Cl ratios had much greater variability, the acceptable range for each ratio was established at ±25% of the average value. These criteria are more restrictive than that used by Vong (1990). Samples that were within 25% of the seasalt Mg/Na seasalt ratio were accepted for further analysis. Since the Cl/Na and Cl/Mg ratios are biased low, range limits were determined differently so as not to exclude reasonable data. Instead of using the accepted seasalt ratio, the average value of each ratio was calculated from the original (n=180) sample data set. The range limits were set at 25% from this average (Cl/Na = 1.013 and Cl/Mg = 4.654). Table 2.9 summarizes the results from applying the criteria.

Table 2.9. Summary of results after applying seasalt ratio criteria. Original number of samples = 180.

Criteria	Acceptable Range	Percentage of samples removed	New Average Value
Charge Balance	0.650-1.350	10.0%	1.062
Cl/Na	0.765-1.276	12.8%	1.019
Cl/Mg	3.428-5.714	12.8%	4.607
Mg/Na	0.171-0.284	5.0%	0.222
All criteria	N/A	23.9%	

Indicators of continental or other non-marine influences

Nitrate/Non-seasalt Sulfate Ratios. Nitrate is typically an indicator of continental and/or anthropogenic influence. (Savoie *et al.*, 1992). A high ratio of NO_3^- to nss-$SO_4^=$ would then indicate air masses of non-marine origin. Prospero *et al.*, (1985) measured aerosol NO_3^- and nss-$SO_4^=$ at several stations in the SEAREX North Pacific network from 1981-

1982. They report concentrations for both dusty (high mineral aerosol resulting from Asian dust transport) and clean seasons. CAChE-3 occurred during the low dust concentration season. The average NO_3^-/nss-$SO_4^=$ mole ratio for the clean season was 0.75 ± 0.39. Assuming equivalent scavenging coefficients, one would expect the aerosol ratio to represent the ratio expected in cloud water.

The average NO_3^-/nss-$SO_4^=$ for the CAChE-3 data set was 0.493 ± 0.244 (number of samples=180). The criterion for maximum NO_3^-/nss-$SO_4^=$ was set at 0.8 and applied to the data set. Of the original 180 samples, 21 samples had ratios higher than 0.8 and therefore failed the criterion. Upon closer inspection, 10 samples were from marine trajectories, 10 samples were from modified marine trajectories, and one sample was from a southerly boundary layer trajectory. The NO_3^-/nss-$SO_4^=$ ratio may not be a good indicator of non-marine influences at Cheeka Peak because most of the samples that failed the criterion were from ostensibly marine origin. This criterion was not applied to the data set as an internal quality check or determinant of marine influence.

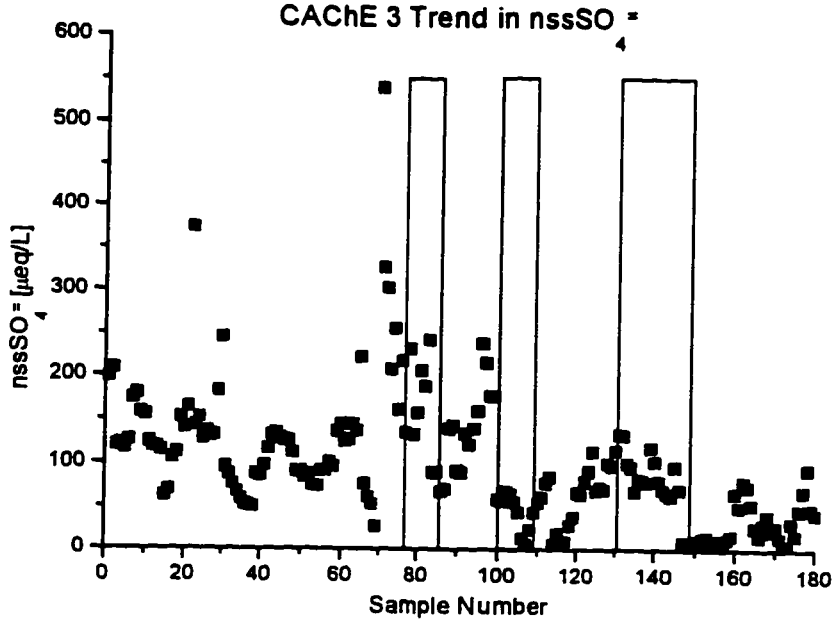

Figure 2.5. The marked areas correspond to events 8, 10, and 14. These events were characterized by high NO_3^-/nss-$SO_4^=$ ratios.

This ratio might be high if the nss-$SO_4^=$ value is unusually low. Figure 2.5 shows the trend in nss-$SO_4^=$ for CAChE-3. The graph indicates that the samples did not have unusually small nss-$SO_4^=$ values. Therefore the first explanation is not a likely one. A second explanation for the high NO_3^-/nss-$SO_4^=$ ratios at Cheeka Peak may relate various specific aspects of the air mass trajectory. If the trajectory shows a fast-moving air parcel from the ocean, the air parcel may have Asian dust in it that had not been removed through cloud cycling. However, this explanation cannot be confirmed with this data set.

Excess K or Excess Ca. Potassium and calcium concentrations beyond that expected from seasalt input are tracers for biomass burning and continental weathering, respectively. There were few instances of high excess values, so these criteria were not used to quality check the data.

2.3c Examination of size dependent droplet concentration

Variations in CAChE 3 cloud droplet chemical concentrations for the two size fractions (average collected droplet size of 12μm and 13μm, respectively) were examined using paired sample t-tests at the α=0.05 confidence level (Moore and McCabe, 1993). In a matched pair study, samples are matched in pairs and the difference for each pair is calculated. The collection of differences forms a single sample, for which t_{calc} can be determined:

$$t_{calc} = \frac{\bar{x} - \mu}{s/\sqrt{n}} \qquad (2)$$

where $\bar{x}$ and s are the mean and standard deviation, respectively, of the "difference" sample set, n is the number of pairs, and μ is the increase in sample concentration between sizes (assumed to be zero for the null hypothesis).. The paired sample t-tests were performed on the overall CAChE 3 data set (n=51 pairs) and on individual events that had greater than five 12μm/13μm cloud water pairs (Events 5, 6, 9, and 17).

2.4 RESULTS AND DISCUSSION

2.4a CAChE 3 average cloud concentrations and comparison to earlier CAChE experiments and other sites

The average cloud concentrations [μeq/L] for major ions collected during CAChE 3 are given in Table 2.10. Concentrations are reported for all blank-corrected, criteria-selected samples (n = 133) and for samples with marine boundary layer (MBL) trajectories only (n = 43). Reported MSA values are blank-corrected but were not subjected to any criteria, other than examination for unusual chromatographic performance. These samples were measured independently (see Section 2.2d) and represent a smaller data set (n = 65 for all samples, n = 21 for marine boundary layer samples).

Table 2.10. Average cloud water concentrations [μeq/L] for CAChE 3 samples. *MSA values were analyzed independently and have a different sample size.

Species	All samples (n=133)	
	Mean	Std Dev
LWC [g/m^3]	0.530	0.387
Cl^-	255.43	344.58
NO_3^-	52.69	39.20
$SO_4^=$	137.40	83.97
$nssSO_4^=$	108.10	68.11
Na^+	242.18	321.20
NH_4^+	28.81	25.36
K^+	6.65	7.04
Mg^{+2}	53.88	72.35
Ca^{+2}	12.66	14.99
H^+	105.24	62.99
$CH_3SO_3^-$ *	5.31	4.39

Acetate, formate and pyruvate were also measured in these samples, but their values are very unreliable (personal communication, Mike Hamilton, NOAA-PMEL). The acetate peak was frequently convoluted with one or more unidentified peaks and deionized water blanks run during the analysis frequently registered unreasonably high values (e.g. 22 ppm). Formate sample blanks were more than half the sample value except in extreme cases where sample concentrations were unusually high (e.g. 20-40 ppm). Pyruvate concentrations were usually below detection limit.

The CAChE 3 major ion concentrations are also graphed in Figure 2.6. The mean and standard deviation of sample sets rarely capture the true range and variability found in most environmental samples. Figure 2.6 shows that the mean concentration often falls far from the median concentration.

Major ion cloud chemistry was also measured during the CAChE 2 sampling campaign. The cloud water samples were not fractionated by size; all drops greater than 5μm were collected. These samples were measured by ion chromatography using the same procedure described in Section 2.2.d. CAChE 2 samples were blank-corrected and criteria selected. Average concentrations for CAChE 1 (Vong, *et al.*, 1997), CAChE 2 and CAChE 3 major ions are compared in Table 2.11. The concentrations represent marine boundary layer samples only, as determined from air mass back trajectories.

There is large variation in ion concentration determined during the three CAChE sampling campaigns. The CAChE 2 samples were more influenced by ocean contact, evidenced by seasalt concentrations that were 2-4 times more concentrated than CAChE 1 or 3 samples. From these limited data sets, there appears to be no seasonal agreement between the spring samples collected in 1993 and 1994 (CAChE 1 and 2) or agreement between samples collected in the same year (CAChE 2 and 3). Long term (multi-year and multi-season) measurements made at Whiteface Mountain, NY also fluctuate widely (Mohnen and Kadlecek, 1989). It may be unreasonable to expect close comparison when emission rates, oxidant processes, and air mass origins do not repeat from year to year or season to season.

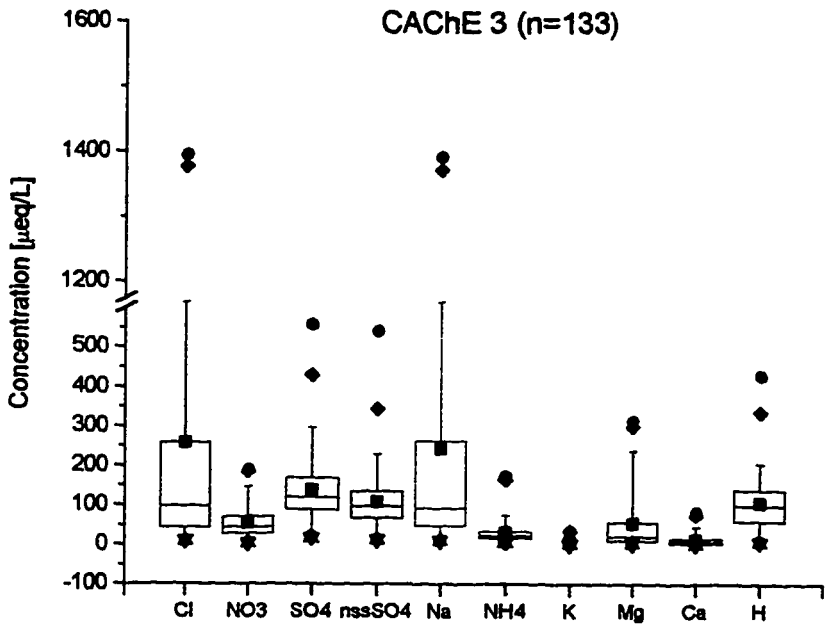

Figure 2.6. Box chart for blank corrected and criteria selected CAChE 3 data. The bottom symbol = minimum value; the second symbol = 1st percentile; the bottom of the box = 25th percentile; the median line = 50th percentile; and the top of the box = 75th percentile. The square symbol in the box marks the mean. The top two symbols mark the 99th percentile and maximum value.

Table 2.11. Average cloud water concentrations [μeq/L] for CAChE 1, 2, and 3 MBL samples. Average LWC for CAChE 1 = 0.3 ± 0.2 g/m^3 (Vong, *et al.*, 1997), CAChE 2 = 0.30 ± 0.08 g/m^3, and CAChE 3 = 0.44 ± 0.16 g/m^3.

	CAChE 1 (n=45) May 5-25, 1993		**CAChE 2 (n=46)** Apr 21-May 22, 1994		**CAChE 3 (n=43)** Aug 10-Sep19, 1994	
Species	Mean	Std Dev	Mean	Std Dev	Mean	Std Dev
Cl^-	432.9	369.6	872.1	787.5	144.27	166.90
NO_3^-	15.1	12.9	68.4	55.9	56.81	48.37
$SO_4^=$	63.5	38.9	185.1	126.7	132.60	107.09
$nssSO_4^=$	27.9	19.8	93.5	59.7	115.03	96.65
Na^+	290.6	236.9	757.1	667.8	145.19	161.12
NH_4^+	11.1	10.1	21.1	20.7	22.05	15.69
K^+	8.1	5.8	17.7	16.2	4.65	3.95
Mg^{+2}	66.4	55.5	173.8	155.2	32.60	37.28
Ca^{+2}	36.1	37.0	39.3	32.2	8.14	7.21
H^+	35.0	16.5	85.0	51.3	113.42	78.40
$CH_3SO_3^-$ *	3.4	3.5	N/A		6.15	3.81

Cloud water composition from other regions in the US and Europe are presented in Table 2.12 for comparison. The CAChE 3 results are comparable to other remote western US sites. However, CAChE 3 concentrations are much higher than those measured at Mary's Peak, OR and during CAChE 1.

2.4b Data Trends

Chloride Depletion

Evidence for chloride depletion was found in Section 2.3.b, however the underlying cause was not explored further. It is widely accepted that acids can replace Cl^- in seasalt aerosol, thereby releasing $HCl_{(g)}$ (c.f. Martens *et al.*, 1973 or Duce, 1969). A Cl^- deficit is clearly seen in aerosol samples but usually not in cloud water samples because the released HCl is efficiently scavenged by cloud droplets and the pH is not low enough to degas Cl^- (Munger et al., 1989). However, CAChE 3 cloud water samples display a Cl^- deficit. A

Table 2.12. Comparison of measured cloud water compositions in the US and Europe.

Location	Sampling Period	$SO_4^=$ [μeq/L]	NO_3^- [μeq/L]	NH_4^+ [μeq/L]	Comments
Western USA:					
Mary's Peak, OR	1984-85	22	5	N/A	Weathers *et al.*, 1988; site 100km from ocean
San Marcos Pass, CA	1983	55	74	97	Jacob *et al.*, 1985; mtn pass in coastal range; no nearby sources
Redwood Nat'l Park, CA	1984-85	160	30	N/A	Weathers *et al.*, 1988; site 2km from ocean, total $SO_4^=$ reported
Pt Reyes, CA	1982	283	152	131	Jacob *et al.*, 1985; Nat'l Seashore, no nearby sources, nss$SO_4^=$ rep'd
San Pedro Hill, CA	1987	868	1185	775	Munger *et al.*, 1989; southern LA, nss$SO_4^=$ reported
Midwestern and Eastern USA					
OH, WV, KY, IN	1990	194	142	87	Burkhard *et al.*, 1994; aircraft platform
Whiteface Mtn, NY	1982-87	158-396	49-243	68-173	Mohnen & Kadlecek, 1989; mean ranges
Shenandoah Mtn, VA	1986-88	176	94	93	Mohnen & Vong, 1993; mean concentrations
Mt. Mitchell, NC	1986-88	489	174	184	Mohnen & Vong, 1993; mean concentrations
Europe:					
Great Dun Fell, England	1987	644	743	N/A	Gallagher, *et al.*, 1988; average from one cloud event
Areskutan Peak, Sweden	1983-84	6-700	2-68	1-17	Ogren & Rodhe, 1986; range of median conc's over all trajectories
Mt. Rigi, Switzerland	1990-91	213	310	460	Collett *et al.*, 1993; volume-weighted averages
Po Valley, Italy	1984	150-6300	80-8200	30-8100	Fuzzi *et al.*, 1988; largest agricultural and industrial area in Italy

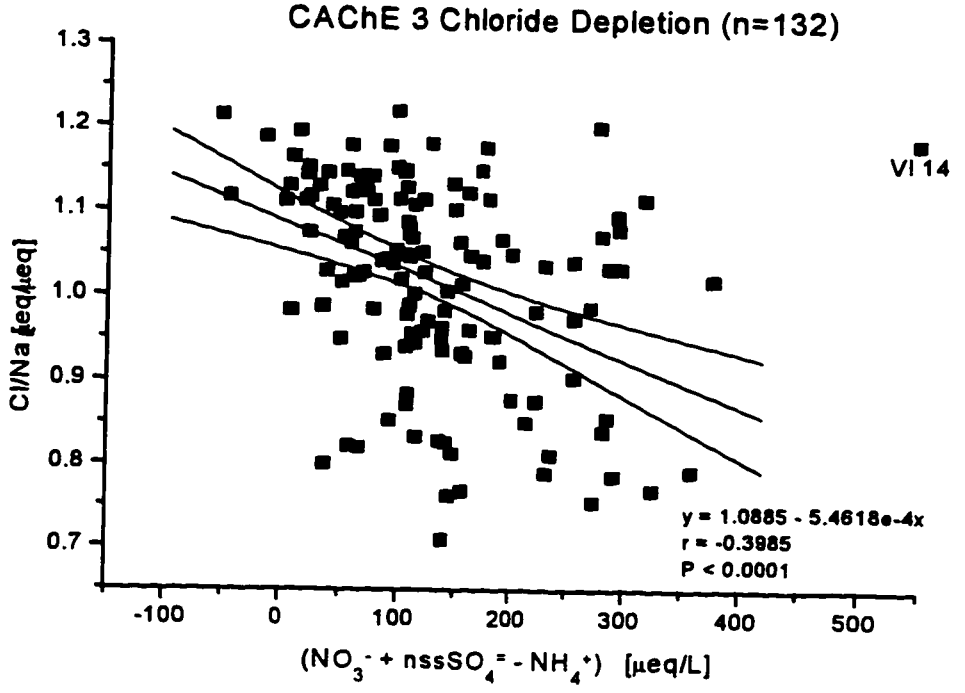

Figure 2.7. Chloride depletion for the CAChE 3 sampling campaign. The probability that the slope is zero is less than 0.0001. Sample VI 14 is an extreme outlier and was not included in the linear regression. Curved lines indicate 95% confidence bands for the fit.

plot of Cl/Na versus an acidity measure was made to determine if the observed chloride depletion could be a result of acid-induced volatilization. Nitrate and $nssSO_4^=$ both contribute to acidity; NH_4^+ neutralizes their effect. Figure 2.7 shows an overall trend for the entire CAChE 3 campaign. The non-zero slope suggests that acidity plays a role.

When individual events are plotted (Figures 2.8 a and b), chloride depletion is more pronounced in some cases than others. Cloud formation could have occurred on already depleted aerosol, so that released HCl would not have the opportunity to be reabsorbed by the cloud. For the aerosol to remain depleted, some mechanism for the preferential removal of the HCl must be present, or else the released HCl(g) would also be incorporated into the cloud drops. A possible, though unsubstantiated, explanation is the deposition of acidic HCl(g) to the seawater surface, which is basic (pH ~ 8.2).

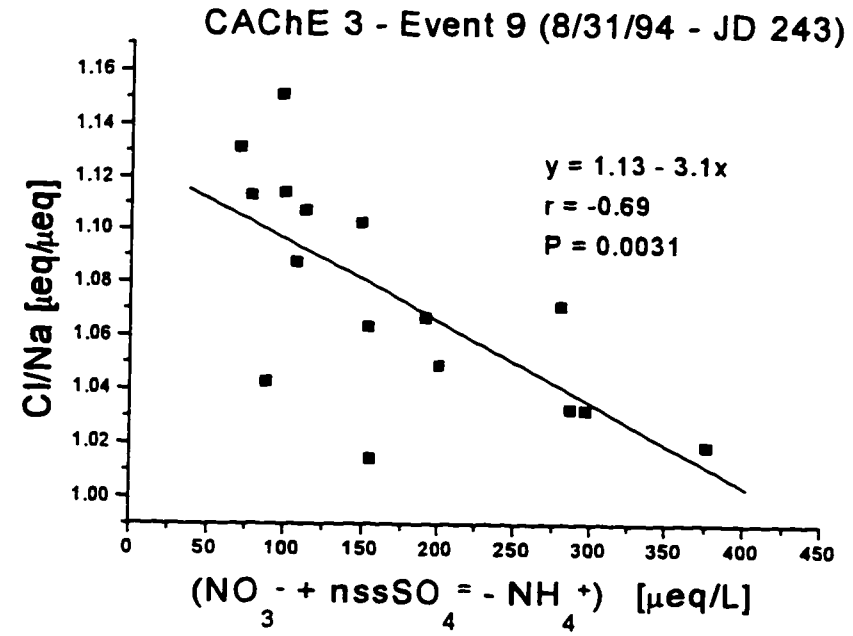

a)

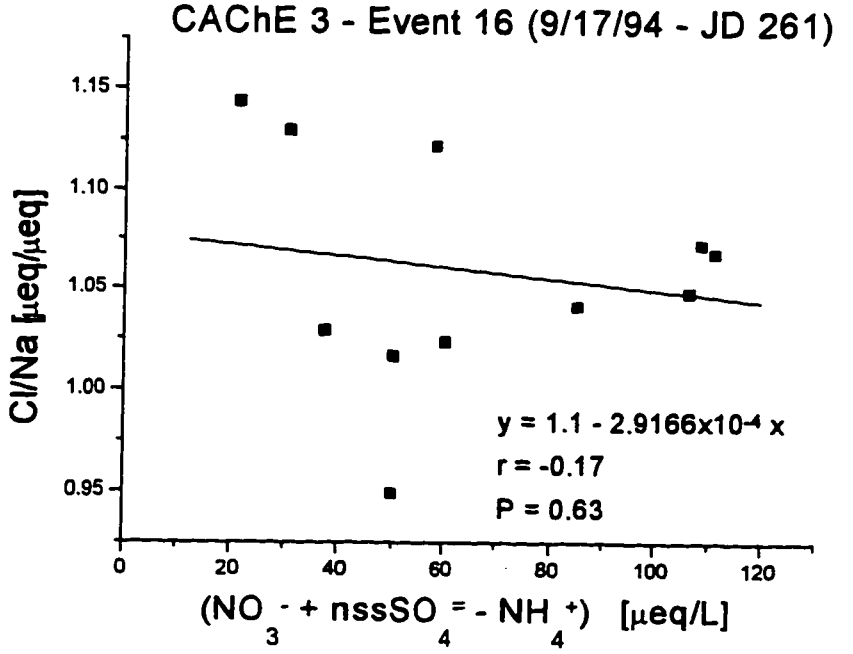

b)

Figure 2.8 a and b. Chloride depletion for two events during CAChE 3. Event 9 demonstrates more chloride depletion than Event 16. The probability that the slope for Event 16 is zero is high.

Acidity Trend

The concentration temporal trends (in μeq/L) for the major ions that influence acidity are given in Figures 2.9 and 2.10. The data plotted were blank-corrected and passed charge balance and seasalt ratio criteria. The data set was split into two parts to facilitate interpretation and to reflect the transition to higher, more variable blanks for NO_3^- and NH_4^+. As described in Section 2.3a, the NO_3^- and NH_4^+ blanks were generally lower for the "TI" and "VI" series samples and were therefore plotted separately from the "XI" and "YI" series samples. Non-seasalt sulfate dominated the acidity, sometimes by a factor of two or more than nitrate. In Figure 2.9.a, a drastic decrease in pH at sample VI14 (Event 7) was accompanied by the highest measured nss-$SO_4^=$ concentration for the entire campaign (note that the sample immediately prior to VI14 is from a different event). The corresponding >5μm sample, VI15, did not pass the criteria and was therefore not shown on the lower graph. The nss-$SO_4^=$ concentrations for the TI and VI series were generally a factor of two higher than concentrations measured for the XI and YI series. This increase in nss-$SO_4^=$ was reflected in a corresponding decrease in the average pH between the two time periods (pH = 3.97 vs. 4.35 for drops greater than 12 μm, pH = 3.92 vs. 4.33 for drops greater than 5 μm). There was an uncharacteristic increase in NH_4^+ concentration in the >12μm drops at samples XI38, XI40, and XI42. These samples comprised a single event (Event 19, southerly boundary layer). Ammonia emissions over land are stronger than over the ocean (Soderlund and Rosswall, 1982), however its trajectory did not indicate any unusual continental contact. Although the NH_4^+ concentration was high, there was not a corresponding increase in pH. Also, the >5 μm drops (samples XI39, XI41, and XI43) did not exhibit a markedly increased NH_4^+ concentration. The additional NH_3 could have originated by local production in coastal waters. It also is possible that the cloud nucleated on neutralized aerosol, i.e. that the NH_4^+ originated from particles and not from gas phase mass transport of NH_3.

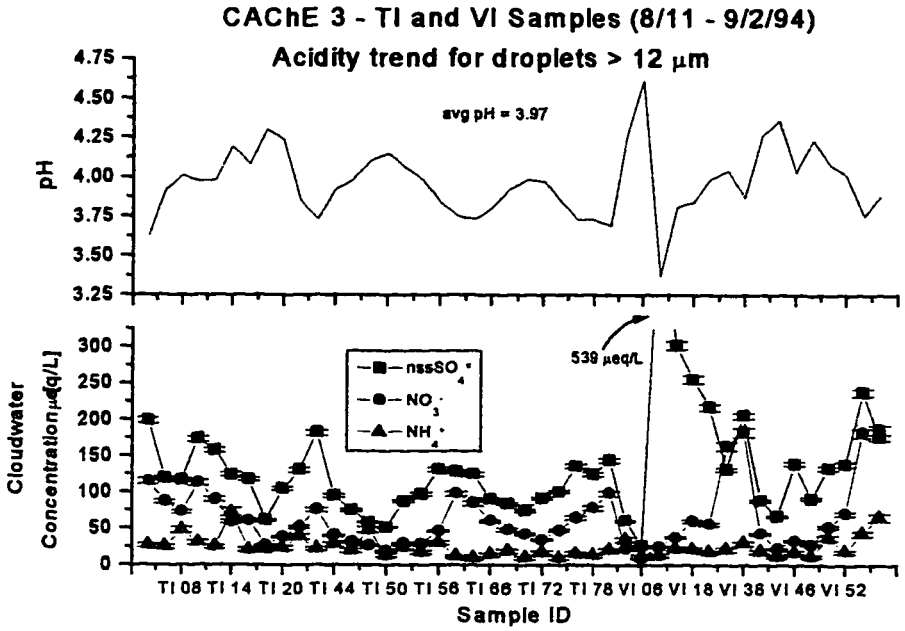

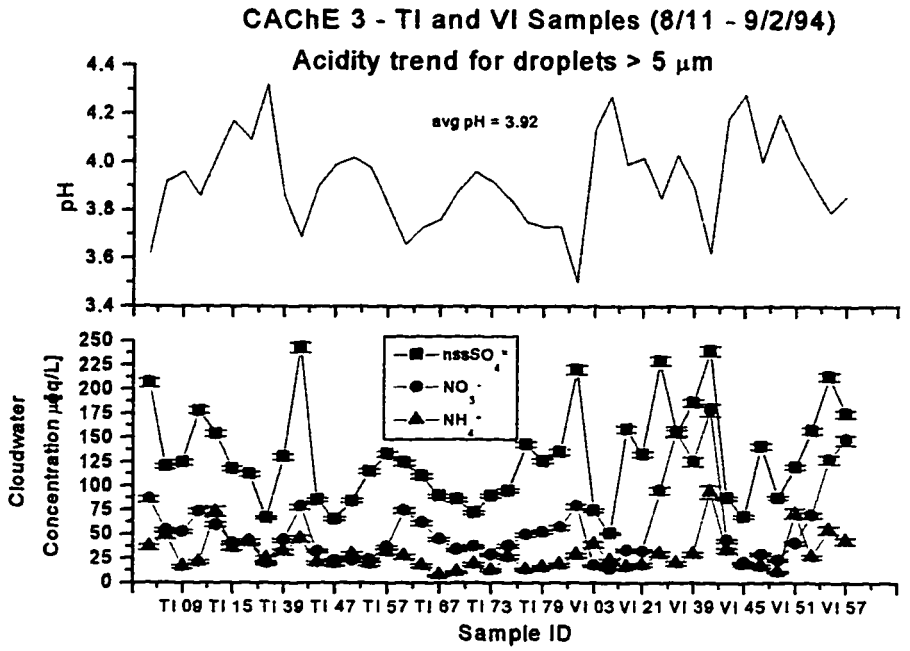

Figure 2.9a and b. Acidity trends for the CAChE 3 "TI" and "VI" series. Data are in sample order and do not reflect a continuous time period. The a & b x-axes are not identical.

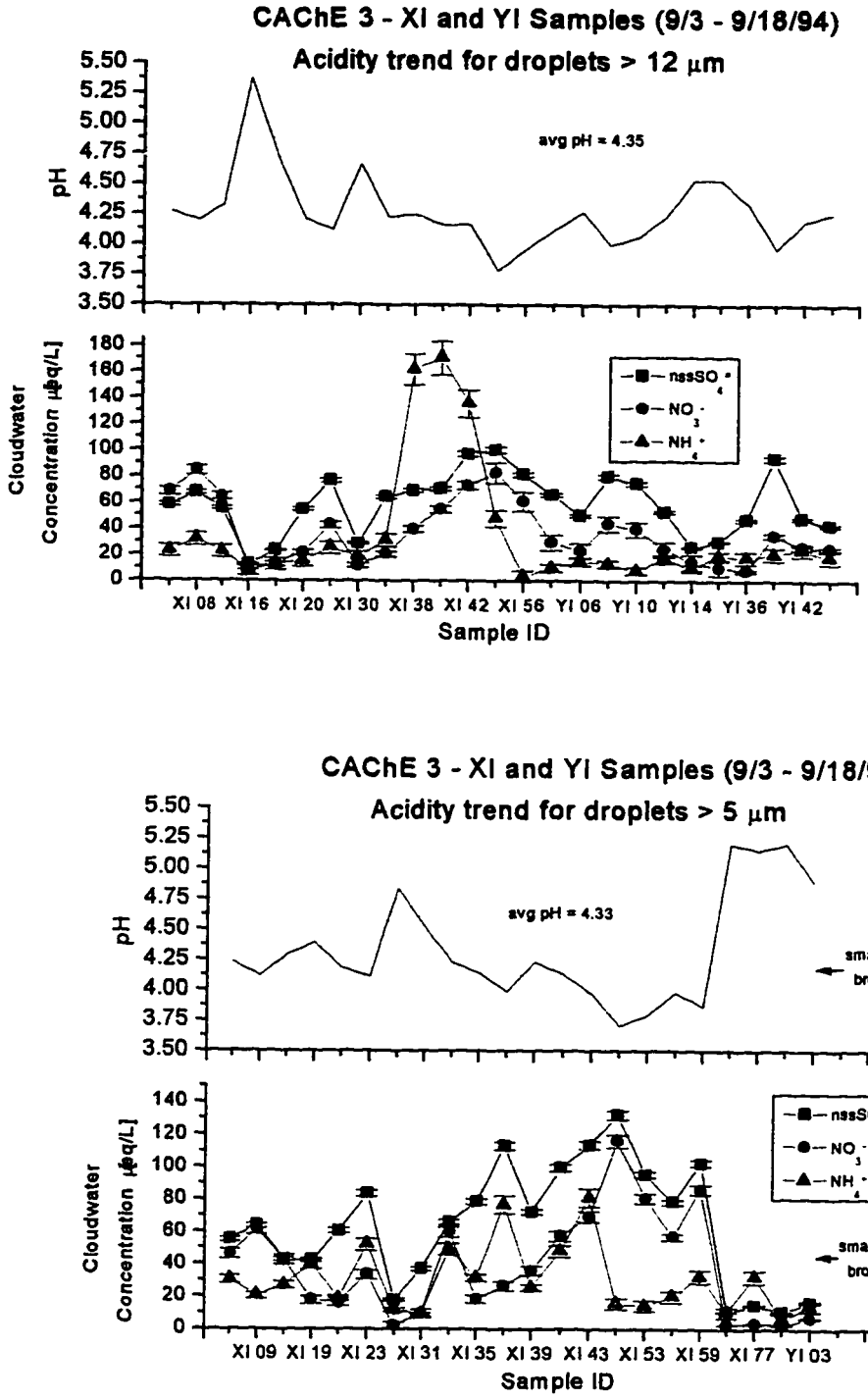

Figure 2.10.a and b. Acidity trends for the CAChE 3 "TI" and "VI" series. Data are in sample order and do not reflect a continuous time period. The a & b x-axes are not identical.

Non-seasalt $SO_4^=/Na^+$ and NO_3^-/Na^+ ratios

An elevated $nssSO_4^=/Na^+$ ratio (in seawater, $SO_4^=/Na^+$=0.120μeq/μeq) could indicate sources of $SO_4^=$ in addition to the scavenging of seasalt aerosol, e.g. aqueous phase oxidation. The trend in $nssSO_4^=/Na^+$ ratio for the collected size fraction representing drops > 5 μm is shown in Figure 2.11. The displayed data were blank-corrected and criteria-checked. In general, the ratios were higher during Events 1, 2, 3, and 4 (all stagnant boundary layer trajectories).

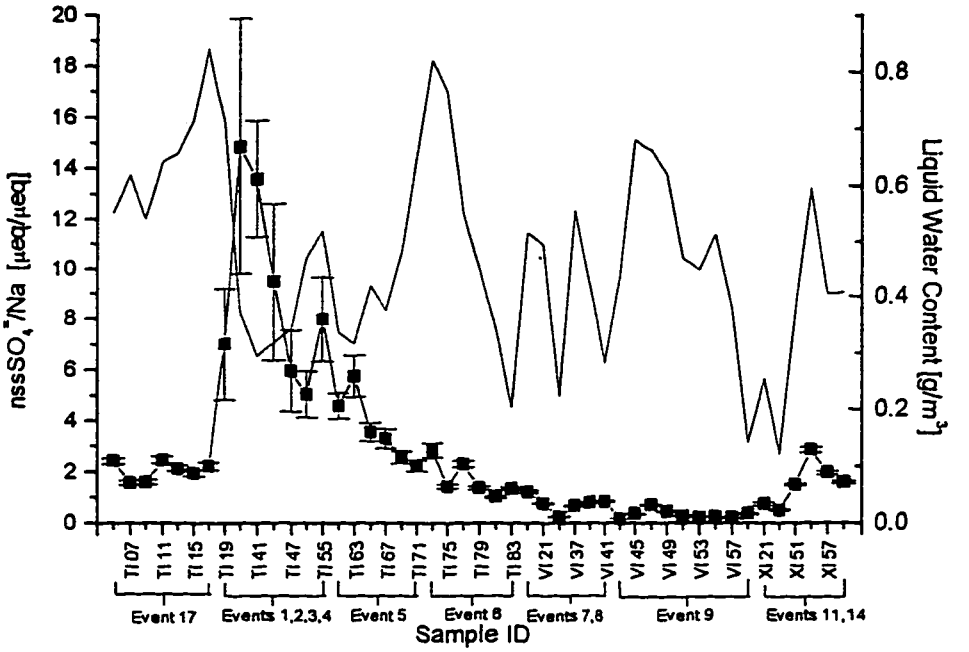

Figure 2.11. Trend in $nssSO_4^=/Na^+$ ratio during CAChE 3 for drops > 5 μm. Graph points represent approximately one-hour samples. See Table 2.1 for event details.

A more interesting comparison would be to compare the $nssSO_4^=/Na^+$ ratio found in the 5-12 μm fraction with that found in the >12 μm fraction. However, the raw data, which consist of chemical composition data for two different sizes of collection rods, yield mean drop sizes (12 μm for the small stage and 13 μm for the large stage) for the two collection aliquots which sometimes scarcely differ. Because the collected fractions reflect cumulative collected water above the rod cutoffs of 5 and 12 μm, and there is relatively

little water mass in the 5 – 12 μm size range, this is not surprising. Nevertheless, it can render concentrations for the two size aliquots nearly identical. To get around this problem and derive size dependent concentrations for distinct size fractions, these distinct fractions are deconvoluted from the available aliquots by treating the concentrations in the collected water above 5 μm as the volume-weighted mean of the concentrations for the 5 - 12 μm and >12 μm size fractions given by:

$$(C_i)_{>5\mu m} = (C_i)_{5-12\mu m}\left(\frac{LWC_{5-12\mu m}}{LWC_{>5\mu m}}\right) + (C_i)_{>12\mu m}\left(\frac{LWC_{>12\mu m}}{LWC_{>5\mu m}}\right) \quad (3)$$

where the LWC's and C's refer to the liquid water contents and chemical species concentrations, respectively for the indicated size ranges. Ratios can also be substituted for C. Hence, for comparison with the already available >12 μm fraction, the concentrations of the chemical species in the 5 - 12 μm fraction are estimated as:

$$(C_i)_{5-12\mu m} = \frac{(C_i)_{>5\mu m} - (C_i)_{>12\mu m}\left(\frac{LWC_{>12\mu m}}{LWC_{>5\mu m}}\right)}{\left(\frac{LWC_{5-12\mu m}}{LWC_{>5\mu m}}\right)} \quad (4)$$

A comparison of the nss$SO_4^=/Na^+$ ratio in the 5 - 12 μm and >12 μm fractions for selected cloudwater sample pairs collected during CAChE 3 are shown in Figure 2.12. The remaining sample pairs were not shown because the 5 - 12 μm ratio exceeded the >12 μm ratio by 5 to 98 times. Because the volume mean cloud drop diameter is usually greater than 12 μm, there is so little water in the 5 – 12 μm fraction that above calculation becomes unstable. In all cases, the nss$SO_4^=/Na^+$ 5 - 12 μm ratio exceeded the >12 μm ratio. Unfortunately, this is caused by marked preferential scavenging of Na into the larger drop fraction and is not evidence for $SO_4^=$ production in the smaller size fraction.

A changing NO_3^-/Na^+ ratio could also indicate NO_3^- production or loss. The NO_3^-/Na ratio suffers from the same systematic error due to preferential scavenging of Na and was therefore not plotted.

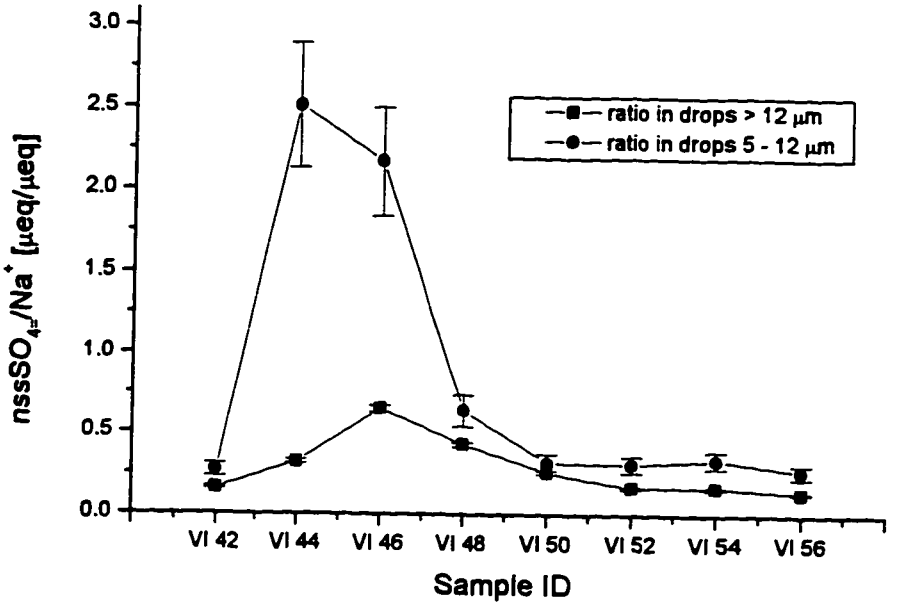

Figure 2.12 Size-differentiated trend in $nssSO_4^{=}/Na^{+}$ ratio for Event 9 during CAChE 3. A total of 41 pairs of samples passed criteria selection, but only 8 pairs are shown here. Graph points represent approximately one-hour samples. See Table 2.1 for event details.

2.4c Size Dependent Chemistry

Table 2.13 represents the size dependence in cloud chemistry for all blank-corrected samples that passed charge balance and seasalt ratio criteria. The 51 pairs of data for ionic species represent non-precipitating cloud only. From the overall data, large droplets (>12µm collected fraction) are more concentrated for the seasalt-derived species (Na^{+}, K^{+}, Mg^{+2}, Ca^{+2}, and Cl^{-}). NO_3^{-} is also more concentrated in the larger drops and is discussed later. Conversely, H^{+} is concentrated in the smaller droplets (>5µm collected fraction). MSA, nss-$SO_4^{=}$, and NH_4^{+} had no statistically significant size dependence.

Four events (Events 5, 6, 9, 17) were chosen for closer examination because these events had the most sample pairs retained following criteria selection (Table 2.14). The rationale for this was to determine if a size dependence might be masked by looking at the overall data instead of each event separately. In the case of K^{+}, the overall data set indicated strong support for size dependence, but one event (Event 6) had no statistically significant difference between fractions. The most unusual finding was for H^{+}; although

the overall data set indicated size dependence, the four individual events indicated no chemical difference at α=0.05 (however significance was shown at the α=0.06 level for two events). This is likely due to the greater degrees of freedom in the overall data set.

The size dependence of the seasalt species agreed with previously observed results (c.f. Munger *et al.*, 1989; Collett *et al.*, 1994; Vong *et al.*, 1997). Under diffusional growth situations, larger droplets nucleate on dust or sea-salt particles whereas smaller droplets nucleate on nss-$SO_4^=$ and other secondary derived aerosols (Andreae *et al.*, 1986; Noone *et al.*, 1988; Ogren and Charlson, 1992). In theory, large droplets experience proportionally less dilution than smaller drops in the same cloud (Ogren and Charlson, 1992), further explaining why coarse mode species like seasalt are more concentrated in large drops.

The observed size dependence of NO_3^- agreed with some results (Collett *et al.*, 1994) but disagreed with other results (Munger *et al.*, 1989). This was largely due to the area in which samples were collected. Munger and coworkers collected cloud water samples at the coast in south Los Angeles. Los Angeles has an abundance of stable particulate nitrate, largely due to gas-phase chemical reactions of NH_3 with other acidic species to form secondary, condensed aerosols (Seinfeld, 1986). Secondary aerosols are mainly sub-micron sized and therefore smaller cloud drops will nucleate on these particles. This is consistent with their observation that NO_3^- was enriched in the smaller droplets relative to the larger droplets. However, in marine environments, nitrate is largely present in the gas phase, albeit at low concentrations relative to urban areas, resulting from oxidation of NO_x. Coastal areas have low concentrations of $(NH_4)_2SO_4$ and NH_4NO_3 secondary aerosol because coastal areas in general are deficient in acid-neutralizing capacity (Jacob et al, 1985). Particulate nitrate that is present is likely associated with seasalt particles from the displacement of HCl (Collett et al., 1994). If NO_3^- is in the gas phase, than it will likely concentrate in large drops where there is greater surface area and greater

Table 2.13. CAChE 3 size dependent chemistry for all samples (blank corrected and criteria selected). Mean concentrations are reported for the two droplet fractions (drops > 5μm and drops > 12 μm). The quantity P(T< t) represents the probability that the difference in concentration is due to randomness; therefore the small P-values indicate strong evidence against the H_o: $x_{>5\mu m} = x_{>12\mu m}$. A significance level of α=0.05 was chosen to assess size dependence. If the P-value was as small or smaller than α, the data was considered statistically significant at that level. The number of observations for MSA are less because only a subset of CAChE 3 samples were analyzed at NOAA PMEL.

SPECIES	MEAN CONC (> 5μm drops)	MEAN CONC (> 12 μm drops)	# PAIRS	P(T<t)	SIZE DEP?
Na^+	239.6	313.2	51	7.24E-05	Yes
NH_4^+	28.5	31.9	51	0.221	No
K^+	6.4	8.6	51	9.21E-06	Yes
Mg^{+2}	53.7	69.1	51	0.0003	Yes
Ca^{+2}	11.9	17.1	51	2.21E-05	Yes
H^+	111.8	107.1	51	0.008	Yes
Cl^-	255.8	327.8	51	0.0001	Yes
NO_3^-	50.4	65.2	51	8.12E-10	Yes
nss-$SO_4^=$	111.1	112.9	51	0.278	No
MSA	5.2	5.5	32	0.210	No

Table 2.14. CAChE 3 size dependent chemistry for samples (blank corrected and criteria selected) of Events 5, 6, 9, and 17. The value *n* is the number of pairs. No MSA data was available for Events 6 and 17. A significance level of α=0.05 was chosen to assess size dependence. If the P-value was as small or smaller than α, the data was considered statistically significant at that level.

	EVENT 5 (n=5)		EVENT 6 (n=5)		EVENT 9 (n=8)		EVENT 17 (n=7)	
SPECIES	P(T<t)	SIZE DEP?	P(T<t)	SIZE DEP?	P(T<t)	SIZE DEP?	P(T<t)	SIZE DEP?
Na^+	7.3E-06	Yes	0.039	Yes	0.044	Yes	4.8E-05	Yes
NH_4^+	0.24	No	0.30	No	0.15	No	0.38	No
K^+	0.022	Yes	0.057	No	0.038	Yes	0.0014	Yes
Mg^{+2}	1.2E-05	Yes	0.025	Yes	0.044	Yes	5.8E-05	Yes
Ca^{+2}	6.2E-06	Yes	0.022	Yes	0.038	Yes	0.00036	Yes
H^+	0.055	No	0.32	No	0.059	No	0.14	No
Cl^-	5.0E-05	Yes	0.050	Yes	0.043	Yes	0.00012	Yes
NO_3^-	0.0043	Yes	0.020	Yes	0.044	Yes	5.8E-05	Yes
nss-$SO_4^=$	0.12	No	0.28	No	0.28	No	0.38	No
MSA	0.17	No			0.17	No		

alkalinity (due to seasalt). If NO_3^- is in the particulate phase, it will be associated with the coarse particles and thus large drops. Both explanations support the observed CAChE 3 results of enriched concentration in the larger drops.

Although researchers have previously observed $SO_4^=$ enrichment in smaller droplets (Munger et al., 1989, Collett et al., 1994), enrichment was not observed for the CAChE 3 samples. This finding is consistent with earlier results found at Cheeka Peak (Vong *et al.*, 1997). Processes other than nucleation scavenging and diffusional growth (e.g. gas phase adsorption, aqueous phase oxidation) likely masked any size effects discernible by the cloud water sampler.

2.5 CONCLUSIONS

Samples (n = 180) from non-precipitating clouds were collected at Cheeka Peak, WA and were analyzed for major anions and cations. Sample collection occurred during August and September 1994 as a part of the third Cloud and Aerosol Chemistry Experiment (CAChE 3). Samples were subjected to blank correction and rigorous quality control. CAChE 3 ion concentrations are higher than previously observed at Cheeka Peak, but comparable to other remote West coast locations.

Chloride depletion was observed overall and was attributed to an increase in acidity; however, individual events varied in the strength of the decreasing relationship. Non-seasalt sulfate dominated the acidity, sometimes by a factor of two or more than nitrate. The nss-$SO_4^=$/Na^+ ratios results were inconclusive due to extreme preferential scavenging of Na^+ into the large drop fraction.

Seasalt ions were more concentrated in the larger drops, consistent with previously observed and modeled results. Size dependence was not observed for MSA, nss-$SO_4^=$, and NH_4^+ and only weakly observed for H^+, consistent with earlier results (Vong *et al.*, 1997). Nitrate was more concentrated in the larger drops, suggesting that the nitrate observed in the cloudwater originated as particulate NO_3^- rather than adsorption of gas phase HNO_3. The observed size dependence is almost surprising given the actual difference in collected cloud water fractions. Although a theoretical difference of 7μm is

expected between the two sampler stages, ambient cloud droplet size and sampler aspiration/collection efficiencies reduce the actual difference to ~1μm (Vong *et al.*, 1997). With such a small difference between the two size fractions, any observed difference in chemistry is even more significant.

CHAPTER 3 - GAS PHASE AND AQUEOUS PHASE MEASUREMENTS OF HYDROGEN PEROXIDE

3.1 INTRODUCTION

3.1.a Importance of H_2O_2

Hydrogen peroxide is one of the most important oxidants in the atmosphere. Photochemical models predict its presence in both remote and polluted air (Chameides, 1984; Kleinman, 1986; Liu and Trainer, 1988). Hydrogen peroxide controls the oxidative capacity of the atmosphere in two ways. In the gas phase, H_2O_2 acts as a reservoir species for hydroxyl radicals (OH) which, in turn, oxidize trace gases such as NO_x, CH_4, and CO (Kleinman, 1986). In the aqueous phase, the reaction between H_2O_2 and HSO_3^- provides the major source of $SO_4^=$ in cloud water. The production of $SO_4^=$ in clouds plays a key role in acidifying precipitation (c.f. Calvert *et al.*, 1985) and modifies the aerosol spectrum to create better cloud condensation nuclei (CCN) and more efficient light-scattering particles (Lelieveld and Heintzenberg, 1992). In this regard, it is noteworthy that the oxidative capacity of the atmosphere is changing; Greenland ice cores have shown a 50% increase in H_2O_2 over the past 200 years (Sigg and Neftel, 1991) and H_2O_2 concentrations are predicted to continue to rise in the next 50 years (Thompson *et al.*, 1989). Higher peroxide concentrations increase sulfate production in oxidant-limited conditions.

3.1.b Sources of H_2O_2

The dominant pathway by which H_2O_2 is formed, in both the gas and aqueous phase, is via the bimolecular self-reaction of the hydroperoxyl radical (Kircher and Sander, 1984; Gunz and Hoffman, 1990):

$$HO_2^{\cdot} + HO_2^{\cdot} \rightarrow H_2O_2 + O_2 \qquad k = 5.6E\text{-}12\ cm^3molec^{-1}sec^{-1} \qquad (1)$$

The hydroperoxy radical disproportionates, meaning it undergoes reduction and oxidation simultaneously (initial oxygen oxidation state of -1/2 to final oxidation states of -1 and 0). This reaction is accelerated when a hydrogen-bonded complex is formed between HO_2 and H_2O (Hamilton and Lii, 1977). The bimolecular self-reaction of OH to form H_2O_2 ($OH + OH \rightarrow H_2O_2$) is kinetically and thermodynamically favorable. However, OH

concentrations in the gas phase are typically two orders of magnitude less than HO_2 and at least four orders of magnitude less in the aqueous phase (Finlayson-Pitts and Pitts, 1986; Chameides, 1984) making this pathway insignificant in comparison to formation from HO_2.

The hydroperoxyl radical can be formed in a variety of ways. In the gas phase, the hydrogen radical, H·, can react with O_2 to form HO_2. The hydrogen radical can be formed via an abstraction mechanism, such as (Finlayson-Pitts and Pitts, 1986):

$$CO + OH\cdot \rightarrow H\cdot + CO_2 \qquad (2)$$

or via a decomposition mechanism, such as (Finlayson-Pitts and Pitts, 1986):

$$HCHO + h\nu(\lambda < 370nm) \rightarrow H\cdot + HCO\cdot \qquad (3)$$

The abstraction mechanism, involving the OH radical, indicates a relationship between HO_2 production and ozone concentration, since OH is produced via decomposition of ozone and subsequent reaction with water vapor:

$$O_3 + h\nu(\lambda < 320nm) \rightarrow O_2 + O(^1D) \xrightarrow{H_2O} 2OH\cdot \qquad (4)$$

Using model predictions, Liu and Trainer (1988) reported that a change in column O_3 could induce changes in tropospheric OH, HO_2, and H_2O_2. Olzyna *et al.* (1988) also reported a positive correlation (r^2 = 0.42) from field observations of O_3 and H_2O_2 concentrations. Conversely, field measurements at Cape Grim, Tasmania (Ayers *et al.*, 1992) show a link between H_2O_2 production and ozone destruction. Although these results appear contradictory, the observed covariance between O_3 and H_2O_2 does not necessarily involve formation of one from the other. The O_3 concentration is many times that of HO_2 and not much O_3 must be lost to explain typical HO_2 levels.

The hydroperoxyl radical can also be formed in the gas phase through the thermal decomposition of peroxyacetyl nitrate ($CH_3C(O)O_2NO_2$) and peroxynitric acid (HO_2NO_2) (Gunz and Hoffmann, 1990) and the photoxidation of isoprene ($CH_2C(CH_3)CHCH_2$) (Gu, *et al.*, 1985; Gaffney *et al.*, 1987; Watkins *et al.*, 1995).

In the gas phase, the HO_2 bimolecular self-reaction competes with NO oxidation and reaction with O_3 (Baulch *et al.*, 1982 and Finlayson-Pitts and Pitts, 1986, respectively):

$$HO_2 + NO \rightarrow OH + NO_2 \qquad k = 8.3E\text{-}12\ cm^3molec^{-1}sec^{-1} \qquad (5)$$

$$HO_2 + O_3 \rightarrow OH + 2O_2 \qquad k = 2E\text{-}15\ cm^3molec^{-1}sec^{-1} \qquad (6)$$

The primary natural source of NO in the Northern Hemisphere marine atmosphere is via lightning. Because lightning is rarely observed in the non-turbulent conditions around Cheeka Peak, oxidation of NO by HO_2 is a minor pathway. In low NO_x conditions, equation 6 becomes the dominant O_3 destroying mechanism; however, the HO_2/O_3 reaction rate is 3 orders of magnitude slower than the bimolecular HO_2/ HO_2 self-reaction. Because radical production is many times greater than NO_x introduction rates in the free troposphere and marine boundary layer, most radicals are removed by self-combination reactions rather than reaction with NO_x (Daum, *et al.*, 1990).

In the aqueous phase, dissolved O_3 can consume the hydroperoxyl radical (Sehested *et al.*, 1984):

$$HO_2 + O_3 \rightarrow OH + 2O_2 \qquad k < 10^4\ M^{-1}s^{-1} \qquad (7)$$

or its dissociated form:

$$HO_2 \leftrightarrow H^+ + O_2^- \qquad K_a = 1.3 \times 10^{-5}\ M \qquad (8)$$

$$O_2^- + O_3 \xrightarrow{H^+} OH + 2O_2 \qquad k = 1.0 \times 10^9\ M^{-1}s^{-1} \qquad (9)$$

However, reaction (7) is slow. At pH >3.5, reaction (8) becomes more significant and net H_2O_2 production declines. However, ozone is not very soluble and thus the hydroperoxyl radical in the aqueous phase mostly reacts to form H_2O_2 at pH<5 (McElroy, 1986).

The hydroperoxyl radical concentration in cloud water is thought to be largely due to scavenging of gas phase HO_2. According to McElroy (1986), this process is dependent on the radiation intensity, scavenging efficiency of precursor radicals, the droplet spectrum, and cloud liquid water content. Free radical chemistry in a cloud droplet is controlled by the ultraviolet density within the cloud. When the solar zenith angle (incident on the cloud) is small, the uv density within the cloud is at least as large as that

found in clear air. For this reason, McElroy proposes that diurnal variations in concentration should be more pronounced in clouds than in clear air. Scavenging efficiency depends on the accommodation coefficient, α, which is estimated to be equivalent to that of water since both molecules are likely to be controlled by strong hydrogen bonding (Pruppacher and Klett, 1978). The supply of HO_2 radicals is also affected by the cloud droplet spectrum, because a favorable surface-to-volume ratio of a small droplet will scavenge precursor gas species (HCHO, H^-, OH^-) before they can make HO_2. Finally, the predicted rate HO_2 scavenging, and hence H_2O_2 production, drops off as the liquid water content increases because precursor radicals are again scavenged and consumption by O_3 becomes favorable.

While many studies have assumed the primary source of atmospheric H_2O_2 is controlled by gas phase reactions, aqueous phase production mechanisms have also been proposed. The impetus for determining aqueous phase production mechanisms came from an inability to explain aqueous phase concentrations from precursor gas phase concentrations in many field studies. A production mechanism for HO_2 involving aqueous formaldehyde oxidation has been proposed (Chameides and Davis, 1983). Anastasio *et al.* (1994) also propose a photochemical production pathway in the aqueous phase for terrestrial clouds, however the mechanism is sketchy and depends on the presence of certain unidentified "chromophores". The chromophores, thought to be organic compounds, absorb ultraviolet radiation and either fluoresce or serve as electron donors that initiate radical reactions in the droplet to form H_2O_2. A more substantiated production mechanism involves the production of H_2O_2 via the photolysis of Fe(III)-organic ligand complexes (Zuo and Hoigne, 1993):

$$Fe(III) - L \xrightarrow{h\nu} Fe(II) + L^{\bullet} \tag{10}$$

$$L^{\bullet} + O_2 \rightarrow O_2^{\bullet -} + oxidized\ L \tag{11}$$

$$2O_2^{\bullet -} + 2H^+ \rightarrow H_2O_2 + O_2 \tag{12}$$

where L stands for organic ligand (commonly oxalic, pyruvic, or glyoxalic acid) and $L^{\bullet}$ stands for organic radical. Siefert *et al.* (1996) demonstrate that sufficient

photochemically available iron is present to make this Fe redox pathway significant for the urban locations studied (Whiteface Mtn., NY and various CA locations). However, the concentration of iron in North Pacific air is much lower due to iron-limited ocean conditions and therefore this aqueous phase pathway is not likely to be as important as gas phase scavenging.

3.1.c Henry's Law and phase equilibria of H_2O_2

Knowledge of the Henry's Law behavior of H_2O_2 is important since most of its oxidizing capacity is realized in the aqueous phase (Lind and Kok, 1986). Henry's Law describes the partitioning of a species between a gas and liquid phase whose equilibrium can be expressed as

$$M(i) = K_H P(i) \qquad (13)$$

where $P(i)$ is the partial pressure of species i in equilibrium with a solution of molar concentration $M(i)$. The Henry's Law constant, K_H, is dependent on the temperature and chemical composition of the system; pressure effects are negligible on the condensed phase. Equation (13) relies on the assumptions that both gas and condensed phases behave ideally (otherwise fugacity and activity should be used) and that the species i must be in the same chemical form in both phases. Fortunately, both criteria are met for H_2O_2. The temperature dependence of K_H takes the form

$$K_H(\text{M atm}^{-1}) = e^{[A/T - B]} \qquad (14)$$

where T is temperature and A and B are constants. At 25°C, $K_H(H_2O_2)$ is 1.02E5 M atm^{-1} (Lind and Kok, 1994). Compared to other atmospheric compounds such as O_3 (1.3E-2 M atm^{-1}), SO_2 (1.24 M atm^{-1}) and NH_3 (62 M atm^{-1}), hydrogen peroxide is very soluble (Finlayson-Pitts and Pitts, 1986).

3.1.d Aqueous phase chemistry of H_2O_2

Hydrogen peroxide controls cloud water acidity through the oxidation of S(IV) to S(VI); H_2O_2 itself doesn't contribute to acidity because its acid dissociation constant is so small ($K^{298} = 2 \times 10^{-12}$ M; Behar *et al.*, 1970). Under typical atmospheric conditions, H_2O_2 reacts almost exclusively with S(IV), meaning that if all the S(IV) were consumed, excess H_2O_2 would have little to react with. In addition, the oxidation of S(IV) by H_2O_2

exceeds the S(IV) reaction with O_3, dissolved O_2, hydroxyl radical, and CH_2O when pH<4.5 (c.f. Penkett *et al.*, 1979; Chameides, 1984; Kelly *et al.*, 1989; Hegg, 1989). However, modeling (Hegg and Larson, 1990) and field measurements (Collett *et al.*, 1994) show that individual drops can have a much different pH than bulk cloud water, and thus conditions of higher pH can exist in individual drops wherein O_3 oxidation becomes dominant. The production of atmospheric acidity through the conversion of N(III) to N(V) by H_2O_2 is considered inconsequential (Daum *et al.*, 1984; Kelly *et al.*, 1985; Lee and Lind, 1986) because HNO_3 is formed primarily by the gas phase reaction of OH with NO_2 (Finlayson-Pitts and Pitts, 1986) or produced in the aqueous phase via other mechanisms (Calvert *et al.*, 1985). A similar case can be made for carboxylic acids (see below). An extensive body of literature describing the reaction of H_2O_2 with S(IV) exists (Gunz and Hoffman, 1990 and references therein).

The mechanism for S(IV) oxidation by H_2O_2 proposed by Hoffman and Edwards (1975) for pH 4 -8 and later verified by McArdle and Hoffman (1983) for pH 0 - 4 is as follows:

$$SO_2(aq) \rightleftarrows H^+ + HSO_3^- \qquad (15)$$

$$HSO_3^- + H_2O_2 \rightleftarrows \begin{matrix} O^- \\ \diagdown \\ S-OOH \\ \diagup \\ O \end{matrix} + H_2O \qquad (16)$$

$$\begin{matrix} O^- \\ \diagdown \\ S-OOH \\ \diagup \\ O \end{matrix} + H^+ \longrightarrow H_2SO_4 \qquad (17)$$

The reaction proceeds via the nucleophilic displacement of HSO_3^- by H_2O_2, followed by a rate-determining acid-catalyzed rearrangement of the peroxymonosulfurous acid intermediate to form H_2SO_4. The rate of reaction follows second order kinetics, first order with respect to [S(IV)] and [H_2O_2], respectively, at pH ranges typical of cloud water (Penkett *et al.*, 1979; Martin and Damschen, 1981, Hoffman and Edwards, 1975; McArdle and Hoffman, 1983). Kunen *et al.* (1983) verified these results using much lower concentrations of reactants, similar to those typically found in cloud water. Unlike other S(IV)-oxidant reactions, the reaction of S(IV) with H_2O_2 is relatively invariant with

respect to pH because the increase in rate due to acid catalysis offsets the decreasing solubility of SO_2 with decreasing pH (Calvert *et al.*, 1985).

Aqueous phase reactions between hydrogen peroxide and species other than SO_2 could also contribute to the acidity in rain and cloud droplets. Carboxylic acids can contribute significant acidity to the precipitation in non-urban troposphere (c.f. Keene and Galloway, 1984). Benner and Bizjak (1988) have demonstrated a possible aqueous-phase HCHO-H_2O_2 reaction; however, it does not compete kinetically with the S(IV)-H_2O_2 reaction and does not produce a carboxylic acid product. Although Chameides and Davis (1983) have suggested aqueous phase formation of formic acid (HCOOH) from OH radical reactions (not H_2O_2), recent field results show no evidence for significant production of HCOOH from aqueous phase reactions (Keene *et al.*, 1995). Furthermore, Talbot *et al.* (1995) observed no correlation between gas phase formic/acetic acids with peroxide species. From these results, one may conclude that H_2O_2 plays no role in carboxylic acid production.

3.1.e Fate of H_2O_2 after cloud processing

In an unpolluted environment, peroxide may not be entirely consumed through reaction with SO_2, resulting in excess peroxide that is present when the cloud evaporates. The fate of peroxide upon cloud evaporation is unclear. Hydrogen peroxide photolyzes through breakage of the O-O bond at wavelengths starting at 300 nm and extending to lower wavelengths (Okabe, 1978). Because most of the radiation below 300 nm is absorbed by O_3, O_2, and atomic oxygen in the atmosphere, destruction by photolysis is unlikely on the time scale of cloud evaporation and detrainment. McElroy (1986) suggests that clouds ultimately act as a sink for excess peroxide because H_2O_2 neither volatilizes (like SO_2) nor remains in the aerosol phase (like NaCl) upon cloud droplet evaporation; rather, it disproportionates in the presence of trace metals like Fe(II) and Fe(III). However, if sufficient trace metal concentration is not present, it is plausible that H_2O_2 volatilizes like other soluble gases, especially since the evaporation process is very rapid compared to most chemical reactions.

3.1.f Organic peroxides

Organic peroxides, collectively referred to as ROOH (where R = various organic functional groups), have been observed in the atmosphere in the form of methyl hydroperoxide (MHP; CH_3OOH), hydroxymethyl hydroperoxide (HMHP; $HOCH_2OOH$) and peroxyacetic acid (PAA; $CH_3C(O)OOH$) (Gaffney *et al.*, 1987; Hellpointner and Gab, 1989; Lee *et al.*, 1993; Fels and Junkermann, 1994). More exotic organic peroxides, like phenylperoxides or substituted methyl peroxides, are unlikely because the R-O_2 bond is much weaker and therefore these precursors don't exist long in the atmosphere (Lightfoot *et al.*, 1992). Organic peroxides have been reported to make up as little as <10% (Barth *et al.*, 1989) to 80% (Lee *et al.*, 1993) of the total peroxides measured. As with other field experiments (c.f. Barth *et al.*, 1989; Simonaities *et al.*, 1991; Tremmel *et al.*, 1994), the organic peroxides measured in this study were not speciated.

When NO_x concentrations are low (< ~10pptv), the competing reaction of RO_2 + NO is negligible and organic peroxides are formed via the following reaction (Lind and Kok, 1986; Lightfoot *et al.*, 1992):

$$RO_2 + HO_2 \rightarrow ROOH + O_2 \qquad (18)$$

The Henry's Law constants (K_H) for MHP and PAA are more than two orders of magnitude less than H_2O_2 (304 M atm^{-1} and 669 M atm^{-1} at 25°C, respectively; Lind and Kok, 1994) whereas the K_H for HMHP is higher (1.68 E 6 M atm^{-1}; Staffelbach and Kok, 1993). Lind *et al.* (1987) determined that the oxidation kinetics of S(IV) by H_2O_2, MHP, and PAA had reaction rate constants that were within a factor of four of one another. Nevertheless, because of their generally lower solubilities and concentrations, the importance of organic hydroperoxides may only become significant when H_2O_2 concentrations are limited and when wet removal is important.

3.1.g This work

The chapter summarizes the results of hydrogen and organic peroxide measurements made in early summer (April/May) and late summer (August/September) 1994 at the Cheeka Peak Research Station. Both gas phase and aqueous phase peroxides were measured, allowing for the examination of Henry's Law equilibrium between the two

phases. The correlation between gas phase O_3 and H_2O_2 is also examined. A principal components analysis is performed to extract maximum variance from a set of measured chemical and microphysical variables, including the major ion chemistry described in Chapter 2 and focuses on these variables' effects on H_2O_2 concentration. Finally, the cloudwater peroxide data is qualitatively examined for evidence of sulfate production.

3.2 EXPERIMENTAL

3.2.a Gas phase measurements of hydrogen peroxide and organic peroxide

Gas phase hydrogen and organic peroxides were collected at Cheeka Peak from April 19 - May 18 and August 30 - September 23, 1994 as a part of the Cloud and Aerosol Chemistry Experiments, CAChE 2 and CAChE 3, respectively. These species were measured using a continuous, fluorometric analyzer based on the horseradish peroxidase method (Lazrus, *et al.*, 1985 and 1986). Analysis is achieved by fluorescence detection of the dimer of p-hydroxy phenylacetic acid (PHOPAA), formed by the reaction of PHOPAA with peroxide and catalyzed by the enzyme peroxidase :

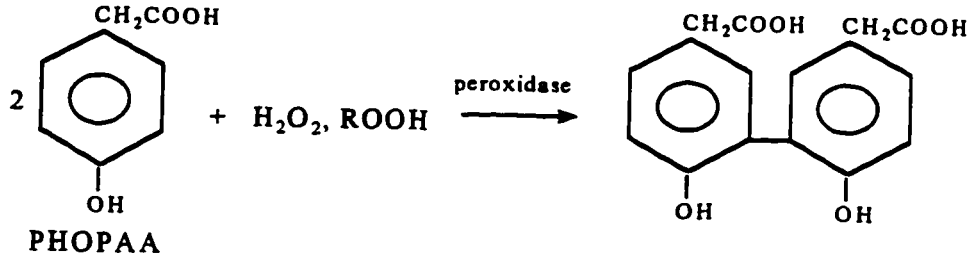

(19)

The PHOPAA dimer fluoresces at a peak excitation wavelength of 320nm and peak emission wavelength of 400 nm and is directly proportional to the peroxide concentration.

In order to differentiate between hydrogen peroxide and organic peroxides, the sample flow is split into two channels. Total peroxide (H_2O_2 + ROOH) is measured in one channel while the H_2O_2 in the second channel is selectively decomposed by the catalase enzyme prior to the addition of peroxidase:

$$2\,H_2O_2 \xrightarrow{\text{catalase}} 2\,H_2O + O_2 \qquad (20)$$

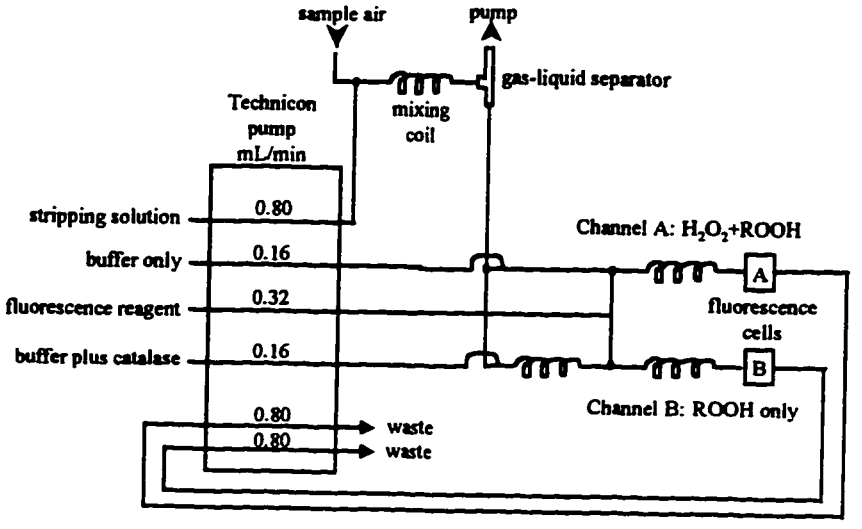

Figure 3.1: Schematic of gas-phase peroxide measurement system.

A dual channel flow system (Figure 3.1), based on the selectivity of the catalase and peroxidase enzymes, provides a simultaneous fluorescence signal resulting from peroxidase reaction pathway (Channel A) and catalase-peroxidase reaction pathway (Channel B). Each channel provides a simultaneous fluorescence signal. The difference between the two channels is a measure of gas phase H_2O_2. The method is described in detail in Lazrus *et al.* (1986).

Ambient air was sampled through approximately twenty feet of ¼" PFA teflon tubing (Fluoroware/Galtek) at a flow rate of 2.1 SLPM. The aqueous flow system was operated with a Ismatec peristaltic pump. The ambient air sample and deionized water

(Millipore milli-Q filtered water with resistivity greater than 18 MΩ/cm) were pulled concurrently through a ten-turn, 2 mm-i.d. Pyrex glass coil, causing soluble peroxides to dissolve in the water. Because H_2O_2 is a highly soluble gas, a collection efficiency of 100% is achieved for H_2O_2 (Lind and Kok, 1986). Following passage through an air-water separator, the flow was split between the two channels and a pH-buffered conditioning solution (0.05 M potassium hydrogen phthalate (KHP) adjusted to pH = 5.8 - 6.0 with 1 N NaOH, J.T. Baker Chemical Co.) was added to the air-scrubbed solution. This pH range gives the best stability of reagent and reaction products (Kok *et al.*, 1986) and minimizes the loss of H_2O_2 caused by reaction with HSO_3^- (Lazrus *et al.*, 1986). Due to an intended imbalance in intake and waste flows, air bubbles were formed and segmented the reaction stream. The flow rate through each channel was approximately 0.6 mL/min.

A fluorescence reagent (1.6 mM PHOPAA [Fairfield Chemical Co.], 12 purpurogalin units/mL of peroxidase [Sigma Chemical Co.] in 0.05M KHP) was added to the "total" peroxide channel and reacted in a five-turn, 2 mm-i.d. mixing coil. The "ROOH" channel received the same treatment, but a catalase reagent (0.05 M KHP containing catalase protein, Sigma Chemical Co.) was added prior to the fluorescence reagent. Each sample stream passed through a nafion membrane immersed in concentrated NH_4OH to raise the pH above 10 and thus optimizing the fluorescence signal of the dimer. Finally, the sample streams passed through fluorometer cells and out to waste. The dual beam fluorometer has been described previously (Lazrus *et al.*, 1985).

The peroxide analyzer was calibrated once daily with aqueous H_2O_2 standards of 2, 5, and 10 ppbm. A commercial 30% H_2O_2 solution was diluted and preserved with EDTA to provide a stock solution of approximately 1%, from which daily standards were made. The stock solution was standardized using $KMnO_4$ at the beginning and end of each CAChE experiment. Although the calibration concentrations are higher than typically observed, standards of lower concentration are more subject to errors from H_2O_2 naturally present in the dilution water. Calibration curves were fit with an intercept of zero; multiple daily calibrations were grouped when the stripping, fluorescence, and catalase reagents were the same (Figure 3.2).

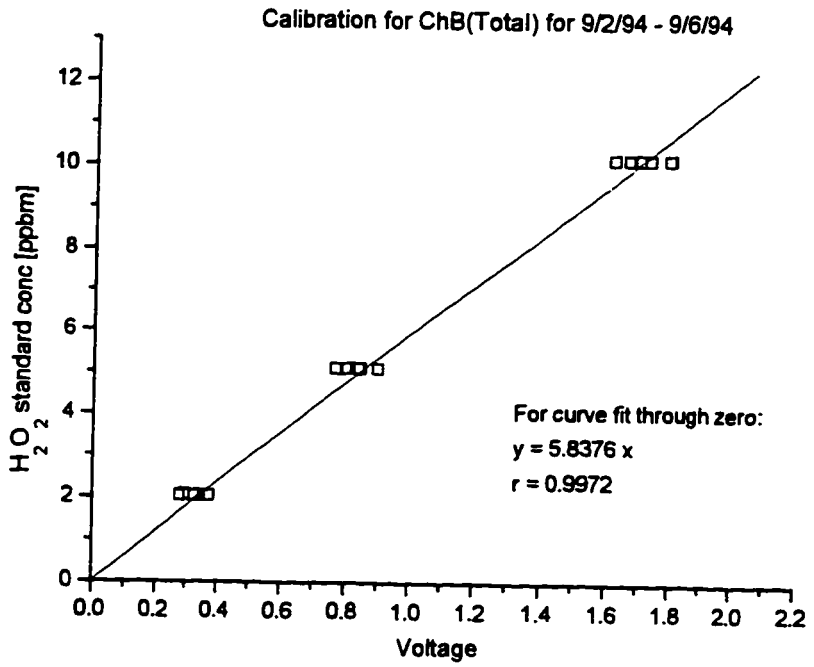

Figure 3.2: Typical set of calibrations for the gas-phase peroxide measurement.

In addition to aqueous calibration standards injected directly into the dual channel flow system, gas phase calibration standards were generated to check system performance and line losses. Line checks performed every 2 weeks throughout the field experiments showed line losses less than 3.5%, with the exception of one measurement that indicated a loss of 8.3%. Lind and Kok (1986) describe the generation of gas phase standards. A schematic of the gas phase calibration setup, along with a sample calculation, is given in Appendix B.

Although catalase does not react with most organic hydroperoxides, it does react slightly with methyl hydroperoxide (MHP). Catalase reacts preferentially with H_2O_2 and then reacts with MHP when all of the H_2O_2 is consumed. To minimize this effect, the strength of the catalase solution was adjusted until the signal from a 10 ppbm H_2O_2 standard registered 3.5% to 7.5% of its original value.

A QUICKBASIC program logged five voltage outputs from an A/D board (AD 1000, Real Time Devices, Inc.) connected to the gas-phase system. Temperature, flow rate, a status signal (indicating zeroing or calibration) and voltage signals from the two fluorimeter cells were collected at a frequency of 1 Hz and saved as 10-second averages. Various calibration and flow constants were used to initialize a FORTRAN program (provided by Greg Kok and later modified) that reduced the collected voltages into gas-phase concentrations. Calculations within the program assumed that all of the ROOH measured was MHP.

The detection limit of each channel is defined as three times the standard deviation of the blank. The blank in this case is ambient air that has passed over a Pd catalyst to decompose all peroxides, prior to dissolution of the sample in deionized water during the stripping step. The instrument measured this "blank" water every three hours. The detection limits for the total peroxide and organic peroxide channels were about 30 pptv and 20 pptv, respectively.

3.2.b Sources of error in gas phase peroxide measurement

Possible sources of error in this measurement include fluctuations in the reagent line flow rates, variable intake air flow rates, presence of interferents, and high proportions of organic peroxides to hydrogen peroxides. The measured standard deviations in the reagent line flow and air intake flow were 0.63 ± 0.03 mL/min (4.6%) and 2.14 ± 0.01 sLpm (0.5%), respectively. The presence of high concentrations of O_3 can cause a positive interference because O_3 can generate H_2O_2 on surfaces in the presence of moisture; however, field experiments using O_3 concentrations of 40 ppbv to 100 ppbv indicated undetectable effects (Lazrus *et al.*, 1986). Ozone concentrations at Cheeka Peak rarely exceeded 30 ppbv. Although a combination of measurements can contribute error to the gas phase peroxide measurement, the largest source of error comes from the process of distinguishing organic peroxides through the selective decomposition of H_2O_2 by the catalase enzyme.

The concentration of catalase has to be carefully controlled because catalase does react slowly with some organic hydroperoxides. Lazrus *et al.* (1985) investigated the

reactivity of catalase with a variety of organic hydroperoxides and found appreciable reaction only with methyl hydroperoxide (MHP). The dual channel system measures the sum of H_2O_2 and partially soluble organic peroxides in one channel (S_p) and partially soluble organic peroxide and some residual hydrogen peroxide on a second channel (S_c) (Heikes, unpublished communication):

$$[H_2O_2] = \frac{\alpha_0^K S_p - S_c}{\alpha_0^K - \alpha_0} \tag{21}$$

where α_0 is the residual fraction of H_2O_2 after reaction with catalase (experimentally determined) and K is the ratio of the pseudo-first order decay rate constants of MHP to H_2O_2 (assumed constant at 1:14). If MHP is destroyed by too much catalase, then the difference between the signals of the two channels would overpredict the H_2O_2 concentration. Conversely, incomplete destruction of H_2O_2 would underpredict the final H_2O_2 value. The residual fraction of H_2O_2 was measured daily during the calibration routine and ranged from 3.5 - 7.5%, within the range recommended by Lazrus *et al.* (1985) and (Heikes, unpublished communication).

Lazrus *et al.* (1985) reported an error of 3.5% in the H_2O_2 measurement when MHP comprises 20% of the total peroxide. However, Heikes (1991) suggested there are larger errors associated with K and the assumed collection efficiency of MHP. Heikes also reported an increasing error with increasing S_c/S_p ratio, i.e. when a greater percentage of organic peroxide is present in the air sample. The sensitivity analysis showed 25% error in H_2O_2 concentration when $S_c/S_p = 0.5$ and $\alpha_0 = 0.05$, increasing exponentially when S_c/S_p exceeded 0.5. The peroxide concentrations obtained during the CAChE experiments frequently reached S_c/S_p ratios of 0.5 or more, usually during cloud events. Since the gas phase concentration dropped to the detection limit during cloud events due to high solubility, these measurements have large error already. Most samples collected under cloud-free conditions had S_c/S_p ratios of 0.3 or less and are therefore largely unaffected by the Heikes error analysis; however some cloud-free data had S_c/S_p ratios greater than 0.3 and would require large error bars according to the Heikes error analysis.

3.2.c Aqueous phase measurements of total peroxide

Aliquots from the cloud water collection described previously (Section 2.2.b) were measured for total peroxide when sample volume permitted. Cloudwater samples for CAChE 3 were size fractionated, whereas CAChE 2 samples were not. A total of 129 cloud water samples were collected: n = 56 for CAChE 2 and n = 73 for CAChE 3. Samples were collected in pre-cleaned 60 mL polyethylene bottles; 1 mL aliquots were transferred into disposable test tubes (KIMAX borosilicate glass, 125mm disposable culture tubes, VWR).

Working standards were prepared immediately prior to each analysis and encompassed the range of concentrations found in the cloud water samples (typically 25-2000ppb). Standards were prepared from deionized water that had trace (less than 1% of that found in typical cloud water samples) amounts of peroxide naturally present in it. Blanks were analyzed in order to quantify this effect and were subtracted from the standards' instrument response.

A derivatization reagent, consisting of pH-buffered 0.5 M KHP (reagent grade, Baker Chemical Co.), 26mM PHOPAA (Fairfield Chemical Co.) and 8 purpurogalin units of horseradish peroxidase (Sigma Chemical Co.), was used to derivatize the standards and cloud water samples (Kok *et al.*, 1986). Most samples were immediately derivatized and refrigerated following each hourly collection. Following the several hour cloud event, the set of derivatized samples was measured as a group; therefore some derivatized samples sat for many hours prior to analysis. An analysis of calibration standard decay and duplicate samples indicated that concentrations had decreased by less than 5% after 12 hours; similar results were found by Kelly *et al.* (1985). Detection was performed by a fluorescence spectrometer (Spectrovision, Model FD-100) using a continuous flow-through cell.

The measurement of peroxides in cloud water did not distinguish between organic peroxide and hydrogen peroxide, because both soluble organic peroxides and hydrogen peroxide were measured in the aliquot. However the Henry's Law coefficients for methylhydroperoxide and peroxyacetic acid are much lower than that of H_2O_2, so that significant scavenging of these species from air by cloud droplets is not likely (Lind and

Kok, 1986 and 1994). If present, hydroxymethyl hydroperoxide (HMHP) would be the only likely interferent. Therefore this technique may overestimate hydrogen peroxide concentration if HMHP is present. Claiborn and Aneja (1991) report that although organic peroxides made up a significant portion of the total gas-phase peroxides at Mt. Mitchell, NC, organic peroxides rarely exceeded 5% of the total peroxides in cloud water. It is likely, then, that the total peroxide signal is a reasonable surrogate for hydrogen peroxide. In any case, the organic peroxides will also oxidize SO_2, so the aqueous peroxide concentration represents the total capability to convert S(IV) to S(VI).

Calibration curves generated by this procedure were fit using a polynomial regression. Instrument response for the duration of CAChE 2 and CAChE 3 was very reproducible. As a result, calibrations for the entire experiment were combined to create a single calibration curve. Calibration results for the CAChE 3 experiment are shown in Figure 3.3.

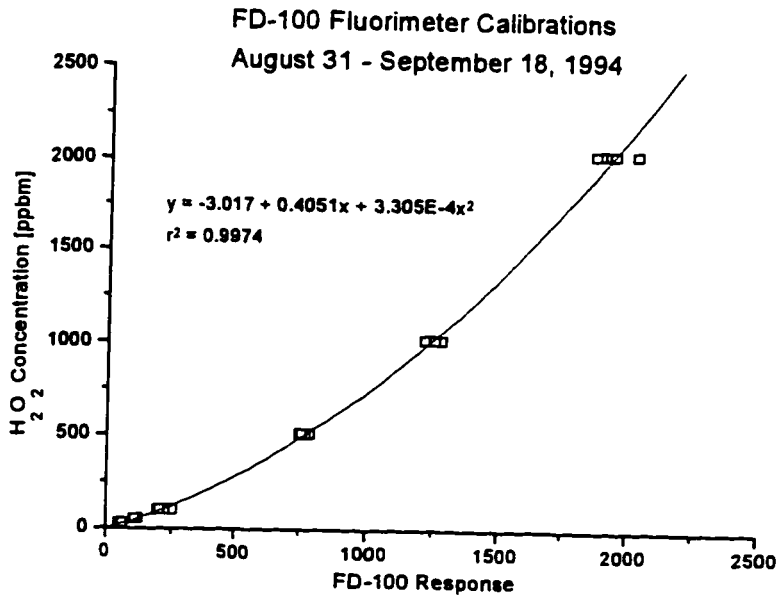

Figure 3.3: Combined calibrations for the CAChE 3 measurement period. Calibrations from six different days are shown.

3.3 RESULTS AND DISCUSSION

3.3.a Time series trends for gas phase peroxide during CAChE 2 and CAChE 3

The time series for CAChE 2 peroxide concentrations, H_2O_2 and methyl hydroperoxide (MHP), are given in Figures 3.4.a-d. The time series was very patchy due to persistent maintenance problems; in particular, one channel was continually plagued by the formation of a brown, gelatinous precipitate that plugged lines until they popped off. It is difficult to discern a clear trend in this data series, diurnal or otherwise, due to the lack of an unbroken trend. Even with a continuous a data record, it is unlikely that a consistent diurnal trend (e.g. Bales *et al.*, 1995) would be present due to the occurrence of multiple cloud events at the peak. Since peroxide is such a soluble species, recurring cloud cover would mask the non-cloud sinks postulated in a diurnal trend. However, a few features are evident.

First, MHP concentrations are sometimes comparable to H_2O_2 concentrations. This result is contrary to some findings that show H_2O_2 usually dominating the organic peroxide species (Barth *et al.*, 1989) but supportive of other studies that show a significant fraction of organic peroxides (Claiborn and Aneja, 1991). On rare occasions (e.g. April 20), the MHP concentration exceeds the H_2O_2 concentration. This time period was characterized by easterly winds and cloud-free conditions. Frequent cloud cover removes both organic and hydrogen peroxide concentrations leaving very low concentrations of peroxide behind. The low concentrations contribute to higher error in calculating the H_2O_2 and MHP concentrations, so that the concentration trends during extended cloud periods (as in the April 20 case) are subject to higher errors.

Second, peaks in H_2O_2 concentration were found on cloudless nights (see locations of "max" on Figures 3.4.a-d). Increases in H_2O_2 concentration frequently peaked near 00:00 (local time) on the nights of April 20-21, April 30-May 1, May 5-6, May 6-7, May 7-8, May 9-10, and May 13-14. With few exceptions, an increase in H_2O_2 concentration

at night was observed when cloud was not present. Claiborn and Aneja (1991) also report nocturnal maxima in both H_2O_2 and O_3 during two summer intensive sampling periods at Mt. Mitchell, NC and have provided a personal communication of nighttime maxima measured at Mauna Loa and Whitetop Mtn, VA. Claiborn and Aneja (1991) attribute this trend to meteorological, rather than chemical, phenomenon wherein the site was above the boundary layer at night allowing mixing to occur from higher-concentration air parcels aloft. Pedersen (1995) reports model results showing increased nighttime hydrogen peroxide production resulting from reactions of nitrate radicals on sulfuric-acid containing aerosols in the lower stratosphere. It is possible that either of these phenomenon could explain the nighttime increases observed at Cheeka Peak.

Third, there were several short-lived (<20 minutes) spikes of H_2O_2 concentration that occur consistently at 8-10 AM. Concentrations spikes occurred seven times during CAChE 2 (one is not shown in the time series due to a dead ROOH channel). All of the spikes occurred during continental influence (wind direction = 77 $\pm$ 11°) with the exception of one spike that occurred under southerly boundary layer influence (wind direction = 193°). The wind speeds were variable during these episodes (0.9 to 7.2 m/s) and likely had no effect. There was also no correlation with O_3 concentration. The spikes did not always occur on sunny mornings with continental air flow; spikes in concentration were not observed on five days with similar conditions. The 8-10AM time frame did not coincide with any routine in measurement. However it appears that these episodes were caused by some type of contamination, either due to some morning activity at CPO or from activities in Neah Bay or beyond. If the concentration spikes were due to an atmospheric process, one would expect to see the spikes consistently when the same atmospheric conditions occurred.

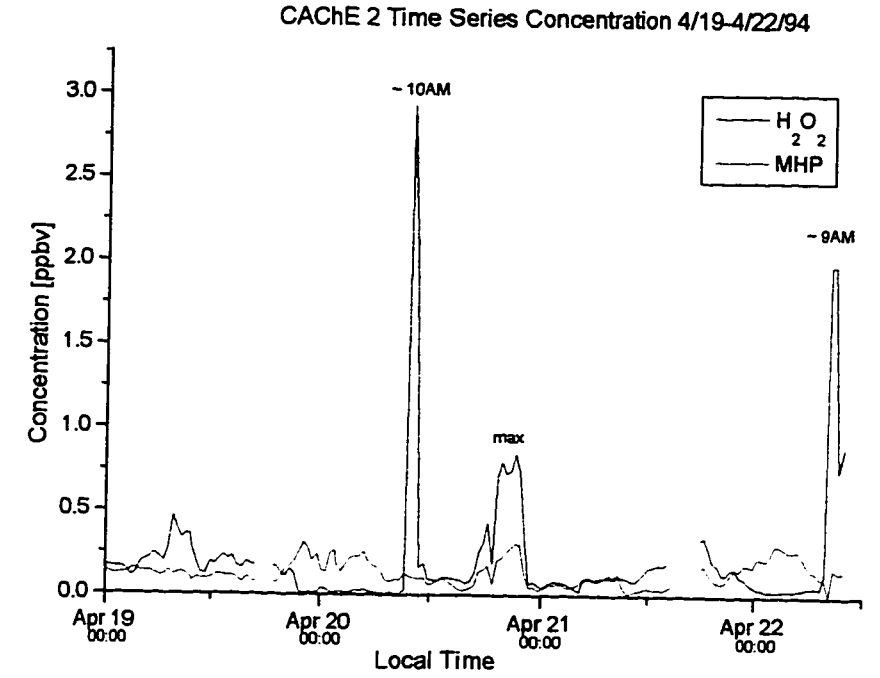

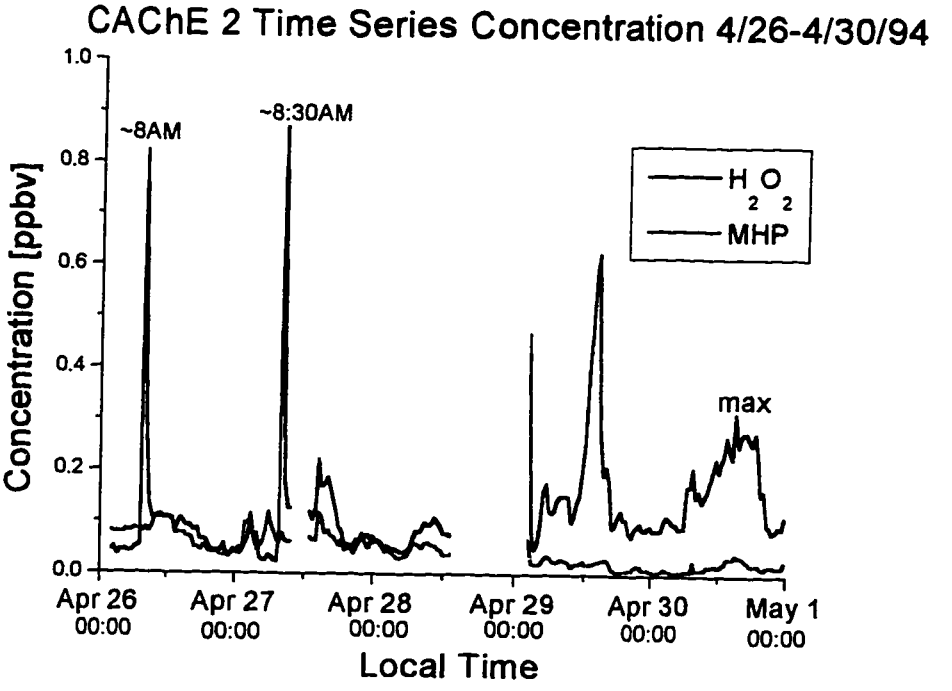

Figure 3.4.a-b: Time series concentrations for CAChE 2.

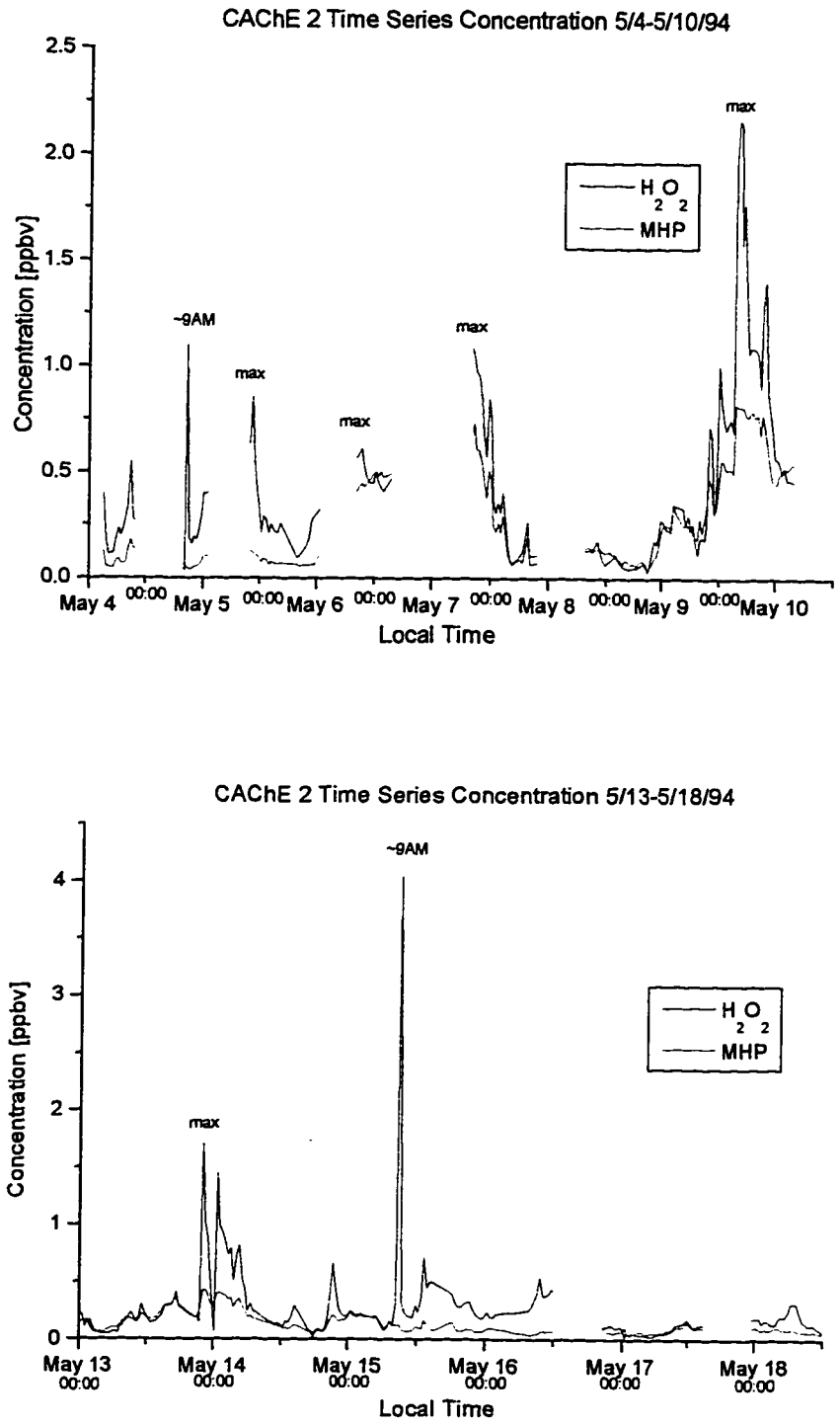

Figure 3.4.c-d: Time series concentrations for CAChE 2.

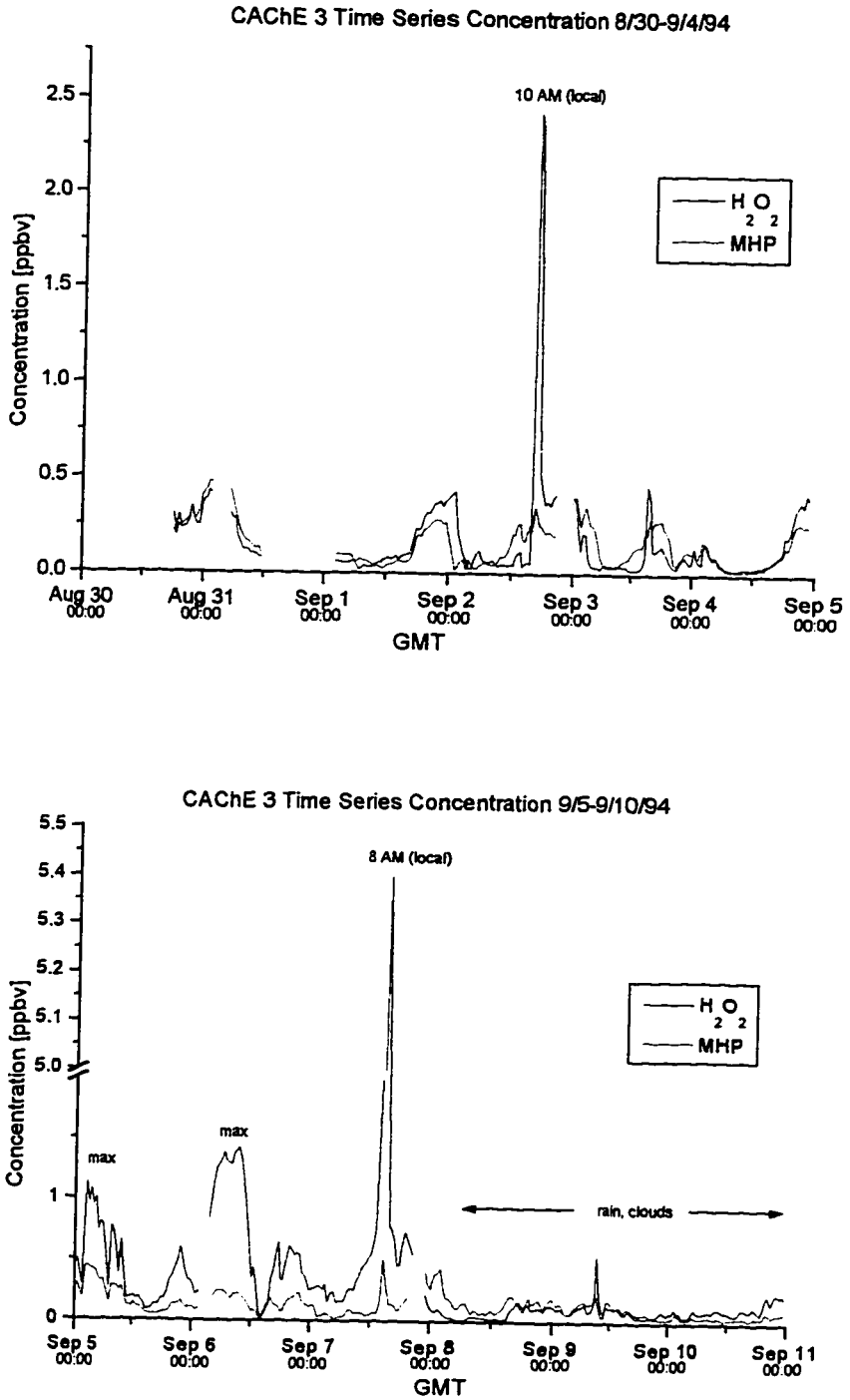

Figures 3.5.a-b: Time series concentrations for CAChE 3. Note: The time scale is presented in GMT (Greenwich Mean Time) for CAChE 3 whereas CAChE 2 data is presented in local time.

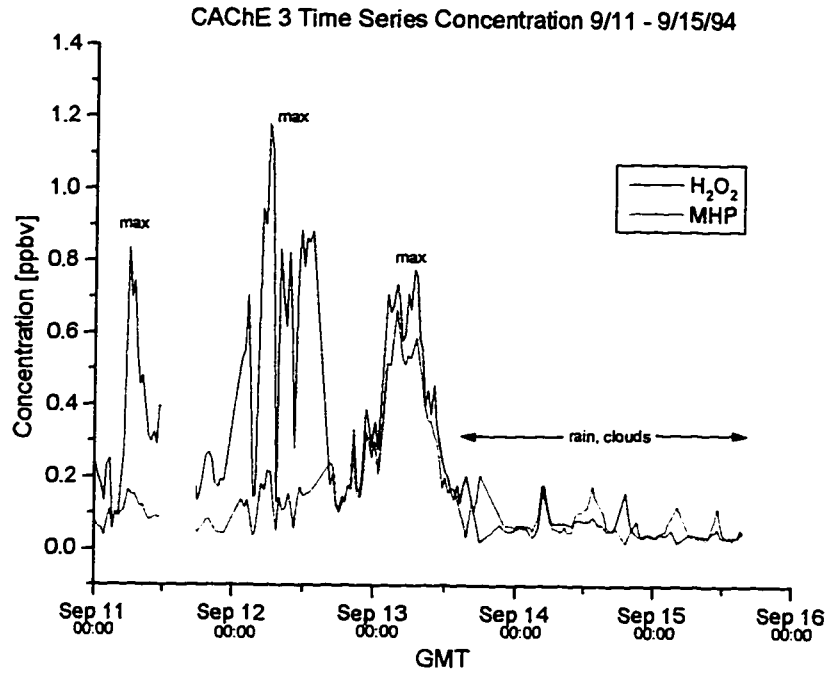

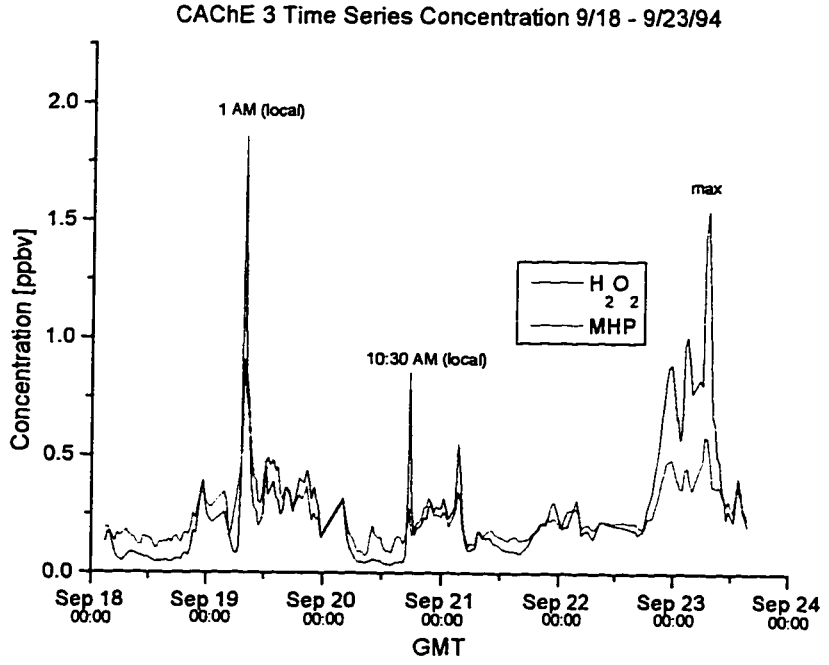

Figures 3.5.c-d: Time series concentrations for CAChE 3.

The time series for CAChE 3 peroxide concentrations, H_2O_2 and methyl hydroperoxide (MHP), are given in Figures 3.5.a-d. The data record is more continuous than CAChE 2. However, CAChE 3 also had more rain events so any diurnal variations would be masked by wet weather. Nighttime maxima in concentrations during cloud-free conditions were also observed during CAChE 3 on 9/5, 9/6, 9/11, 9/12, 9/13, and 9/23/94. The morning spikes that characterized the CAChE 2 data series were also present in the CAChE 3 data series, only not as prevalent; three episodes of short-lived concentration increases were observed (9/2, 9/7, and 9/20/94). However, a concentration spike also occurred at 1 AM on 9/19 that represents the only atypical episode of that type.

Previous field and modeling studies show that ambient HO_2 and OH concentrations are dependent on sunlight (Cantrell *et al.*, 1984), therefore suggesting a diurnal cycle in H_2O_2 if one considers production alone. Furthermore, the characteristic lifetime of H_2O_2 is on the order of 10 to 20 hours (Kleinman, 1986) and also suggests a measurable diurnal cycle. A diel pattern has been reported for peroxides in the equatorial Pacific (SAGA 3, Thompson *et al.*, 1993) and at Cape Grim (Ayers *et al.*, 1992). In the both cases, the maximum mixing ratio was 50% higher than the minimum mixing ratio and concentrations built throughout the day to reach a daily maximum around sunset.

A fourier analysis was employed on the CAChE data to detect any cyclical component that was not immediately obvious by visual inspection. A fourier analysis decomposes a cyclical series into a set of sine and cosine waves of different frequencies. In this case, the data were inspected for a postulated diurnal cycle. Data were selected to encompass times that had the fewest holes and experienced minimal cloud cover or rain. Two time periods during CAChE 3 satisfying these requirements were chosen: 9/4/94 17:35 - 9/9/94 02:15 GMT and 9/19/94 21:10 - 9/23/94 15:45 GMT. Because the discrete fourier transform requires data that is evenly spaced and without holes, the data were matched to the nearest five minute increment and holes were filled by using the average of the two nearest points. The 9/4-9/9 data set contained 1257 data points and 16% filled data, with the longest time gap of 3 hours and 55 minutes. The 9/19-9/23 data set contained 1376 data points and 24% filled data, with the longest time gap of 6 hours

and 40 minutes. A power spectral density diagram, showing the probability of repetition in different time intervals, indicated no diurnal or other periodicity.

3.3.b Average gas phase peroxide concentrations by sector for CAChE 2 and CAChE 3

Table 3.1 lists the average peroxide concentration at Cheeka Peak for non-cloudy conditions by sector and by sampling experiment. Three sectors are defined by wind direction: continental influence (*CBL*) 331-149°; southern boundary layer (*SBL*) 150-209°; and marine boundary layer (*MBL*) 210-330° (see Figure 2.9). The cloud-free criterion was established using fog visiometer data. The fog visiometer records data in a binary format, registering 1 if the visiometer detects cloud above a certain threshold cloud water content. In this case, the instrument threshold was set at 0.05 g H_2O/m^3 of air ($Fog_{0.05}$). The criteria for determining cloud-free air was when $Fog_{0.05} < 0.1$, meaning that fewer than 10% of the visiometer readings during the 5-minute average period exceeded 0.05 g/m^3. The spiked data described in section 3.3.a is likely not representative of ambient concentration and was not included in this tabulation.

Table 3.1 Average peroxide concentrations for cloud-free conditions by sector. All concentrations are in ppbv. N is the number of 5-minute samples included in that category. Median concentrations are listed in parentheses.

		CAChE 2			CAChE 3	
	N	H_2O_2	MHP	N	H_2O_2	MHP
Marine BL	888	0.28 ± 0.28 (0.18)	0.15 ± 0.16 (0.10)	973	0.35 ± 0.28 (0.29)	0.20 ± 0.14 (0.16)
Southern BL	324	0.32 ± 0.30 (0.23)	0.20 ± 0.19 (0.13)	524	0.23 ± 0.23 (0.12)	0.15 ± 0.09 (0.13)
Continental BL	794	0.38 ± 0.41 (0.23)	0.22 ± 0.21 (0.11)	1356	0.36 ± 0.34 (0.24)	0.21 ± 0.13 (0.19)

A total of 3582 5-minute average points were collected during CAChE 2, amounting to 299 hours of gas-phase peroxide data. Of that data, approximately 56% was collected during cloud-free conditions. During CAChE 3, 4819 5-minute average points were collected (402 hours), of which 60% was cloud-free. The maximum H_2O_2 concentration for each sector ranged from 1.292 ppbv (CAChE 3, SBL) to 2.819 ppbv (CAChE 3, MBL) to 3.561 ppbv (CAChE 2, CBL) whereas the minimum concentration for all sectors was below detection limit. The continentally influenced samples experienced higher concentrations, likely due to increased UV intensity from a lack of high-level cirrus clouds that accompanied easterly flow. Increased UV intensity may also explain the slight increase in MBL concentrations from the early spring samples of CAChE 2 to the late summer samples of CAChE 3. These concentrations are somewhat lower than that observed at other mountaintop sites. Claiborn and Aneja (1991) measured a mean concentration of 0.76 ppbv in summer of 1998 at Mt. Mitchell, NC whereas Olszyna *et al.* (1988) measured a mean concentration of 0.8 ppbv in the summer of 1986 at Whitetop Mtn., VA. The concentrations measured at Cheeka Peak are more comparable to autumn concentrations measured at these two sites (0.20 ppbv, Mt. Mitchell; 0.15 ppbv Whitetop Mtn.). The concentrations at Cheeka Peak are also lower than those measured in the equatorial Pacific (mean H_2O_2 = 600 pptv, ROOH = 650 pptv, Thompson *et al.*, 1993).

3.3.c Correlation of H_2O_2 with O_3 in the gas phase

The correlation between H_2O_2 and O_3 in cloud-free air was examined for the marine boundary layer case during CAChE 2 and CAChE 3. Marine boundary layer air masses were chosen for simplicity because air masses from other trajectories are complicated by continental influence. Samples with concentrations greater than 1 ppbv H_2O_2 were considered outliers and excluded because these unusually high samples were occurred during spike events and did not experience similar peaks in O_3. As in Section 3.3.b, conditions were considered cloud-free when fewer than 10% of the visiometer readings during the 5-minute average period exceeded 0.05 g/m^3.

The visiometer and trajectory criteria yielded a data set with n = 850 for CAChE 2 and n = 939 for CAChE 3. To more easily determine any trend present, the data were

grouped into "bins" that were 1 ppbv wide in ozone concentration. Figure 3.6 and 3.7 represent the results from this data treatment. Prior to bin averaging, the correlation coefficients, r, for the CAChE 2 and CAChE 3 data sets were 0.2470 and 0.1864, respectively. Following bin averaging, r = 0.8326 and 0.7783 for CAChE 2 and CAChE 3, respectively. A large change in r occurred because bin averaging serves to significantly reduce the noise in large data sets by removing extraneous points that otherwise mask a correlation. The significant correlation between these two species during CAChE 2 and CAChE 3 data indicates that conditions favorable for the production of the two species are similar. Measurement of UV radiation (200-320 nm) may have clarified this correlation, however the measurement was not available.

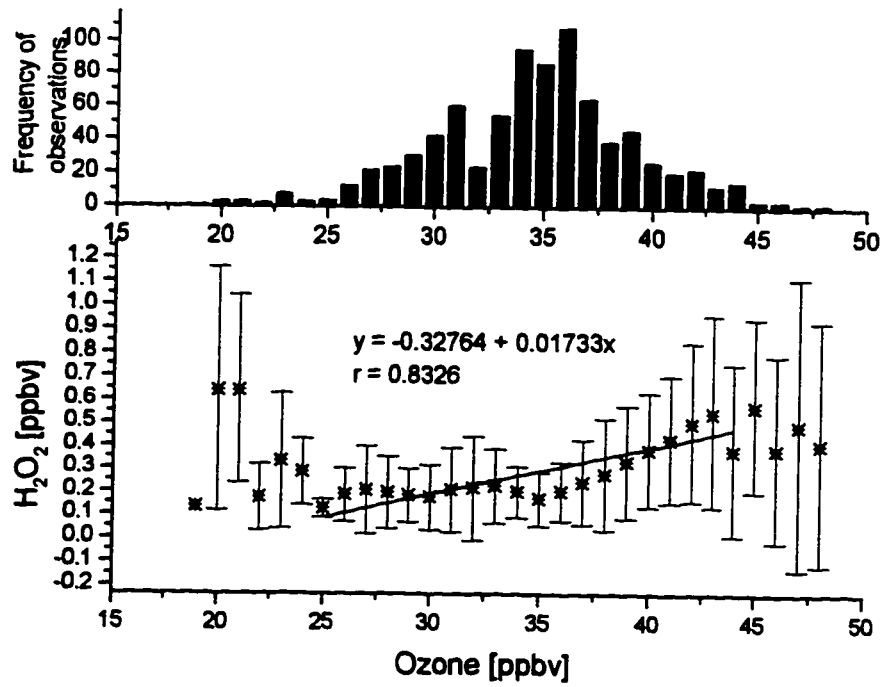

Figure 3.6. H_2O_2 vs. ozone for samples collected in the marine boundary layer during cloud-free conditions ($Fog_{0.05} < 0.1$) for CAChE 2. The error bars represent the standard deviation in H_2O_2 concentration for that bin.

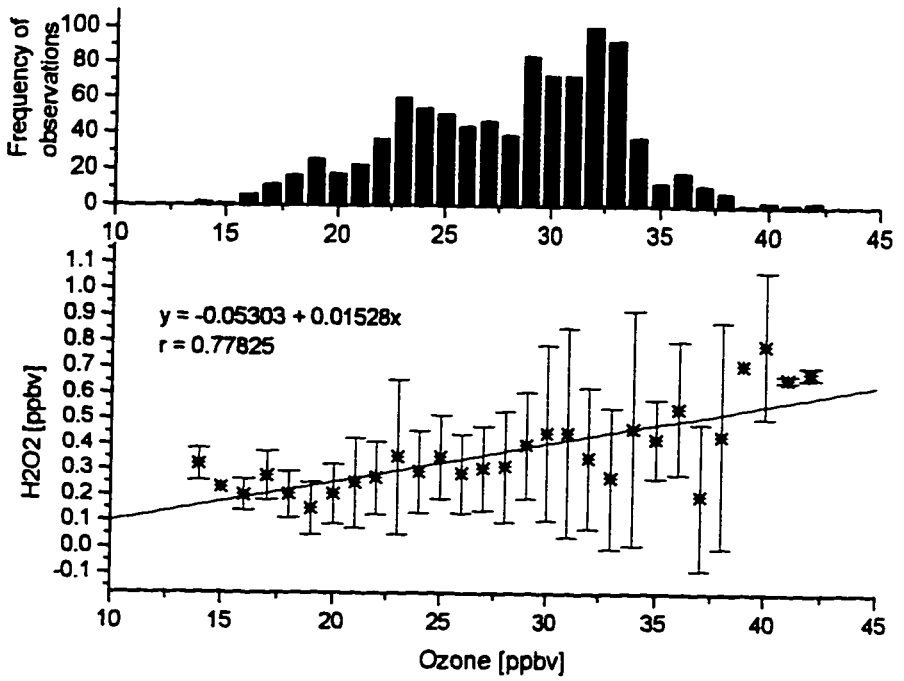

Figure 3.7. H_2O_2 vs. ozone for samples collected in the marine boundary layer during cloud-free conditions ($Fog_{0.05} < 0.1$) for CAChE 3. The error bars represent the standard deviation in H_2O_2 concentration for that bin.

The relationship between H_2O_2 and O_3 is a varied one. A positive correlation between H_2O_2 and O_3 has been previously observed (Whitetop Mtn, VA; Olszyna *et al.*, 1988). However, Ayers et al. (1992) observed the opposite trend, i.e. O_3 decreased when H_2O_2 increased, at Cape Grim. The difference between these two results can likely be ascribed to hemispheric differences in NO_x concentrations. In the Southern Hemisphere, NO_x concentrations are very low because anthropogenic sources found in the Northern Hemisphere are lacking. In a low NO_x regime, photochemical destruction of O_3

$$O_3 + h\nu(\lambda < 320nm) \rightarrow O_2 + O(^1D) \xrightarrow{H_2O} 2OH^{\cdot} \qquad (22)$$

exceeds photochemical O_3 production

$$NO + HO_2 \rightarrow OH + NO_2$$

$$NO_2 + h\nu \rightarrow NO + O$$
$$O + O_2 \rightarrow O_3 \qquad (23)$$

because NO_x (and hydrocarbons) concentrations are too low (Thompson *et al.*, 1993 and references therein). However, odd hydrogen radicals (OH and HO_2) continue to be produced that, in turn, form peroxides. In this regime, the O_3 source is probably replenished primarily from stratospheric injection. In the Northern Hemisphere, even at a relatively remote site like Cheeka Peak, the NO_x concentrations are sufficient (~100 pptv during marine on-shore flow, Dan Jaffe, personal communication) for O_3 production to exceed O_3 destruction. Thus, at the Cape Grim site, stratospheric injection controls the O_3 concentration and the regime is O_3 destroying, causing a negative correlation with H_2O_2. In contrast, a positive correlation is observed at Cheeka Peak because sufficient NO_x concentration is present to cause photochemical production of both H_2O_2 and O_3.

3.3.d Henry's Law behavior of H_2O_2

An attempt was made to compare observed gas phase H_2O_2 concentrations during cloud events to concentrations calculated based on the loss of H_2O_2 to the aqueous phase as described by Henry's Law. Calculations are taken from Seinfeld (1986) and assume that the peroxide is in a closed system so that the total quantity of H_2O_2 is fixed. This assumption generally holds because clouds at Cheeka Peak typically form when a parcel of air is adiabatically lifted, causing cloud droplets to form. Gas phase H_2O_2 from within the parcel adsorbs into the droplets increasing the aqueous phase concentration, while gas phase concentrations decrease with time as H_2O_2 is depleted from the gas phase. From Seinfeld (1986), the total pre-cloud H_2O_2 distributed between the gas and aqueous phases in cloud is given by:

$$[H_2O_2]_{total} = \frac{p_{H_2O_2}}{RT} + [H_2O_2(aq)]L \qquad (24)$$

where p_{H2O2} is the interstitial gas phase partial pressure, $[H_2O_2(aq)]$ is the aqueous phase concentration, L is the liquid water content expressed as a dimensionless volume fraction and R is the gas constant (L atm mol^{-1} K^{-1}). The fraction of the total quantity of H_2O_2 that is in the gas phase is given by:

$$\frac{[H_2O_2]_{gas}}{[H_2O_2]_{total}} = \frac{\frac{p_{H_2O_2}}{RT}}{\frac{p_{H_2O_2}}{RT} + [H_2O_2(aq)]L} \tag{25}$$

If Henry's Law is assumed to hold, then the expression $H_{H2O2}\, p_{H2O2}$ can be substituted for $[H_2O_2\ (aq)]$, yielding the expression:

$$[H_2O_2]_{gas} = [H_2O_2]_{tot} \times \frac{1/RT}{1/RT + H_{H_2O_2}L} \tag{26}$$

The comparison between calculated and observed H_2O_2 concentrations are given for two CAChE 3 cases in Figures 3.8 and 3.9. The average gas phase H_2O_2 concentration one-hour prior to cloud onset was used for $[H_2O_2]_{tot}$. The choice of $[H_2O_2]_{tot}$ is critical in these calculations and assumes that variation in H_2O_2 concentration before cloud onset is small. Variation in calculated H_2O_2 concentration is derived from a changing cloud liquid water content because H_{H2O2} and $[H_2O_2]_{tot}$ are fixed. Cloud liquid water content was measured using a forward scattering spectrometer (PMS FSSP-100; see section 2.2b) mounted on a 10-m tower.

Examination of both figures indicates that Henry's Law is not closely followed, or more likely, that the application of Henry's Law is not suitable for this type of measurement. The predicted H_2O_2 concentration exceeds the observed concentration for

Event 12, whereas this relationship is reversed for Event 14. The initial $[H_2O_2]_{tot}$ chosen can move the "predicted" line up or down and so this measurement appears to be fairly arbitrary. Although a one-hour average of H_2O_2 concentration seems reasonable, concentrations can fluctuate by 20% or more during that hour. The $[H_2O_2]_{tot}$ used for Event 12 was calculated for a time period 2 ½ hours prior to cloud start because closer data was not available.

It is interesting to note that the difference in meteorological conditions for the two cases may explain why Event 14 has better predicted/observed agreement. The wind speed for Event 14 was ~4 m/s (versus >10 m/s for Event 12). The slower wind speed translates into a longer transit time from the coast to the peak, meaning that the air parcel had a greater time to reach equilibrium. The mean droplet size for Event 14 was also smaller (14.4 μm vs. 18.6 μm), also allowing for a faster attainment of equilibrium.

Noone *et al.* (1991) and Macdonald *et al.* (1995) performed similar analyses for clouds sampled from a ground station at Mt. Areskutan, Sweden and from aircraft over central Canada, respectively. Noone *et al.* (1991) measured an average partitioning ratio (measured cloud water concentration divided by calculated cloud water concentration) of 0.87 ± 0.28 using a CVI (counterflow virtual impactor). They concluded that Henry's Law equilibrium was followed for their case study. The use of the CVI was suitable for this type of measurement because it provided rapid, in-situ, size-resolved measurements. Macdonald *et al.* (1995) found fair agreement between measured and calculated concentrations for warm clouds, but found that supercooled clouds differed significantly from equilibrium. Their observation of general agreement with Henry's Law equilibrium was likely due to the ability to accurately measure the pre-cloud H_2O_2 prior to the aircraft's entrance to the cloud. The assumptions of a closed system and accurately measured pre-cloud H_2O_2 hold more for a cloud sampled from an aircraft than from a station on the ground.

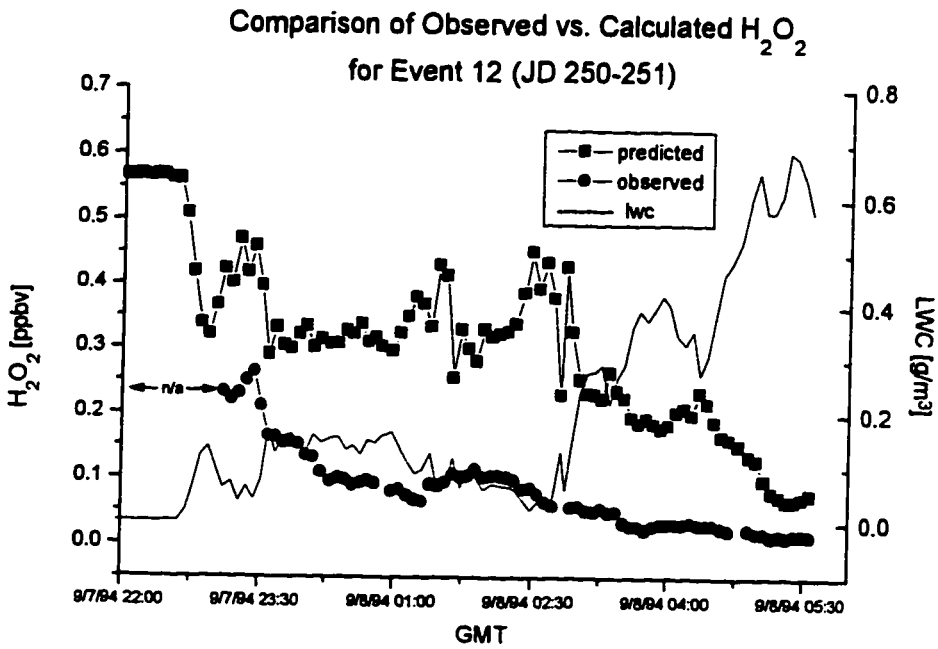

Figure 3.8. Comparison of concentrations predicted by Henry's Law for Event 12.

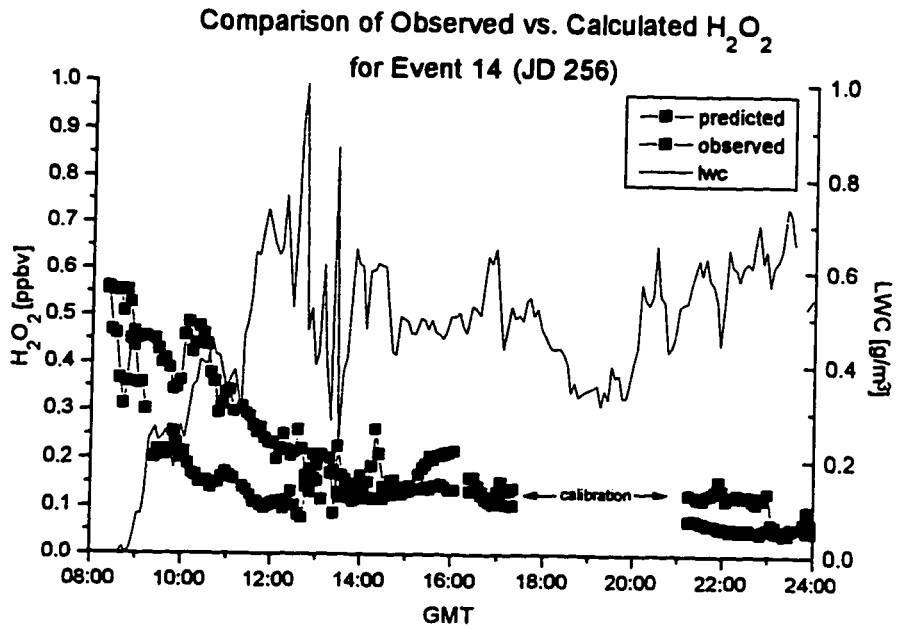

Figure 3.9. Comparison of concentrations predicted by Henry's Law for Event 14.

3.3.e Cloudwater total peroxide

The cloudwater data for CAChE 2 and CAChE 3 are summarized in Table 3.2 and Figure 3.10. Cloudwater samples were differentiated into two size fractions during CAChE 3; the impaction d_{50}'s (droplet diameter collected with a 50% efficiency) for the two collected fractions were 12 μm and 5 μm. However CAChE 2 samples were not fractionated by size; all drops greater that 5 μm were collected. For this reason, Table 3.2 represents summary data for the d_{50}(5 μm) cloudwater samples only. Appendix C contains all of the cloudwater sample concentrations for both sampling campaigns.

Concentrations from only non-precipitating clouds were used in Table 3.2. However, excluding samples from precipitating clouds had a negligible effect on the overall average and other values. For CAChE 2, five samples were removed from the total and the average changed from 32.06 to 32.38 mM. For CAChE 3, six samples were removed from the total and average changed from 34.71 to 37.69 μM. The minimum and maximum values were unchanged in both cases.

Table 3.3 lists concentrations obtained at other sites, typically in the eastern U.S. Many researchers have observed highest concentrations of H_2O_2 in the summer, which is consistent with the formation of H_2O_2 by secondary photochemical processes involving free radicals (Kleinman, 1986). However, there is no apparent difference in concentration from the late spring (April - May 1994) CAChE 2 concentrations and late summer (August - September 1994) CAChE 3 concentrations, probably because the solar angles are about the same for the two time periods. In general, the H_2O_2 concentrations found at Cheeka Peak are comparable to other sites and may be slightly lower than the other summertime concentrations measured. CAChE cloudwater samples were also always well above detection limit, in contrast to observations at other sites. Daum *et al.* (1984), Kelly *et al.* (1985) and Heikes *et al.* (1987) conclude that cloudwater H_2O_2 and SO_2 rarely coexist in measurable concentrations, because the species in excess will fully consume the other. Although continuous gas phase SO_2 measurements were not made, the measured cloudwater concentrations of H_2O_2 indicate that SO_2 was likely never in excess during the CAChE experiments.

Table 3.2 Summary of values for cloudwater peroxide levels from non-precipitating clouds collected at Cheeka Peak, WA .

Sampling Period	N	Mean [μm/L]	Standard Deviation	Median	Minimum	Maximum
CAChE 2	51	32.38	12.56	31.39	8.37	72.48
CAChE 3	23	37.69	27.10	30.47	3.76	92.70

Table 3.3 Examples of hydrogen peroxide measurements at other locations

LOCATION	SEASON	RANGE [μM]	AVG CONC'N [μM]	REFERENCE
Ontario, Canada[a]	Aug 1988 Mar-Apr 1990	1.5 - 60 most < 5	29	Macdonald *et al.* (1995)
Mt. Mitchell, NC[g]	May-Jun 1988 Jul-Aug 1988 Sept 1988	0.2 - 219.1 3.2 -219.1 1.9 - 54.6	54.2 46.9 16.8	Claiborn and Aneja (1991)
Carolina coast[a]	Jan-Mar 1986	0.3 - 112		Barth *et al.*, (1989)
Whitetop Mtn, Va[g]	Apr-May 1986 Jul-Aug 1986 Oct 1986	<0.04 - 62.8 2.4 -247 0.3 - 130	7.6 57.3 15.2	Olszyna *et al.* (1988)
several nonurban sites in NE US[a]	Sept 1982 - Aug 1983	<0.1 - 71		Kelly *et al.*, (1985)

[a]aircraft measurement
[g]ground-based measurement

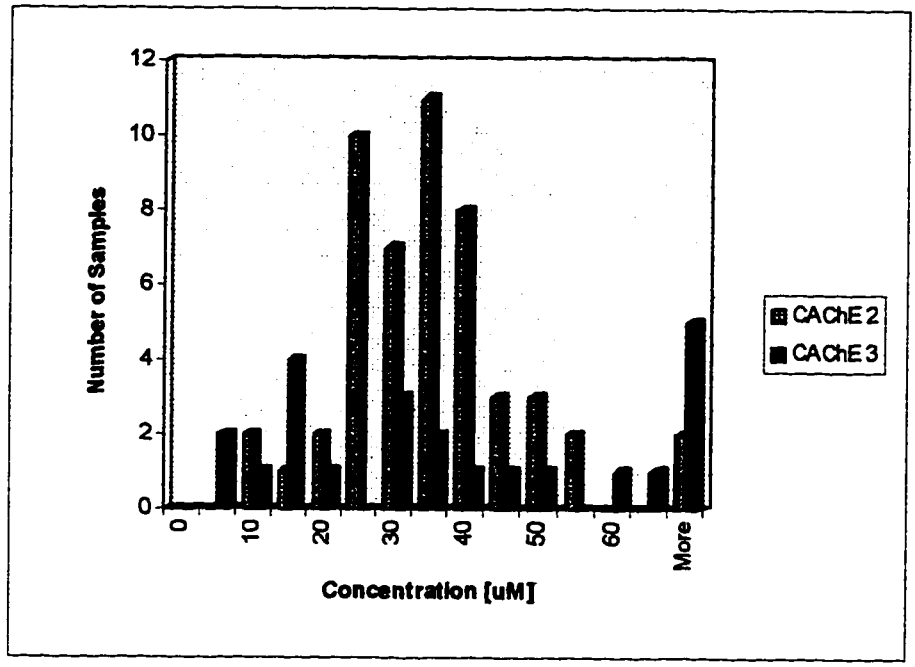

Figure 3.10. Frequency distribution for CAChE 2 and CAChE 3 cloudwater concentrations.

Eighteen paired samples from CAChE 3 non-precipitating clouds were also examined for size dependence using a paired sample t-test at the α=0.05 confidence level (previously described in Section 2.3.d). The t-test yielded the result P(T<3.050) = 0.0036 for the null hypothesis that the means are the same. The quantity P(T< t) represents the probability that the difference in concentration is due to randomness; therefore the small P-value indicates that the difference in means is statistically significant at greater than the 95% (α=0.05) level. The means for the d_{50}=5μm and d_{50}=12μm size fractions were 32.79 μM and 28.09 μM, respectively. It is likely that the difference in collection would be even larger if droplets 5-12 μm in diameter were compared to drops greater than 12 μm, however the collection method prevents this comparison.

If the concentration of H_2O_2 in cloudwater were dictated by diffusion, i.e. the transport of the gas to the surface of the droplet, then one would expect higher concentrations in smaller drops because the surface area-to-volume ratio is higher. Other gaseous species, like SO_2, would also be more concentrated in the smaller drops. If the concentration of SO_2 were comparable to H_2O_2, oxidation would occur thereby

consuming the H_2O_2 and masking any preferential scavenging of H_2O_2 in the smaller drops. However, if the concentration of SO_2 was low and $[H_2O_2]$ was much greater than $[SO_2]$, one would expect to observe a difference in concentration between small drops and large drops. Sulfur dioxide was measured for three size-differentiated events (Event 9, $[SO_2]$=205 pptv, $[H_2O_2]$ = 226 pptv; Event 11, $[SO_2]$=15 pptv, $[H_2O_2]$ = 493 pptv; and Event 14, $[SO_2]$=31 pptv, $[H_2O_2]$ = 467 pptv) during CAChE 3. Referring to Appendix C, the difference in drop size H_2O_2 concentration is smallest for Event 9 (highest SO_2 interstitial concentration) and highest for Event 11 (lowest SO_2 interstitial concentration) supporting the above hypothesis.

3.3.f Principal components analysis of cloud water chemistry

A principal components analysis was performed to investigate the relationships between the many variables measured in the CAChE 2 and CAChE 3 data sets. Principal components analysis is a statistical technique used to identify a relatively small number of factors (or components) that are linear combinations of the observed variables (Norusis, 1994). The objective is to describe the data using fewer factors than original variables and thereby removing redundancy in the data set. The analysis matrices consisted of sample concentrations and other meteorological variables collected only during cloud events. The CAChE 2 data matrix consisted of 16 variables by 42 cases whereas the CAChE 3 data matrix consisted of 17 variables by 28 cases (see Appendix D); net radiation was not available during CAChE 2. Analysis was performed using the *FACTOR* routine and varimax rotation in Systat (Version 5.01, ©1992, Systat, Inc.). Varimax rotation is an orthogonal axes rotation that serves to simplify the factor matrix so that each factor has fewer non-zero variable loadings than in the unrotated matrix.

To reduce the effect of changing cloud liquid water content, all cloudwater concentrations were converted to gas phase equivalent concentrations. The gas phase equivalent concentration (the concentration that results from transforming the measured aqueous phase into the gaseous state) was calculated by multiplying the cloudwater ion concentration by the cloud liquid water content. The H_2O_2 gas phase equivalent concentration is the concentration that results from transforming the aqueous phase

concentration to the gaseous state and summing it to the H_2O_2 calculated to be present in the gas phase, assuming Henry's Law equilibrium (Kelly *et al.*, 1985):

$$p = [H_2O_2](LRT + H_L^{-1}) \tag{27}$$

where $[H_2O_2]$ is the molar concentration of peroxide in the aqueous phase, L is the liquid water content, R is the universal gas constant, and H_L is the Henry's Law constant for peroxide.

The percent variance captured by the first four principal components (PC's) for the CAChE 2 and 3 data sets are given in Table 3.4. Most of the variance in the two data sets are captured in the first two PC's; the third and fourth PC's describe at best 11.5% of the variance. Although a thorough, propagated error analysis was not performed, it is not uncommon for an environmental data set to have errors that exceed 10%. It is therefore likely that the third and fourth PC are approaching the noise of the data.

Table 3.4 Percent of total variance explained for the first four rotated principal components for CAChE 2 and CAChE 3.

	PC 1	PC 2	PC 3	PC 4
CAChE 2	32.7%	29.1%	10.0%	9.0%
CAChE 3	40.8%	19.9%	11.5%	11.0%

The degree of contribution (loading) of the variables to each PC is given in Tables 3.5 and 3.6. The component loadings are covariances of the original variables with the components. Variables with loading close to zero make little contribution to the PC. There appears to be an overall lack in variability between cases for the CAChE 3 data set, as even the rotated loadings have high values in both PC 1 and PC 2. This is probably

also due to the small number of cases for the CAChE 3 data set. For this reason, the majority of the discussion will focus on the larger CAChE 2 data set.

For both CAChE experiments, seasalt dominates PC 1 and accounts for the largest amount of variance in the data. This effect is more clearly seen in the CAChE 2 data. Hydrogen peroxide is very negatively correlated with seasalt in the CAChE3 data (-0.470) set and moderately so in the CAChE 2 data set (-0.198). This is reasonable if one considers that basic sea salt particles are more likely to absorb acidic SO_2, which in turn reacts with the H_2O_2, resulting in peroxide concentration that is low when seasalt concentration is high even though S(IV)-H_2O_2 kinetics are not as favorable at higher pH's.

The CAChE 2 NO_3^+, nss-$SO_4^=$ and H^+ load very heavily in PC2, suggesting a pollution effect. The number of droplets (Nd) is also positively correlated to the pollution tracers because polluted air tends to have more activatable drops. Droplet number and volume mean diameter are inversely correlated here because with more drops, there are fewer ways to distribute the available water vapor and so the drops sizes are smaller. Hydrogen peroxide is positively correlated with nss-$SO_4^=$ probably because it is an S(IV) oxidant; however it's descriptive power is diluted because it is equally weighted in the fourth PC. Wind direction is also weighted in this PC, but it is also loaded in the other PC's and likely has little descriptive power.

The third principal component in the CAChE 2 data set is close to the level of the error present in this data set, and lacks concrete information to attribute any chemical basis for the component. Radon is heavily loaded in this PC (-0.777). Radon is a tracer for continental input and therefore an air mass with high radon may have less water vapor than an air mass originating from the ocean. If this were a strong effect, one would expect an inverse correlation in H_2O_2 because less water vapor typically means less peroxide is produced. However, this effect is not present, as the H_2O_2 loading is nearly zero (0.074). The fourth PC is also hard to interpret and likely in the level of the noise.

Table 3.5 CAChE 2 rotated loadings

Variable	PC 1	PC 2	PC 3	PC 4
Na	0.995	0.060	0.002	-0.036
Mg	0.994	0.079	0.004	-0.031
Cl	0.993	0.044	0.032	-0.021
K	0.986	0.044	-0.008	0.010
Ca	0.977	0.094	0.085	0.031
H	0.020	0.946	0.057	0.072
NO_3^-	0.112	0.938	0.132	0.004
nss-$SO_4^=$	-0.059	0.910	0.146	0.027
Nd	0.077	0.874	-0.393	0.024
VMD	-0.193	-0.741	0.223	-0.163
H_2O_2	-0.198	0.519	0.074	0.542
wind dir	-0.255	-0.503	-0.247	0.556
Radon	0.120	-0.111	-0.777	-0.271
O_3	0.330	-0.071	0.698	-0.078
NH_4^+	0.107	0.113	0.156	0.778
CPC1	0.207	0.394	-0.395	0.335

Table 3.6 CAChE 3 rotated loadings

	PC 1	PC 2	PC 3	PC 4
Na	0.973	0.146	-0.028	0.030
Mg	0.972	0.102	-0.055	0.053
Cl	0.971	0.123	-0.035	0.027
Ca	0.971	0.151	0.036	0.017
K	0.966	0.191	0.032	0.018
Nd	0.678	0.617	0.111	-0.002
NH_4^+	0.639	0.319	0.149	0.143
CPC1	0.600	0.544	0.073	-0.054
nss-$SO_4^=$	0.526	0.708	0.227	-0.011
NO_3^-	0.366	0.903	-0.061	0.086
H	0.172	0.836	-0.142	0.416
wind dir	-0.176	0.540	0.435	0.079
O_3	0.100	0.044	-0.910	0.125
net rad	0.239	0.096	0.892	0.072
radon	-0.028	-0.070	-0.069	-0.909
H_2O_2	-0.470	0.417	-0.087	0.637
VMD	-0.495	-0.056	0.113	-0.628

3.3.g Comparison of aqueous phase peroxide and formic/acetic acid concentrations

The aqueous phase reaction between hydrogen peroxide and organic species such as HCHO was discussed in Section 3.1d. This reaction is of interest because it can contribute to the acidity in rain and cloud droplets. Cloud water formate and peroxide were measured concurrently during only one cloud event in CAChE 3. The correlation between these two species is shown in Figure 3.11. Although there appears to be some correlation between the two species at lower concentrations, the $HCOO^-$ average blank level was quite high (~13 μM) and thus these samples are highly suspect as they exceeded the blank by less than 3 times. The three samples that did exceed the blank by several times (V43, V49, and V57) do not show any particular trend. These results lend support for earlier findings (e.g. Talbot *et al.*, 1995) that H_2O_2 plays no role in carboxylic acid production.

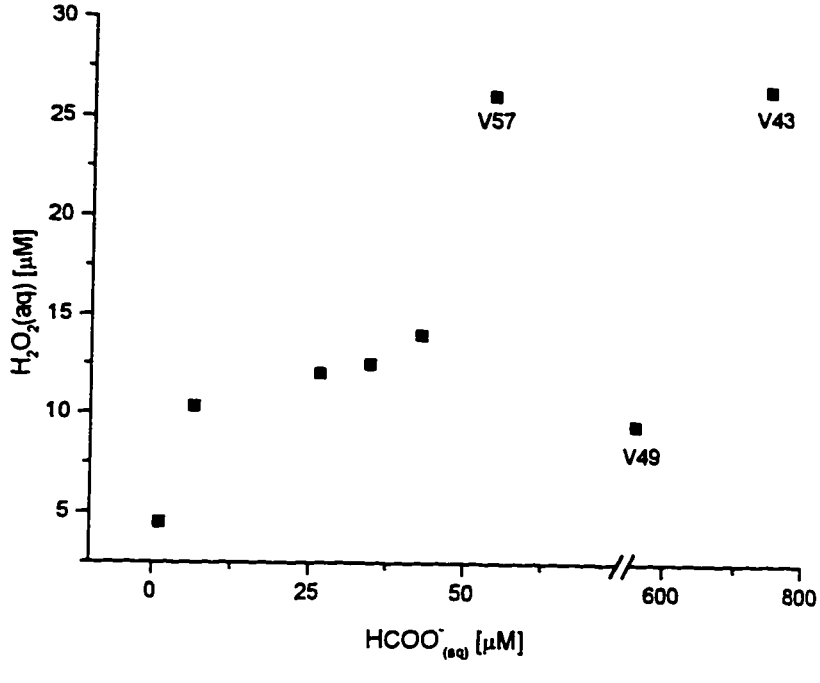

Figure 3.11 Cloud water formate concentration vs. cloud water peroxide concentration for Event 9 (JD 243), d_{50}(5 μm) samples only.

3.3.h Evidence for sulfate production in clouds

The sulfate measured in cloudwater is due to one of two processes: incorporation of particulate sulfate via nucleation scavenging and/or absorption of interstitial gas-phase SO_2 that is subsequently oxidized to $SO_4^=$. The data collected during the CAChE experiments cannot explicitly distinguish between sulfate that is scavenging or produced in-cloud. In addition, H_2O_2 is always in excess relative to SO_2 and so detection of sulfate production using H_2O_2 data is difficult because increasing $SO_4^=$ depends on the limiting species; a continuous gas phase SO_2 measurement would have been a better indicator but was not available. However, an attempt was made to qualitatively determine if the measured variables had some explanatory value. Pre-cloud nonseasalt (nss) $SO_4^=$, cloudwater nss-$SO_4^=$ and the decrease in H_2O_2 in both the gas and aqueous phase were examined for consistency in explaining the change in nss-$SO_4^=$. The number of cases was constrained by available pre-cloud nss-$SO_4^=$ data (obtained from Tad Anderson; data represent continuous, sector-controlled daily filter collection). Therefore, only two cloud events from CAChE 2 (events 8 and 11) and one cloud event from CAChE 3 are analyzed (event 16). Table 3.7 contains a comparison of the H_2O_2 and nss-$SO_4^=$ gas phase equivalent concentrations (as described in Section 3.3f) measured in these three events.

For all three cases, the cloudwater nss-$SO_4^=$ exceeds the pre-cloud nss-$SO_4^=$. However, Kelly *et al.* (1989) considers a simple increase in nss-$SO_4^=$ concentration only as the weakest indication of in-cloud oxidation of SO_2. To attribute in-cloud oxidation to a particular reaction, one would need to demonstrate simultaneous and stoichmetrically decrease in oxidant concentration (e.g. H_2O_2) and decrease in reactant concentration (SO_2) and increase in product concentration (nss-$SO_4^=$). Following an analysis similar to that by Daum *et al.* (1984), evidence for peroxide-S(IV) reaction is examined by plotting the two molar quantities of oxidant and product versus one another (see Figures 3.12 a-c).

Table 3.7. Comparison of changing H_2O_2 and nss-$SO_4^=$ concentrations during three CAChE cloud events.

Sample	Liquid Water Content [g/m^3]	Equivalent gas phase nss-$SO_4^=$ [μmol/m^3]	Equivalent gas phase H_2O_2 [μmol/m^3]	pH	Ozone [ppbv]
CAChE 2 - Event 8	pre-cloud nss-$SO_4^=$ = 0.96 μg/m^3 or 0.010 μmol/m^3				
M10	0.210	0.0254	0.0210	3.71	35.1
M12	0.282	0.0303	0.0171	3.70	36.1
M14	0.313	0.0272	0.0150	3.78	36.1
M16	0.357	0.0174	0.0146	4.00	34.5
M18	0.315	0.0142	0.0136	4.01	35.2
M20	0.239	0.0127	0.0119	3.85	26.3
CAChE 2 - Event 11	pre-cloud nss-$SO_4^=$ = 0.81 μg/m^3 or 0.0084 μmol/m^3				
M76	0.119	0.0126	0.0116	3.85	34.4
M80	0.196	0.0092	0.0108	4.15	34.6
M82	0.249	0.0051	0.0111	4.30	33.0
M84	0.260	0.0076	0.0125	4.35	33.1
M86	0.216	0.0083	0.0143	4.27	31.8
M88	0.201	0.0090	0.0122	4.16	32.5
CAChE 3 - Event 16	pre-cloud nss-$SO_4^=$ = 0.85 μg/m^3 or 0.00885 μmol/m^3				
Y04	0.380	0.0125	0.0156	4.12	18.6
Y06	0.324	0.0081	0.0189	4.27	18.9
Y08	0.428	0.0171	0.0145	4.00	19.4
Y10	0.474	0.0177	0.0130	4.07	18.1

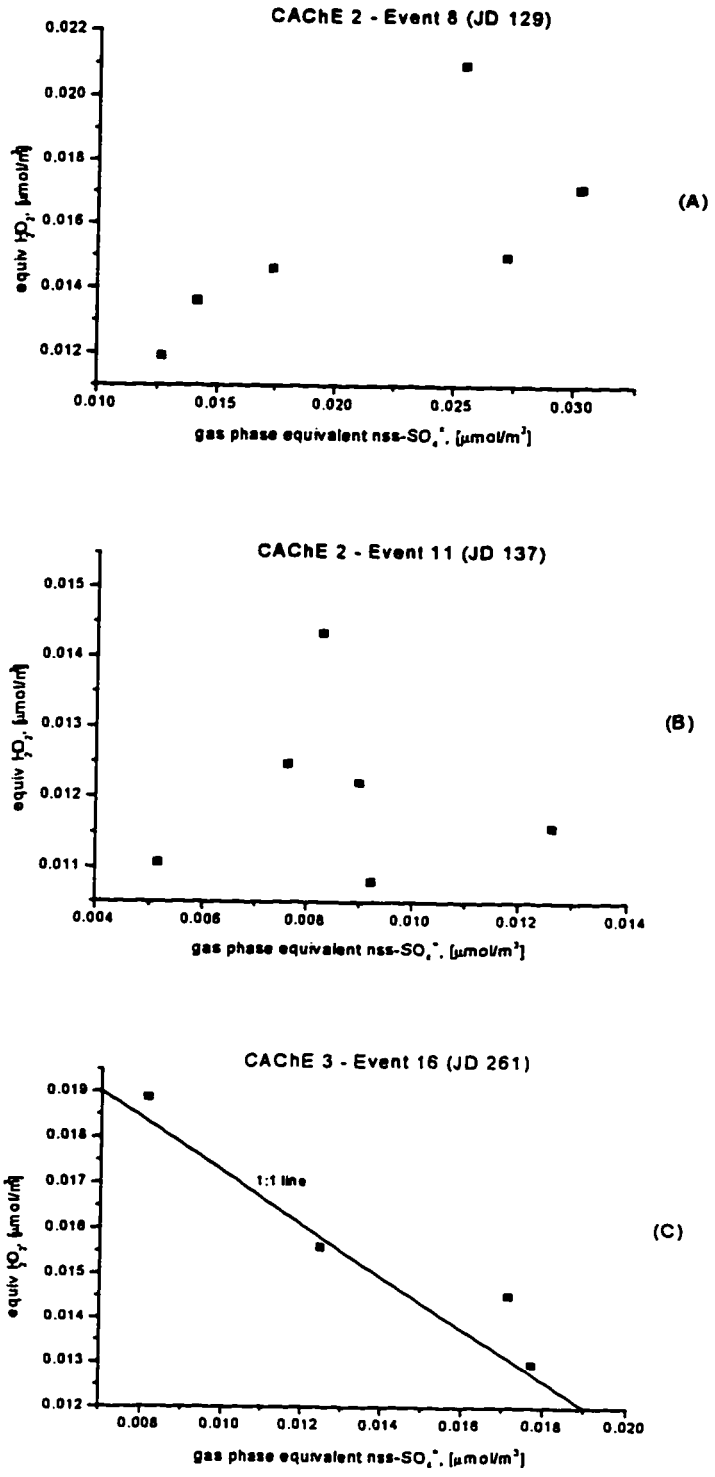

Figure 3.12 a-c. Gas phase equivalent H_2O_2 concentration vs. nss-$SO_4^=$ concentration for three cloud events during CAChE 2 and CAChE 3.

The three plots are dissimilar in their H_2O_2/S(VI) relationship. Event 16 is the only cloud event that experienced the expected 1:1 molar decrease in H_2O_2 concentration with increase in nss-$SO_4^=$ concentration. Daum *et al.* (1984) state that finding such a case required a "fortuitous set of conditions" and therefore may not be typical.

It is possible that H_2O_2 is the dominant oxidant in Event 16 but not in Events 11 or 8. Oxidation by ozone may be competitive in the other two cases, thus obscuring a clear 1:1 relationship. The ozone concentration is much lower in Event 16 suggesting that H_2O_2 may be the dominant oxidant, but the pH does not clearly favor H_2O_2 over O_3 oxidation. To verify this, kinetic calculations were performed to compare the contributions from either O_3 or H_2O_2 oxidation. In general, the reaction and rate of sulfate formation can be expressed as:

$$S(IV) + oxidant \xrightarrow{k^{(2)}} S(VI) \tag{28}$$

$$\frac{-d[S(IV)]}{dt} = k^{(2)}[oxidant][S(IV)] \tag{29}$$

where $k^{(2)}$ is a second order rate constant and [oxidant] and [S(IV)] are the concentrations of oxidant and unoxidized sulfur present in solution (Penkett *et al.*, 1979; Lee *et al.*, 1986). When comparing the rates of oxidation for the same cloud conditions, the rate equation is simplified to:

$$\frac{-1}{[S(IV)]}\frac{d[S(IV)]}{dt} = k^{(2)}[oxidant] \tag{30}$$

The second order rate constants for the two oxidants vary differently with pH, and are expressed as follows (Lee *et al.*, 1986 and Maahs, 1983, respectively):

$$k(H_2O_2) = 8.1 \times 10^7\ M^{-2}\ s^{-1} * [H^+ \text{ (in M)}] \tag{31}$$

$$k(O_3) = k_a + k_b K_w/[H^+] \tag{32}$$

where $k_a = 3.8 \times 10^5\ M^{-1}\ s^{-1}$

$k_b = 1.05 \times 10^{16}\ M^{-2}\ s^{-1}$

K_w = water dissociation constant, $1 \times 10^{-14}\ M^2$

Table 3.8 gives a comparison of reaction rates for the two oxidants, using the concentrations from Table 3.4. Oxidation by H_2O_2 dominates oxidation by O_3 in all cases; Event 16 does not exhibit any extraordinary rate difference. Therefore, the explanation that H_2O_2 oxidation is favored over O_3 in Event 16 (explaining the observed 1:1 relationship) but not in Events 8 and 11 is not substantiated. Significant initial S(VI) prior to cloud formation would also obscure the 1:1 relationship; however Event 16 had as much pre-cloud S(VI) as the other two events. It is possible that Events 8 and 11 experienced entrainment while Event 16 did not, thus preserving the 1:1 relationship. A comparison between observed LWC and adiabatic LWC would address this question but adiabatic LWC was not available.

Table 3.8 Comparison of S(IV)-oxidant reaction rates for the three cases in Table 3.4.

Sample	Reaction rate [s^{-1}] H_2O_2 oxidation only	Reaction rate [s^{-1}] O_3 oxidation only	Reaction rate ratio H_2O_2/O_3
CAChE 2 - Event 8			
M10	1.057	4.191E-04	2522
M12	0.715	4.253E-04	1682
M14	0.479	4.753E-04	1009
M16	0.254	6.414E-04	396
M18	0.254	6.656E-04	381
M20	0.388	3.841E-04	1010
CAChE 2 - Event 11			
M76	0.596	5.024E-04	1186
M80	0.205	8.381E-04	245
M82	0.126	1.062E-03	119
M84	0.123	1.175E-03	105
M86	0.193	9.654E-04	200
M88	0.221	8.018E-04	276
CAChE 3 - Event 16			
Y04	0.170	4.266E-04	399
Y06	0.161	5.738E-04	281
Y08	0.191	3.606E-04	530
Y10	0.135	3.797E-04	356

3.4 CONCLUSION

Measurements of cloudwater and gas phase peroxide concentrations collected during two sampling intensives at the Cheeka Peak Observatory during late spring and late summer 1994 are reported. Contrary to diurnal variations measured at other sites, the concentrations at CPO did not experience a diurnal trend, likely due to persistent cloud cover which masked variation expected from uv intensity. The data trend was marked by several nighttime maxima in H_2O_2 concentration (similar to that observed at Mt. Mitchell, NC) and spike events (>3 ppbv) that were uncharacterized but suspected due to contamination. Average cloud-free gas phase H_2O_2 and MHP concentrations were on the order of a few hundred ppt and did not vary much by wind sector; slightly higher concentrations were observed from the continental sector. In general, these concentrations were lower than those measured at other east coast sites.

A positive correlation between gas phase H_2O_2 and O_3 was observed for both CAChE data sets. In contrast to the low NO_x, ozone-destroying regime of the Southern Hemisphere where a negative correlation has been observed, both H_2O_2 and O_3 are photochemically produced at Cheeka Peak and account for the positive correlation.

An attempt was made to investigate consistency with Henry's Law equilibrium using simultaneously-collected cloudwater and gas phase H_2O_2 data. Henry's Law behavior was difficult to model using the field data and divergence from Henry's Law is due more to the deficiency of the data rather than non-equilibrium conditions in the atmosphere.

Cloudwater H_2O_2 concentrations (~30 μM) were slightly lower than concentrations observed at other sites during summertime. Peroxide concentrations always dropped to below detection limit during episodes of rain and cloud and were always present so that reaction of dissolved S(IV) with H_2O_2 was never oxidant-limited. Size dependence was observed for H_2O_2 as H_2O_2 was more concentrated in the smaller drops, likely because the observed cloudwater concentration was a diffusion-limited process.

A principal components analysis was performed on 16 variables present in both of the cloudwater CAChE data sets. Hydrogen peroxide did not lend particular descriptive capability to the analysis, and typical seasalt and pollution components were observed.

Although it is accepted that H_2O_2 is the predominant oxidant in the aqueous phase, thereby making clouds potentially large producers of sulfate, the quantitation of this amount was a difficult to measure. Without an appropriate tracer, direct measurement of sulfate production is difficult because the amount of sulfate produced through oxidation is usually a small fraction in comparison to the sulfate incorporated into cloudwater droplets through scavenging. A comparison of cloudwater nss-$SO_4^=$ and H_2O_2 yielded one case in which a 1:1 inverse molar relationship was observed. However an examination of oxidant rates of the other two non-conforming cases did not verify that H_2O_2 oxidation was clearly responsible for the observed 1:1 trend.

CHAPTER 4 - A MODEL-DATA INTERCOMPARISON OF HETEROGENEOUS CLOUD CHEMISTRY

4.1 INTRODUCTION

The ability of the environmental scientist to fully constrain and describe a complex atmospheric system is often limited. For example, current experimental techniques make it impossible to fully describe the complexity and heterogeneity theoretically postulated in clouds through field observation alone. For this reason, numerical cloud models which attempt to describe heterogeneous chemistry as a function of droplet size are employed to elucidate processes that otherwise are difficult to observe *in situ*.

Numerous examples of numerical cloud models exist which incorporate heterogeneous chemistry into their structure (e.g., Ahr *et al.*, 1989; Seidl, 1989; Ayers and Larson, 1990; Hegg and Larson, 1990; Lin and Chameides, 1991; Roelefs *et al.*, 1993). These models differ from earlier bulk parameterized models, which represented the cloud droplet spectrum with a single drop size and uniform chemical composition. Explicit microphysical models have suggested that heterogeneity in the chemistry across the droplet size spectrum can have very significant impacts on such diverse issues as sulfate production (Twohy *et al.*, 1989; Hegg and Larson, 1990), the impact of cloud-processing on the optical properties of processed aerosols (Hegg *et al.*, 1992; Yuen *et al.*, 1994), the nucleation scavenging efficiency of clouds (Ahr *et al.*, 1989) and the chemical wet deposition from clouds (Lin and Chameides, 1991).

Observational support for heterogeneous cloud chemistry has slowly accumulated in the last few years (e.g., Noone *et al.*, 1988; Munger *et al.*, 1989; Ogren *et al.*, 1992; Collett *et al.*, 1994) but has fallen well short of the specificity and detail necessary to validate models. Indeed, the observations are not always consistent with one another (c.f., Ogren *et al.*, 1992) and in no instance have model-observation comparisons been undertaken on a case-by-case basis. However it is only by such case-by-case comparisons, no matter how crude, that confidence in specific model predictions can be improved.

In this chapter, a preliminary comparison is made between predictions of a size-resolved cloud chemical model and limited observations of size-resolved cloud chemistry for three case studies. The model is used in a diagnostic sense to help elucidate cloud chemistry, particularly the role of NO_3^-. Due to current limitations in measurement technology with regard to size-resolved sampling of cloud water (only two size-segregated cloudwater fractions were collected during CAChE 3), and a lack of a complete suite of initial variable values necessary for model initialization, the comparison must be considered preliminary.

4.2 EXPERIMENTAL

4.2.a Description of the cloud model

The model used in this study is a modified version of the Ayers-Larson parcel model (Ayers and Larson, 1990) as described in Hegg *et al.* (1992). The model is a kinematic[1], Lagrangean parcel[2] model with explicit cloud microphysics and size resolved cloud drop chemistry. The model is composed of two distinct parts: a physical part describing the growth of each droplet class, and a chemical part which calculates cloud droplet chemical composition based on gas-aqueous equilibria and kinetic rate equations for the oxidation of S(IV). The separation of these two processes is reasonable because the time scale associated with the aqueous phase chemical reactions is long in comparison to the time scale associated with droplet growth. The two parts of the model only interact during the initialization phase of the model, in which an iteration is performed to achieve consistency between the specified initial $NH_3(g)$ concentration and the degree of ammoniation of the initial sulfate nuclei , which is assumed to be 1:1.

The model is initialized with a bi-modal log-normal size distribution covering the size range from 0.01 to 5.0 μm radius with 30 discrete size classes per mode. An example

---

[1] A kinematic model pre-specifies the vertical velocity profile of a parcel of air (Hegg and Larson, 1990) as opposed to a dynamic model, which allows the velocity profile to change with time.

[2] In a Lagrangean parcel model, the parcel of air is followed through a trajectory as predicted by prevailing meteorology, as opposed to a Eulerian model where species concentrations are calculated at a fixed geographical location at specified times (Finlayson-Pitts and Pitts, 1986).

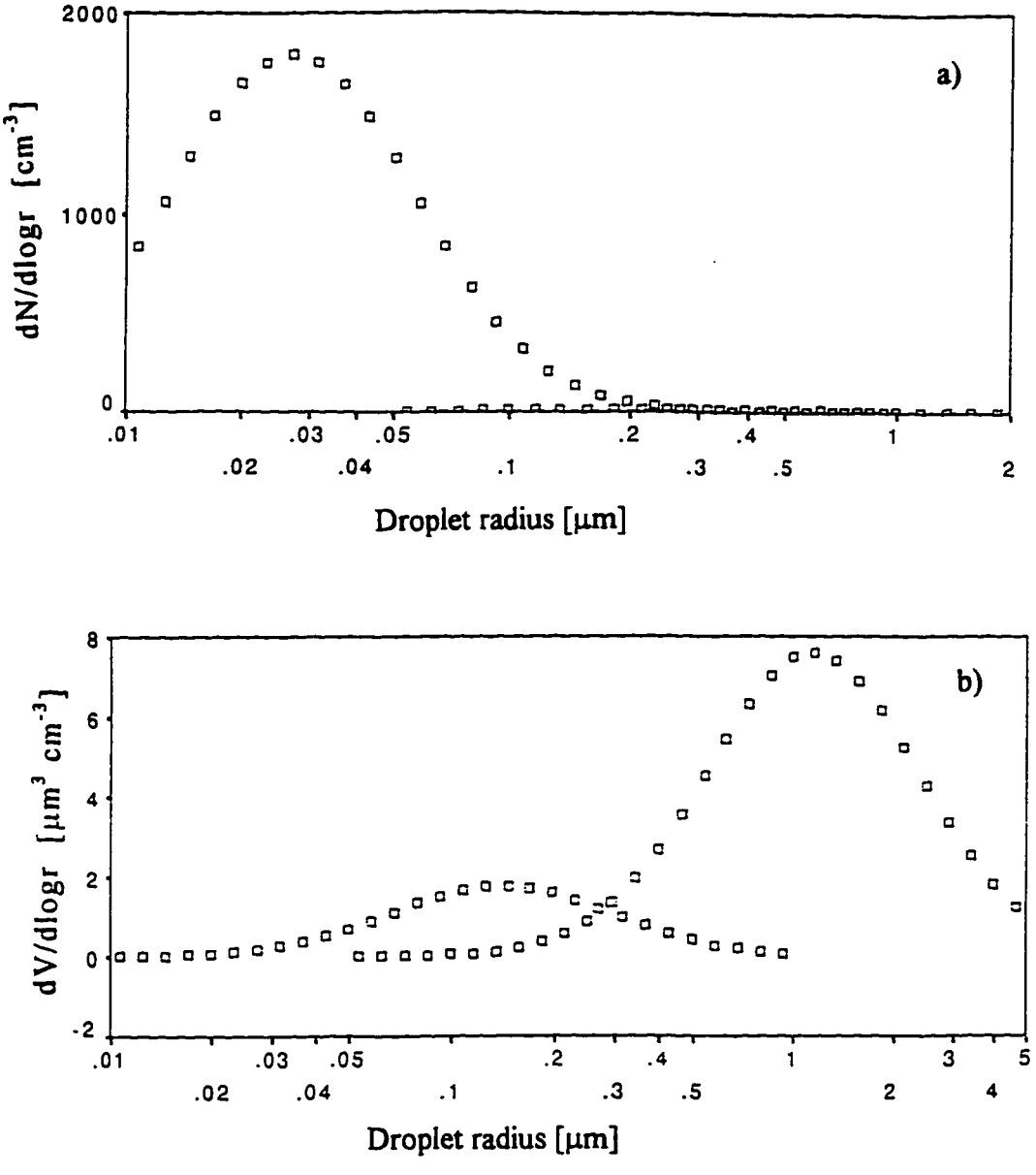

Figures 4.1.a and b. Number and volume size distributions, respectively, for case JD 243.

of this size distribution for case JD 243 is given in Figures 4.1.a and b. Each mode may have a distinct chemical composition. For the model simulations performed in this study, the smaller, or accumulation, mode (0.01 to 1.0 μm) consisted of NH_4HSO_4 and the larger, or coarse, mode (0.05 to 5 μm) consisted of seasalt. Trace gases which must be initialized are SO_2, NH_3, H_2O_2, O_3 and HNO_3. These trace gases are initially assumed to be at equilibrium with the unactivated particle size distribution but are then allowed to vary in phase partitioning by explicit calculation of mass transfer to and from each particle using the well-known Fuchs-Sutugin formulation (Fuchs and Sutugin, 1970). Sulfate production is formulated in terms of kinetic rate extensions for S(IV) oxidation by both H_2O_2 and O_3.

Discussion of the derivation of the kinematic trajectory to be used in the cases examined here is deferred to the section on model initialization.

4.2.b Description of the data base

The three case studies reported here are based on data acquired during the third Cloud and Aerosol Chemistry Experiment (CAChE 3), which took place at the CMDL Regional Research Station at Cheeka Peak Observatory (CPO) from August 12 through September 17, 1994. A more thorough description of the site is given Section 2.2.a. Numerous previous studies have taken place at this well-characterized site (c.f., Quinn *et al.*, 1995; Vong *et al.*, 1997).

Four distinct measurements most relevant to the current study are: cloud droplet characterization including composition, gas-phase concentrations of key species, the particle size distribution and synoptic meteorological data. The most important measurement is that of the cloud water droplet mass, number concentration and composition. The cloud droplet size distribution is measured with PMS FSSP-100 spectrometer. Both the total number of droplets and droplet mass over any size range are then determined by integration of the measured size distribution. It is noteworthy that the LWC as determined by the FSSP-100 was found to be in excellent agreement with a co-located Gerber PVM-100 probe (Kowalski *et al.*, 1997). Composition was determined from ion chromatographic analyses of bulk cloud water samples collected with the two-

stage rod collector described in Section 2.2.d. This device collected cloud droplets via impaction with two distinct size cutoffs; droplets greater than 5 μm and droplets greater that 12 μm, the latter category being a subset of the former.

A second data set utilized was that for the partial pressures of several key gas-phase species. Ozone concentration was monitored continuously by means of chemiluminescence by standard commercial instrument (Dasibi Model 1003 PC). Hydrogen peroxide was also monitored continuously with a dual-channel fluorimeter utilizing the horseradish peroxidase reaction (Lazrus *et al.*, 1986; also described previously in Section 3.2.a). However, SO_2 was only measured intermittently by means of base-impregnated filters (Ferek *et al.*, 1991). Hence, for the cases examined here, the SO_2 concentrations utilized were based on a single filter commencing at the time of cloud water sampling in the cases of JD 243 and JD256 but by more than 12 hours prior to the cloud start in the case of JD 251.

Two additional gas concentrations must be estimated to initialize the model. The first of these is NH_3. Because no NH_3 measurements were available, estimates were made based on measured cloud water composition for the first few samples of an event (essentially an assumption of gas-aqueous phase equilibrium) coupled with an assessment based on literature sources (e.g. Quinn *et al.*, 1990). This procedure yielded estimates of NH_3 of ~15 pptv for the cases of JD 243 and 256 (in accord with the average value reported by Quinn *et al.* for the NE Pacific Ocean) but an appreciably higher value of ~32 pptv for the case of JD 251 – though still well within the bounds of the Quinn *et al.* data set.

The second gas which must be estimated in HNO_3. Sources of this gas in the unperturbed marine boundary layer are very slight and concentrations are expected to be quite low. While nitrate is commonly found in both background aerosol (Prospero *et al.*, 1985) and precipitation (Vong *et al.*, 1988) over the NE Pacific, it is likely largely in particulate form. This results in an initialization problem. As currently configured, the model only initializes nitrate as HNO_3 – no particulate nitrate is initially present. Hence, the amount and distribution of nitrate in the aerosol is determined by the model itself based

on gas-aqueous phase equilibrium with the unactivated sulfate and seasalt haze particles. This equilibrium will be modulated by the amount of NH_3 gas present as well. In short, introducing nitrate into the model solely as HNO_3 could produce problems in both the NO_3^- and NH_4^+ distributions over drop size if the nitrate were actually mostly in particulate form initially. Nevertheless, such a single-phase introduction has been necessary, with initial HNO_3 values being used to reproduce observed total cloudwater nitrate.

The third data set employed in the analysis consisted of particle size distributions covering the range from 0.02 to 7.1 μm. These distributions were measured with a combination of a Differential Mobility Analyzer (DMA, TSI Model 3071) and an Aerodynamic Particle Spectrometer (APS, TSI Model 3300). Also available are "total" particle number concentrations (actually the number concentrations between ~0.02 μm and 0.5 μm diameter) from a TSI 3760 CN counter. A more detailed description of these instruments, and their utilization to obtain measurements, is given in Quinn *et al.* (1996). In this study, the size distributions are fitted to bimodal log-normal distribution functions. The functions are then integrated and the derived modal masses are compared with the measured masses of sea salt and non-seasalt sulfate. The fit parameters are then adapted to yield the best agreement with the measured masses and number concentrations obtained from the CN counter. The adjusted distribution functions are then used to initialize the cloud model.

The rationale for such adjustment is straightforward because the credibility of the various aerosol measurements is not uniform. The estimates of aerosol mass (e.g., sulfate, sodium, nitrate, etc.) concentrations are the most reliable. Slightly less certain are the measures of total aerosol concentration derived from the TSI 3760. Coming in a distant third are the aerosol and cloud size distribution measurements. Hence, where the mass, number concentration and size distribution of the aerosol have not been consistent, most weight is given to achieving agreement in initial species masses. However, some consideration has also been given to the other variables. For example, in the case of JD 256, the initial sulfate mass utilized was only 69% of that observed because to raise it

further would have grossly distorted both the number concentrations and size distributions.

The final data set employed consisted of synoptic meteorological data used both for back trajectory calculations and to initialize the model. The model initialization was based on the temporally nearest sounding to the sample time taken at the NWS station at Quillayute, WA, which is located on the coast ~30 km south of CPO.

4.2.c Model initialization

Although twenty distinct cloud events were sampled during the course of the CAChE 3 experiment, in no instance was so complete a data set obtained that a definitive model initialization was feasible. This situation is typical of models that have explicit microphysics and chemistry. However, in three cases sampled, the suite of measurements obtained was sufficiently complete to permit a reasonably constrained model initialization and hence a commensurably objective comparison of the model predictions with observations.

The trace gas concentrations, thermodynamic data (sounding of temperature and dewpoint) and particle size distributions necessary to initialize the model are derived from the measurements in a straightforward manner. The values used for each of the variables required by the model are shown in Table 4.1. With regard to particle composition, the accumulation mode and coarse mode are assumed to be NH_4HSO_4 and seasalt, respectively. Values for the mass of these two species are based on integration of the respective modes and are later compared with observations as described above.

The kinematic airflow necessary to initialize the model was derived from a combined assessment of the synoptic flow, the winds from the Quillayute sounding and the topography of the area surrounding the CPO. Winds for all three cases were westerly, varying between 280 and 320°. For such a flow regime, with only modest wind sheer between the surface and the CPO, the flow field can be effectively modeled as a simple case of upslope flow with an induced vertical velocity given by:

$$W = \overline{V}_{mbl}\overline{V}_h \qquad (1)$$

where $\overline{V}$ is the average velocity and h is the height (above sea level) of the terrain (Houze, 1993). The gradient of the terrain height was determined from detailed topographic charts. Specifically, the heights along the direction of flow (the problem may be treated as two-dimensional) was fitted to a polynomial in distance along the direction of flow and then differentiated to obtain a smooth functional form for the streamline needed in the model.

This procedure implicitly assumes that the cloud at the CPO is essentially purely orographic, independent of larger scale synoptic forcing. Clearly this is not always the case and certainly not for cloud well above the surface. However, at the CPO itself, where sampling was done within 10 m of the surface, the orographic flow appeared to be the main (though perhaps not the sole) source of vertical velocity for the cases examined here.

4.3 RESULTS AND DISCUSSION

4.3a Cloud microphysical and bulk chemical parameters

Prior to analysis of key variables indicative of the heterogeneity of the cloud chemistry, some assessment must be made of the success of the model in predicting more standard parameters such as cloud liquid water content, cloud drop number concentration and various (or volume mean) bulk chemical species concentrations. Hence, a model-observation comparison of a selected set of such parameters is next examined. The six variables chosen for comparison are shown in Table 4.2 for each of the three cases examined. Also shown is the source of the air sampled base on 10-day isentropic back trajectories from CPO for synoptic reporting times (12 hour intervals) bracketing the observations (see Appendix A).

Table 4.1 Initial values for parameters used in the cloud model. Observed values are shown in parentheses. When no observed value was available, NA has been entered. Discrepancies in the initial/observed pairings are largely due to inconsistencies among observed values within the framework of the model utilized (see text).

CASE	JD 243	JD 251	JD 256
LCL Temperature (K)	285.9 (285.9)	286.5 (286.5)	285.2 (285.2)
LCL Altitude (m)	300 (300)	250 (250)	263 (263)
LCL Pressure (mb)	975 (975)	984 (984)	986 (986)
$\overline{U}$, vertical wind (m s^{-1})	4 (4)	10 (10)	4 (4)
Accumulation Mode N (cm^{-3})	1457 (950)	328 (300)	870 (700)
Accumulation Mode σ_g	2.1 (2.1)	2.1 (1.4)	1.68 (1.68)
Accumulation Mode $\bar{r}$ (μm)	0.027 (0.027)	0.04 (0.03)	0.04 (0.03)
Coarse Mode N (cm^{-3})	10.7 cm^{-3} (NA)	10.2 (NA)	2.0 (NA)
Coarse Mode σ_g	2.1 (NA)	2.1 (NA)	2.0 (NA)
Coarse Mode $\bar{r}$ (μm)	0.23 (NA)	0.23 (NA)	0.20 (NA)
nss-sulfate (μg m^{-3})	2.1 (2.2)	1.5 (1.4)	1.1 (1.6)
sea salt (μg m^{-3})	3.8 (3.8)	3.7 (3.7)	0.4 (0.4)
SO_2 (pptv)	205 (205)	25 (15-31)	31 (31)
O_3 (ppbv)	25 (25)	25 (25)	28 (28)
H_2O_2 (pptv)	500 (500)	400 (400)	700 (700)
NH_3 (pptv)	15 (NA)	16 (NA)	32 (NA)
HNO_3 (pptv)	4.8 (NA)	5.9 (NA)	101 (NA)

For the three microphysical parameters examined (LWC, drop number concentration and volume mean drop diameter), the model predictions are in reasonable accord with the observations except for the cloud drop number concentrations in JD 243 and JD 251 (and a consequent underprediction in volume mean radius). In the case of JD 243, this discrepancy is simply due to the high initial aerosol number concentration utilized to provide mass closure. For JD 251, however, the source of the discrepancy is less clear. Such a phenomenology would be consistent with the entrainment of air with lower moisture content and higher particle concentration than those for the lifting condensation level at which the model was initialized. While very plausible, there are no data available to confirm or refute this hypothesis. In any case, the model-observation agreement is still sufficiently close to suggest that gross distortions in distributed droplet chemical properties will not occur.

Table 4.2 Comparison of observed and predicted values for selected parameters for the cases examined. Observed values are given in parentheses.

Parameter	JD 243	JD 251	JD 256
Cloud liquid water content ($g\ m^{-3}$)	0.40 (0.50)	0.45 (0.48)	0.44 (0.48)
Cloud drop number conc. (cm^{-3})	333 (220)	214 (140)	327 (314)
Volume mean drop diameter (μm)	12.8 (17)	15.6 (18.6)	13.6 (14.4)
Droplet NO_3^- mass ($\mu g\ m^{-3}$)	0.86 (0.96)	0.50 (0.53)	1.1 (1.6)
Droplet NH_4^+ mass ($\mu g\ m^{-3}$)	0.51 (0.29)	0.37 (0.32)	0.31 (0.15)
Volume mean drop pH	4.1 (4.0)	4.4 (4.2)	4.3 (4.0)
Isentropic back trajectory	Gulf of Alaska	Central N. Pacific	Gulf of Alaska

The three chemical parameters examined also show reasonable agreement for the three cases, although the best agreement is now for the case of JD 251. Particularly important are the pH predictions of the model since most of the size-distributed properties

of the cloud chemistry are associated with the pH. The ratios of predicted to observed pH's suggest discrepancies in hydrogen ion concentration ranging from ~25% for JD 243 to close to a factor of 2 for JD 256. This discrepancy is related to the relative amounts of nitrate and sulfate present in the ambient aerosols, coupled with the manner in which the initial nitrate is phase-partitioned by the model itself. In light of the importance of the nitrogen species to the overall chemistry, it is worthwhile to discuss this issue further.

Because of uncertainties in the size distribution of particulate nitrate, it is not directly specified in the model as it is now formulated. Instead, an initial HNO_3 partial pressure is specified and the model iterates to phase equilibrium with the unactivated haze particles prior to model integration. Hence, implicitly, the particulate nitrate concentration is dependent on the initial NH_3 partial pressure and, conversely, the NH_4^+ in the condensed phase is modulated by the particulate nitrate. For example, in the case of JD 256, for which the observed particulate nitrate is quite high, the initial NH_3 must also be set quite high because the NH_3 titrates with the available NO_3^-. Enough NH_3 must be leftover to maintain the prescribed 1:1 ratio of the initial unactivated NH_4HSO_4 aerosol and achieve a corresponding proper model initialization. When the nitrate-to-sulfate equivalence ratio is simultaneously quite high, as in the case for JD 256, this can seriously distort the NH_4^+/S(VI) equivalence ratio. If, in the actual cloud water, the nitrate is associated with basic cations other than NH_4^+ (e.g. Na^+, Ca^{+2}, Mg^{+2}, etc.) then significant discrepancies between the observed and predicted pH's can occur. It is interesting to note, in this regard, that the size of the model-observation discrepancy in pH from Table 4.2 scales directly with the nitrate-to-sulfate ratio and also with the amount of NH_3 initially present. This nitrate-ammonium-pH linkage suggests that, if the nitrate present in the case to be modeled is indeed mostly associated with the NH_4^+ cation (as would be expected if the NO_3^- originated primarily in the gas phase), then model predictions of phase partitioning and size-resolved chemistry will likely be in agreement with observations. If, however, such is not the case, then anomalies may be expected.

In summary, the cloud microphysical and bulk chemical parameters examined suggest that, while model-observation agreement is far from perfect, there is sufficient agreement to render a comparison of size-distributed properties feasible.

4.3.b Chemical properties distributed over drop size

The first step in the analysis of size-distributed properties is to derive them. The raw data, which consist of chemical composition data for two different sizes of collection rods, yield mean drop sizes (12 μm for the small stage and 13 μm for the large stage) for the two collection aliquots which scarcely differ. Because the collected fractions reflect cumulative collected water above the rod cutoffs of 5 and 12 μm, and there is relatively little water mass in this size range, this is not surprising. Nevertheless, it renders concentrations for the two size aliquots nearly identical. To get around this problem and derive size dependent concentrations for distinct size fractions, these distinct fractions are deconvoluted from the available aliquots by treating the concentrations in the collected water above 5 μm as the volume-weighted mean of the concentrations for the 5 - 12 μm and >12 μm size fractions (described earlier in Section 2.4.b), given by:

$$(C_i)_{>5\mu m} = (C_i)_{5-12\mu m}\left(\frac{LWC_{5-12\mu m}}{LWC_{>5\mu m}}\right) + (C_i)_{>12\mu m}\left(\frac{LWC_{>12\mu m}}{LWC_{>5\mu m}}\right) \qquad (2)$$

where the LWC's and C's refer to the liquid water contents and chemical species concentrations, respectively for the indicated size ranges. Hence, for comparison with the already available > 12 μm fraction, the concentrations of the chemical species in the 5 - 12 μm fraction are estimated as:

$$(C_i)_{5-12\mu m} = \frac{(C_i)_{>5\mu m} - (C_i)_{>12\mu m}\left(\frac{LWC_{>12\mu m}}{LWC_{>5\mu m}}\right)}{\left(\frac{LWC_{5-12\mu m}}{LWC_{>5\mu m}}\right)} \qquad (3)$$

The most obvious parameter upon which to employ this deconvolution is the hydrogen ion concentration. Values for the pH for each of the two size fractions for the case of JD 243 are plotted against the model-predicted distribution of pH over drop size in

Figure 4.2. The figure demonstrates that the sense of the model prediction, with higher pH in the smaller drops, is replicated in the measurements. However, the model somewhat overestimates cloud drop acidity, suggesting the presence of cations other than those currently indicated in the model.

A major problem associated with the deconvolution technique is that the uncertainty in the liquid water contents, particularly the small aliquot for the 5 - 12 μm fraction, render the uncertainties in the absolute amounts of a species present highly uncertain. For example, the observed pH's shown in Figure 4.2 are uncertain to ± 5%. Hence, while the small droplet pH's are systematically higher than those for the larger drops, the pH's for the two size classes do not differ significantly. To get around this issue, one can employ concentration ratios instead of absolute concentrations. Of the various ratios available, the one of most interest is NH_4^+ / $SO_4^=$. This arises because, in the model, the ammonium and sulfate ions are the dominant base cation and acid anion, respectively. Hence, their relative distributions define the distribution of acidity. Furthermore, based on the study of Hegg and Larson (1990), the ammonium ion distribution over drop size is quite sensitive to the distribution of other trace constituents over size and is thus a good indicator of droplet chemical heterogeneity.

The ratios of NH_4^+ to S(VI) as a function of drop size, both as predicted by the model and as derived from the observation for the case of JD 243, are shown in Figure 4.3. As was the case with droplet pH, the sense of the model-predicted and observed ratios as a function of size are in agreement, with the higher ratios occurring in the smaller drop sizes. However, the model-predicted ratios are systematically higher than those observed, by about a factor of two. Much of the relative enhancement in the NH_4^+/S(VI) ratio is simply due to the higher NH_3 concentration necessary to stabilize the particulate nitrate at initialization. Indeed, the ratio of the model predicted NH_4^+ to that observed is also about a factor of 2 (see Table 4.2).

Also shown in Figure 4.3 are the uncertainties in the NH_4^+/S(VI) ratios for the two size fractions available in the observations. From these, it is clear that the smaller droplets

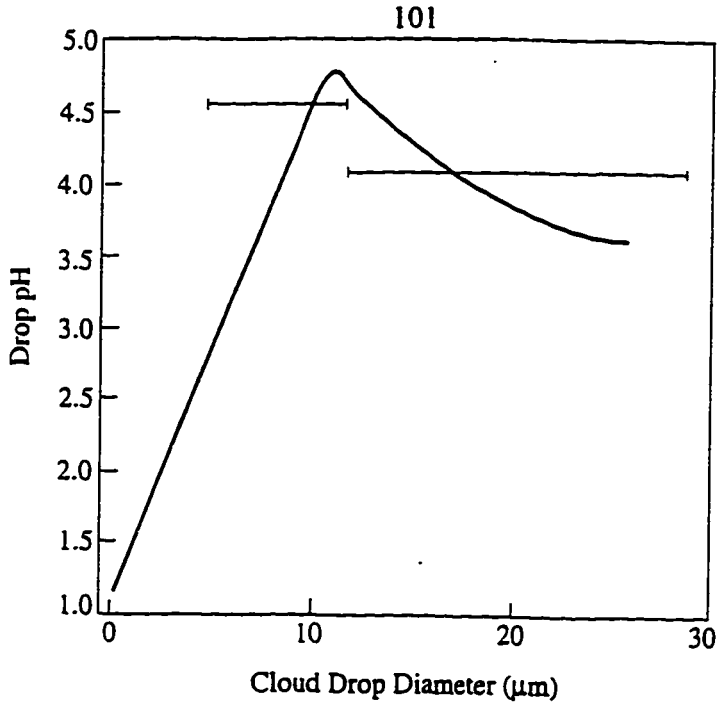

Figure 4.2. A comparison of the size-dependent cloud drop pH distribution predicted by the model (continuous curve) with the observed pH for the two cloudwater size fractions collected (horizontal bars). The case is that of JD 243.

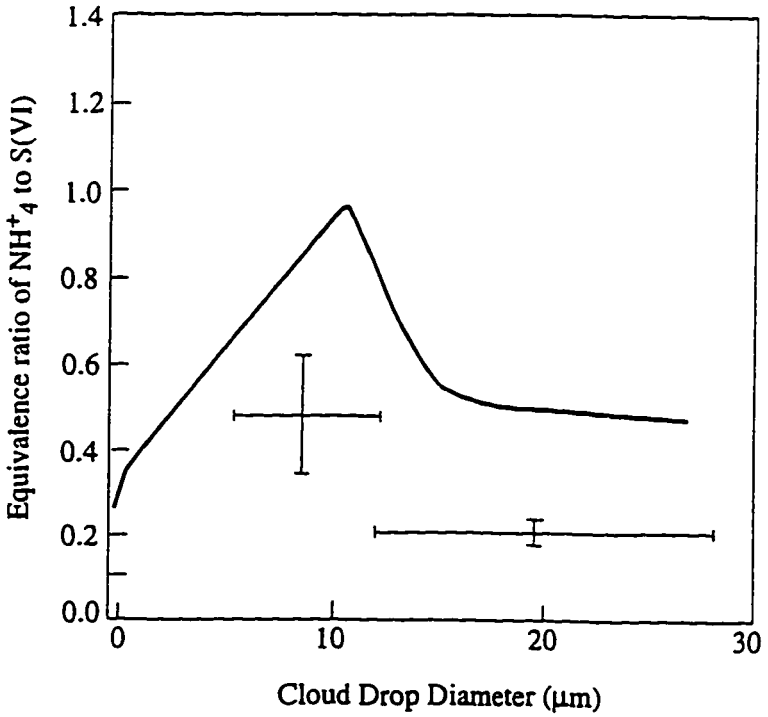

Figure 4.3. A comparison of the NH_4^+ to S(VI) equivalence ratio as a function of size, predicted by the model (continuous curve) with observed ratios in the two cloudwater size fractions collected (horizontal bars, with error bars). The case is that of JD 243.

have a significantly, as well as systematically, higher ratio than do the larger drops, as predicted by the model.

Turning to the other cases examined, an interesting contrast is observed. For the case of JD 256 (Figure 4.4), the model-observation comparison is much like that for JD 243. The sense of the size dependence of the NH_4^+/S(VI) ratio is similar in the model prediction and the observations but the model-predicted ratios are systematically high, though for this case the discrepancy is much more acute for the larger size droplets. Again, this is in accord with the higher than observed NH_3 levels necessary at initialization to stabilize the particulate nitrate. On the other hand, JD 251 (Figure 4.5) shows a marked discrepancy in the sense of the model prediction of size dependence as compared with observations. While the relatively large uncertainties in the observed NH_4^+/S(VI) ratios for this case render values for the two size fractions statistically indistinguishable, the measurements clearly suggest that the predicted size dependence of the ratio is in error. It is interesting to note that the NH_4^+/S(VI) ratio prediction for the large drops is actually in reasonable agreement with the observations, consistent with the fact that no excess NH_3 was necessary in the model simulation of this case. It is only in the 5 - 12 μm size faction that a discrepancy now occurs.

4.3.c Correlations of NO_3^- with other relevant chemical species

As suggested in Section 4.2.b., one possible cause for the model-observation discrepancy seen in this case is the presence of particulate nitrate associated with cations other than NH_4^+. While it is difficult to directly assess this possibility, an analysis of the relationship between nitrate and other key ions in the cloud water is enlightening, particularly if one contrasts these relationships for JD 251 with the other two cases examined.

Linear correlation coefficients between nitrate and three other key ions measured in the cloud water are shown for all three cases in Table 4.3. Perhaps the most important contrast between JD 243/256 and JD 251 is that NH_4^+ and NO_3^- are well correlated in the 243 and 256 data but essentially uncorrelated ($r=0.22$, $p=0.641$) in 251. This is consistent

with the hypothesis that, while for 243 and 256, the nitric acid present is in fact stabilized in solution by NH_3 as assumed in the model, this is not the case for 251. It is the presence of some other cation(s) – not included in the model – that controls the gas/aqueous nitrate partitioning. In line with this, for 243 and 256 NO_3^- is also well correlated with Na, as would be expected for nitrate initially present as an acid vapor. For 251 on the other hand, Na and NO_3^- are not correlated. Finally, turning to nss-sulfate, it is noteworthy that NH_4^+ and nss-$SO_4^=$ are significantly better correlated in 251 than in either 243 or 256, where the NH_4^+ must be shared between nitrate and sulfate. Conversely, nss-$SO_4^=$ and NO_3^- are well correlated in 243 and 256 but not correlated in 251.

All of the above ionic relationships in the cloud water samples suggest that, while in JD 243 and JD 256 the nitrate present was initially nitric acid whose gas/aqueous partitioning was controlled by NH_3 (as in all of the model runs), for JD 251 this was not the case; rather, the particulate nitrate was stabilized by some other cation (e.g. Na^+, Ca^{+2}, Mg^{+2}, etc.). The contrast between the model-observation agreement in the size distribution of NH_4^+/S(VI) found in JD 243 and 256 with the lack of such agreement for 251 is explicable in these terms.

One final observation regarding the ionic correlations in Table 4.3 is noteworthy. For all three cases, the correlation between Na^+ and nss-$SO_4^=$ is quite good, showing the impact of sea salt on nss-$SO_4^=$ production, as predicted by most heterogeneous chemistry models (e.g. Twohy *et al.*, 1989; Yuen *et al.*, 1996).

4.4 CONCLUSIONS

The observational data on size-dependent cloud chemistry presented, while decidedly limited, have permitted a preliminary assessment of the validity of some key predictions of an explicit microphysical model used to explore heterogeneous cloud chemistry. In two out of the three cases examined, the sense of the size distribution of the NH_3/S(VI) ratio was correctly predicted. For the unsuccessful case, the lack of agreement

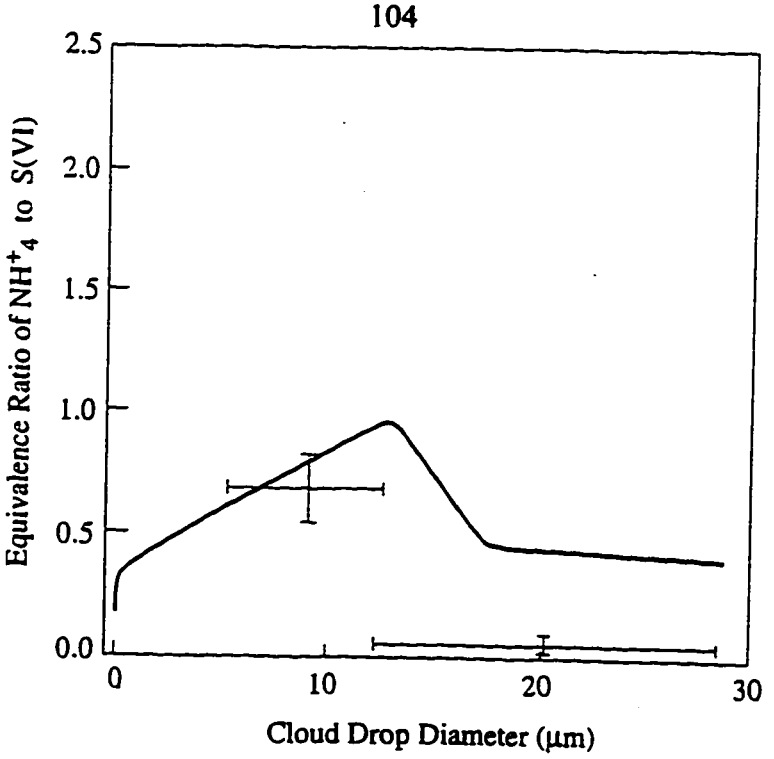

Figure 4.4. As in Figure 4.3 but now for the case of JD 256.

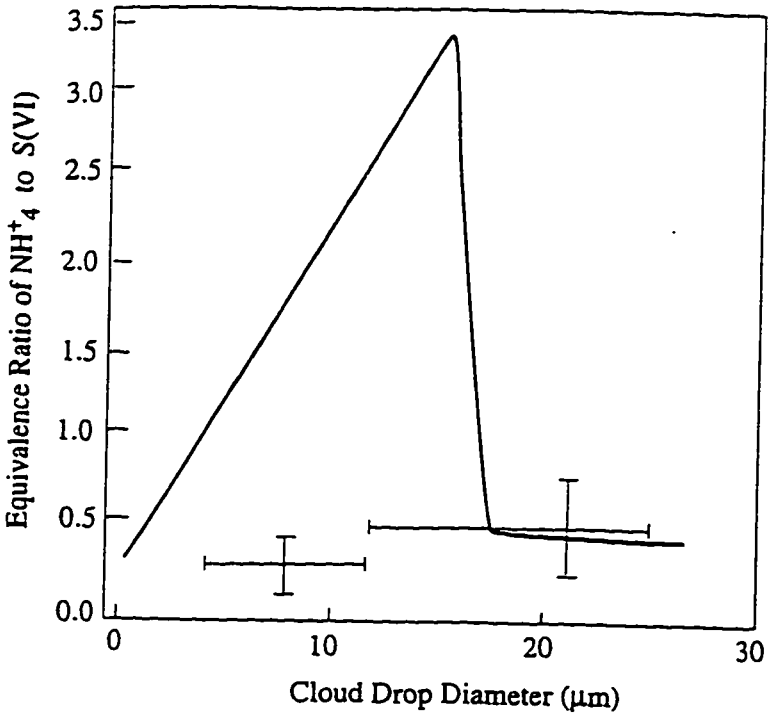

Figure 4.5 As in Figure 4.3 but now for the case of JD 251.

Table 4.3 Linear correlation coefficients, together with chance probability values (P), for selected ions in the cloud water samples for the cases examined.

JD 243 data set				
	Na	NH_4^+	NO_3^-	nss-$SO_4^=$
Na	*1.000 (P = 0)*	0.6385 (P=0.008)	0.9467 (P=0.000)	0.8116 (P=0.000)
NH_4^+	0.6385 (P=0.008)	*1.000 (P = 0)*	0.6519 (P=0.006)	0.5710 (P=0.021)
NO_3^-	0.9467 (P=0.000)	0.6519 (P=0.006)	*1.000 (P = 0)*	0.8498 (P=0.000)
nss-$SO_4^=$	0.8116 (P=0.000)	0.5710 (P=0.021)	0.8498 (P=0.000)	*1.000 (P = 0)*
JD 251 data set				
	Na	NH_4^+	NO_3^-	nss-$SO_4^=$
Na	*1.000 (P = 0)*	0.8335 (P=0.020)	-0.0036 (P=0.99)	0.8032 (P=0.030)
NH_4^+	0.8335 (P=0.020)	*1.000 (P = 0)*	0.2168 (P=0.641)	0.8991 (P=0.006)
NO_3^-	-0.0036 (P=0.99)	0.2168 (P=0.641)	*1.000 (P = 0)*	0.0757 (P=0.872)
nss-$SO_4^=$	0.8032 (P=0.030)	0.8991 (P=0.006)	0.0757 (P=0.872)	*1.000 (P = 0)*
JD 256 data set				
	Na	NH_4^+	NO_3^-	nss-$SO_4^=$
Na	*1.000 (P = 0)*	0.4746 (P=0.063)	0.8766 (P=0.000)	0.8599 (P=0.000)
NH_4^+	0.4746 (P=0.063)	*1.000 (P = 0)*	0.5800 (P=0.019)	0.4434 (P=0.085)
NO_3^-	0.8766 (P=0.000)	0.5800 (P=0.019)	*1.000 (P = 0)*	0.9092 (P=0.000)
nss-$SO_4^=$	0.8599 (P=0.000)	0.4434 (P=0.085)	0.9092 (P=0.000)	*1.000 (P = 0)*

between model and observation is explicable in terms of a substantial particulate nitrate component not associated with the NH_4^+ cation, contrary to the assumed model structure. To appropriately deal with this type of scenario, more information on the size distribution of particulate nitrate, and its molecular form in background marine air, will be required than is currently available.

CHAPTER 5 - SUMMARY, CONCLUSIONS, AND RECOMMENDATIONS FOR FUTURE RESEARCH

5.1 SUMMARY

Measurements of various aerosol, trace gas, and cloud water constituents were made during two intensive observation periods at the Cheeka Peak Observatory (CPO) on the Washington state coast. These measurements were a part of the second and third Cloud and Aerosol Chemistry Experiments (CAChE 2 and CAChE 3) conducted from April 19 to May 18, 1994 and August 30 to September 23, 1994, respectively. Gas phase hydrogen peroxide was measured continuously using the horseradish-peroxidase method during these two time periods. Cloud water samples were analyzed for major ion constituents and aqueous hydrogen peroxide. The cloud water samples collected during CAChE 2 represented bulk collection, whereas the cloud water samples collected during CAChE 3 were segregated into two size fractions, with mean droplet diameter of approximately 12 μm and 13 μm. Finally, a preliminary comparison was made between predictions of a size-resolved cloud chemical model and limited observations of size-resolved cloud chemistry for cases upon which the model was initialized.

5.1 CONCLUSIONS

Cloudwater major ion concentrations (e.g., Na^+, NH_4^+, H^+, NO_3^-, $SO_4^=$, etc.) were higher than previously observed at Cheeka Peak, but comparable to other West coast locations. Despite the small difference in collected droplet size, size dependence was observed for several species. Seasalt ions and NO_3^- were more concentrated in the larger drops, whereas peroxide was more concentrated in the smaller drops. Size dependence was not observed for MSA, non seasalt sulfate (nss-$SO_4^=$), and NH_4^+, and was only weakly observed for H^+.

Cloud-free gas phase H_2O_2 and organic peroxide average concentrations were on the order of a few hundred ppt and did not vary much by wind sector; slightly higher

concentrations were observed from the continental sector. In general, these concentrations were lower than those measured at east coast sites. Cloudwater H_2O_2 concentrations (~30 μM) were slightly lower than summertime concentrations observed at other sites. Evidence for sulfate production via H_2O_2 oxidation was observed but was not conclusive.

Finally, a preliminary comparison was made between predictions of a size-resolved cloud chemical model and limited observations of size-resolved cloud chemistry. The sense of model prediction regarding size-distributed properties agreed with observed values for two of the three cases. For the unsuccessful case, the lack of agreement between model and observation is explicable in terms of a substantial particulate nitrate component not associated with the NH_4^+ cation, contrary to the assumed model structure.

5.3 RECOMMENDATIONS

Several factors could have improved the current study and are worthy of future exploration:

- An improved cloud water collection system that collects more than two fractions would facilitate a more complete picture of heterogeneous cloud chemistry. The two size fractions collected in this study were not distinct from one another (one was a subset of the other) and required, in some instances, mathematical manipulation for comparison. In addition, the rod sizes could be modified to better reflect the ambient cloud drop distribution (e.g., rods with impaction d_{50} of 10 and 15 μm, instead of the current 5 and 12 μm), thus collecting more distinct size classes.
- This study would have benefited from better characterization of organic peroxides, because errors in this measurement can effect the hydrogen peroxide results. More advanced measurement techniques involve HPLC separation prior to detection. Since peroxides have not been well-characterized at remote, marine sites like Cheeka Peak, further study of this important atmospheric oxidant are warranted.
- Evidence of sulfate production via H_2O_2 oxidation was found but, like many other studies, was not conclusively supported or quantified. Although this study failed to

quantitate sulfate production using selenium as a tracer for particulate sulfate, I feel that improvements in sampling, sample irradiation, and γ-ray detection would allow for the detection of low-levels of selenium. I believe that the correct choice for reactor irradiation (Dr. Liaquat Husain, personal communication) and use of more sophisticated detection equipment like that available at Pacific Northwest Laboratory in Richland (Dr. Ron Brodzinski, personal communication) would improve the success of this method.

- The preliminary model-observation comparison suggests several features that could profitably be incorporated into future field studies aimed at model validation. First, both the particulate nitrate and sulfate size distribution would be very useful measurements to have. Second, though difficult, it is important to try to obtain more than two size fractions for bulk cloud water collections. Finally, better characterization of the commonly alkaline coarse mode of the aerosol size distribution is in order. On the modelling side, the most acute need is for a more realistic treatment of particulate nitrate in the model utilized for these studies.

BIBLIOGRAPHY

Ahr, M., Flossman, A. I. and Pruppacher, H. R. (1989) On the effect of the chemical composition of atmospheric aerosol particles on nucleation scavenging and the formation of a cloud interstitial aerosol. *J. Atmos. Chem.*, **9**, 465-478.

Anastasio, C., Faust, B. C. and Allen, J. M. (1994) Aqueous phase photochemical formation of hydrogen peroxide in authentic cloud waters. *J. Geophys. Res.*, **99**, 8231-8248.

Andreae, M.O., Charlson, R.J., Bruynseels, F., Storms, H., Van Grieken, R., and Maenhaut, W. (1986) Internal mixture of sea salt, silicates, and excess sulfate in marine aerosols. *Science*, **232**, 1620-1623.

Ayers, G. P. and Larson, T. V. (1990) Numerical study of droplet size dependent chemistry in oceanic, wintertime stratus clouds at southern mid-latitude. *J. Atmos. Chem.*, **11**, 143-167.

Ayers, G. P., Penkett, S. A., Gillett, R. W., Bandy, B., Galbally, I. E., Meyer, C. P., Elsworth, C. M., Bentley, S. T. and Forgan, B. W. (1992) Evidence for photochemical control of ozone concentrations in unpolluted marine air. *Nature*, **360**, 446-449.

Bales, R. C., McConnell, J. R., Losleben, M. V., Conklin, M. H., Fuhrer, K., Neftel, A., Dibb, J. E., Kahl, J. D. W. and Stearns, C. R. (1995) Diel variations of H_2O_2 in Greenland: a discussion of the cause and effect relationship. *J. Geophys. Res.*, **100**, 18661-18668.

Barth, M. C., Hegg, D. A. and Hobbs, P. V. (1989) Measurements of atmospheric gas-phase hydrogen peroxide concentrations in winter on the east coast of the United States. *Tellus*, **41B**, 61-69.

Baulch, D. L., Cox, R. A., Crutzen, P. J., Hampson, R. F., Jr., Kerr, F. A., Troe, J. and Watson, R. P. (1982) Evaluated kinetic and photochemical data for atmospheric chemistry: Supplement 1. CODATA Task Group of Chemical Kinetics, *J. Phys. Chem. Ref. Data*, **11**, 327-496.

Behar, O., Czapski, G. and Duchovny, I. (1970) Carbonate radical in flash photolysis and pusle radiolysis of aqueous carbonate solutions. *J. Phys. Chem.*, **74**, 2206-2210.

Benner, W. H. and Bizjak, M. (1988) Pseudo first-order reaction rate constant for the formation of hydroxymethylhydroperoxide from formaldehyde and hydrogen peroxide. *Atmos. Env.*, **22**, 2603-2605.

Burkhard, E.G., Dutkiewicz, V.A. and Husain, L. (1994) A Study of SO_2, $SO_4^=$, and Trace Elements in Clear Air and Clouds Above the Midwestern United States. *Atm. Env.*, **28**, 1521-1533.

Calvert, J. G., Lazrus, A., Kok, G. L., Heikes, B. G., Walega, J. G., Lind, J. and Cantrell, C. A. (1985) Chemical mechanisms of acid generation in the troposphere. *Nature*, **317**, 27-35.

Cantrell, C. A., Stedman, D. H. and Wendel, G. J. (1984) Measurement of atmospheric peroxy radicals by chemical amplification. *Anal. Chem.*, **56**, 1496-1502.

Chameides, W. L. (1984) The photochemistry of a remote stratiform cloud. *J. Geophys. Res.*, **89**, 4739-4755.

Chameides, W. L. and Davis, D. D. (1982) The free radical chemistry of cloud droplets and its impact upon the composition of rain. *J. Geophys. Res.*, **87**, 4863-4877.

Chameides, W. L. and Davis, D. D. (1983) Aqueous-phase source of formic acid in clouds. *Nature*, **304**, 427-429.

Chandler, A. S., Choularton, T. W., Dollard, G. J., Eggleton, A. E. J., Gay, M. J., Hill, T. A., Jones, B. M. R., Tyler, B. J., Bandy, B. J. and Penkett, S. A. (1988) Measurements of H_2O_2 and SO_2 in clouds and estimates of their reaction rate. *Nature*, **336**, 562-565.

Claiborn, C. S. and Aneja, V. P. (1991) Measurements of atmospheric hydrogen peroxide in the gas phase and in cloud water at Mt. Mitchell, North Carolina. *J. Geophys. Res.*, **96**, 18771-18787.

Cocks, A. T. and Fletcher, I. S. (1982) Possible effects of dispersion on the gas phase chemistry of power plant effluents. *Atmos. Env.*, **16**, 667-678.

Collett, J.L., Jr., Oberholzer, B. and Staehelin, J. (1993) Cloud chemistry at Mt. Rigi, Switzerland: dependence on drop size and relationship to precipitation chemistry. *Atm. Env.*, **27A**, 33-42.

Collett, J. L., Bator, A., Rao, X. and Demoz, B. B. (1994) Acidity variations across the cloud drop size spectrum and their influence on rates of atmospheric sulfate production. *Geophys. Res. Letters*, **21**, 2393-2396.

Daum, P. H., Kelly, T. J., Schwartz, S. E. and Newman, L. (1984) Measurements of the chemical composition of stratiform clouds. *Atm. Env.*, **18**, 2671-2684.

Daum, P. H., Kleinman, L. I., Hills, A. J., Lazrus, A. L., Leslie, A. C. D., Busness, K. and Boatman, J. (1990) Measurement and interpretation of concentrations of H_2O_2 and related species in the upper midwest during summer. *J. Geophys. Res.*, **95**, 9857-9871.

Dollard, G.J., Unsworth, M.H. and Harve, M.J. (1983) Pollutant transfer in upland regions by occult precipitation. *Nature*, **302**, 241-243.

Duce, R.A. (1969) On the Source of Gaseous Chlorine in the Marine Atmosphere. *J. Geophys. Res.*, **74**, 4597-4599.

Fels, M. and Junkermann, W. (1994) The occurrence of organic peroxides in air at a mountain site. *Geophys. Res. Letters*, **21**, 341-344.

Ferek, R. J., Hegg, D. A., Herring, J. A. and Hobbs, P. V. (1991) An improved filter pack technique for airborne measurement of low concentrations of SO_2. *J. Geophys. Res.*, **96**, 22373-22378.

Finlayson-Pitts, B. J. and Pitts, J. N., Jr. (1986) Atmospheric Chemistry: Fundamentals and Experimental Techniques. John Wiley & Sons, New York.

Fuchs, N. A. and Sutugin, A. G. (1970) Highly Dispersed Aerosols. Ann Arbor Science Publisher, Ann Arbor, MI., p. 105.

Fuzzi, S., Orsi, G., Nardini, G., Facchini, M, McLaren, S., McLaren, E. and Mariotti, M. (1988) Heterogeneous processes in the Po Valley radiation fog. *J. Geophys. Res.*, **93**, D9, 11141-11151.

Fuzzi, S., Facchini, M., Orsi, G., Lind, J., Wobrock, W., Kessel, M. *et al.* (1992) The Po Valley fog experiment 1989: an overview. *Tellus*, **44B**, 448-468.

Gaffney, J. S., Streit, G. E., Spall, W. D. and Hall, J. H. (1987) Beyond acid rain. *Env. Sci. Tech.*, **21**, 519-524.

Gallagher, M.W., Choularton, T.W., Morse, A.P. and Fowler, D. (1988) Measurements of the Size Dependence of Cloud Droplet Deposition at a Hill Site. *Q. J. R. Meteorol. Soc.*, **114**, 1291-1303.

Gervat, G. P., Clark, P. A., Marsh, A. R. W., Teasdale, I., Chandler, A. S., Choularton, T. W., Gay, M. J., Hill, M. K. and Hill, T. A. (1988) Field evidence for the oxidation of SO_2 by H_2O_2 in cap clouds. *Nature*, **333**, 241-243.

Graedel, T. E. and Weschler, C. J. (1981) Chemistry within aqueous atmospheric aerosol and raindrops. *Reviews Geophys. Space Phys.*, **19**, 505-539.

Gu, C., Rynard, C. M., Hendry, D. G. and Mill, T. (1985) Hydroxyl radical oxidation of isoprene. *Env. Sci. Tech.*, **19**, 151-155.

Gunz, D. W. and Hoffmann, M. R. (1990) Atmospheric chemistry of peroxides: a review. *Atmos. Env.*, **24A**, 1601-1633.

Hamilton, E. J. and Lii, R. R. (1977) The dependence on H_2O and on NH_3 of the kinetics of the self-reaction of HO_2 in the gas-phase formation of HO_2-H_2O and HO_2-NH_3 complexes. *Int. J. Chem. Kinetics*, **9**, 875-885.

Harris, J.M. and Kahl, J.D. (1994) Analysis of 10-day Isentropic Flow Patterns for Barrow, Alaska: 1985-1992. *J. Geophys. Res.*, **99**, No. D12, 25845-25855.

Hegg, D. A. and Hobbs, P. V. (1982) Measurements of sulfate production in natural clouds. *Atmos. Env.*, **16**, 2663-2668.

Hegg, D. A. and Hobbs, P. V. (1988) Comparisons of sulfate and nitrate production in clouds on the mid-Atlantic and Pacific Northwest coasts of the United States. *J. Atmos. Chem.*, **7**, 325-333.

Hegg, D. A. (1989) The relative importance of major aqueous sulfate formation reactions in the atmosphere. *Atmos. Res.*, **22**, 323-333.

Hegg, D.A. and Larson, T.V. (1990) The effects of microphysical parameterization on model prediction of sulfate production in clouds. *Tellus*, **42B**, 272-284.

Hegg, D. A., Yuen, P.-F. and Larson, T. V. (1992) Modeling the effects of heterogeneous cloud chemistry on the marine particle size distribution. *J. Geophys. Res.*, **97**, 12927-12933.

Heikes, B. G., Kok, G. L., Walega, J. G. and Lazrus, A. L. (1987) H_2O_2, O_3 and SO_2 measurements in the lower troposphere over the eastern United States during fall. *J. Geophys. Res.*, **92**, 915-931.

Hellpointner, E. and Gab, S. (1989) Detection of methyl, hydroxymethyl and hydroxyethyl hydroperoxides in air and precipitation. *Nature*, **337**, 631-634.

Hoffman, M. R. and Edwards, J. O. (1975) Kinetics of oxidation of sulfite by hydrogen peroxide in acidic solution. *J. Phys. Chem.*, **79**, 2096-2098.

Husain, L. (1989) A technique for determining in-cloud formation of $SO_4^=$. *Geophys. Res. Letters*, **16**, 57-60.

Husain, L., Dutkiewicz, V. A., Hussain, M. M., Kwaja, H. A., Burkhard, E. G., Mehmood, G., Parekh, P. P. and Canelli, E. (1991) A study of heterogeneous oxidation of SO_2 in summer clouds. *J. Geophys. Res.*, **96**, 18879-18805.

Iribarne, J. V. and Cho, H. R. (1989) Models of cloud chemistry. *Tellus*, **41B**, 2-23.

Jacob, D.J., Waldman, J.M., Munger, J.W. and Hoffman, H.R. (1985) Chemical composition of fogwater collected along the California coast. *Environ. Sci. Technol.*, **19**, 730-736.

Keene, W. C. and Galloway, J. N. (1984) Organic acidity in precipitation in North America. *Atmos. Env.*, **18**, 2491-2497.

Keene, W. C., Mosher, B. W., Jacob, D. J., Munger, J. W., Talbot, R. W., Artz, R. S., Maben, J. R., Daube, B. C. and Galloway, J. N. (1995) Carboxylic acids in clouds at a high-elevation forested site in central Virginia. *J. Geophys. Res.*, **100**, 9345-9357.

Kelly, T. J., Daum, P. H. and Schwartz, S. E. (1985) Measurements of peroxides in cloudwater and rain. *J. Geophys. Res.*, **90**, 7861-7871.

Kelly, T. J., Schwartz, S. E. and Daum, P. H. (1989) Detectability of acid producing reactions in natural clouds. *Atmos. Env.*, **23**, 569-583.

Kleinman, L. I. (1986) Photochemical formation of peroxides in the boundary layer. *J. Geophys. Res.*, **91**, 10889-10904.

Kircher, C. C. and Sander, S. P. (1984) Kinetics and mechanism of HO_2 and DO_2 disproportionations. *J. Phys. Chem.*, **88**, 2082-2091.

Kok, G. L., Thompson, K., Lazrus, A. L. and McLaren, S. E. (1986) Derivatization technique for the determination of peroxides in precipitation. *Anal. Chem.*, **58**, 1192-1194.

Kunen, S. M., Lazrus, A. L., Kok, G. L. and Heikes, B. G. (1983) Aqueous oxidation of SO_2 by hydrogen peroxide. *J. Geophys. Res.*, **88**, 3671-3674.

Lazrus, A. L., Kok, G. L., Gitlin, S. N. and Lind, J. A. (1985) Automated fluorometric method for hydrogen peroxide in atmospheric precipitation. *Anal. Chem.*, **57**, 917-922.

Lazrus, A. L., Kok, G. L., Lind, J. A., Gitlin, S. N., Heikes, B. G. and Shetter, R. E. (1986) Automated fluorometric method for hydrogen peroxide in air. *Anal. Chem.*, **58**, 594-597.

Lee, J. H., Leahy, D. F., Tang, I. N. and Newman, L. (1993) Measurement and speciation of gas phase peroxides in the atmosphere. *J. Geophys. Res.*, **98**, 2911-2915.

Lee, Y. N. and Lind J. A. (1986) Kinetics of aqueous-phase oxidation of N(III) by hydrogen peroxide. *J. Geophys. Res.*, **91**, 2793-2800.

Lee, Y. N., Shen, J., Klotz, P. J., Schwartz, S. E., and Newman, L. (1986) Kinetics of hydrogen peroxide-sulfur(IV) reaction in rainwater collected at a northeastern U.S. site. *J. Geophys. Res.*, **91**, 13264-13274.

Lelieveld, J. and Heintzenberg, J. (1992) Sulfate cooling effect on climate through in-cloud oxidation of anthropogenic SO_2. *Science*, **258**, 117-120.

Levi, B. G. (1995) Clouds cast a shadow of doubt on models of earth's climate. *Physics Today*, May issue, 21-23.

Lewis, D.L. (1988) *Assessing and Controlling Sample Contamination*, in Principles of Environmental Sampling, ed. by L. Keith, American Chemical Society, USA.

Lightfoot, P. D., Cox, R. A., Crowley, J. N., Destriau, M., Hayman, G. D., Jenkin, M. E., Moortgat, G. K., and Zabel, F. (1992) Organic peroxy radicals: Kinetics, spectroscopy and tropospheric chemistry. *Atmos. Env.*, **26A**, 1805-1961.

Lin, X. and Chameides, W. L. (1991) Model studies of the impact of chemical inhomogeneity on SO_2 oxidation in warm stratiform clouds. *J. Atmos. Chem.*, **13**, 109-129.

Lind, J. A. and Kok, G. L. (1986) Henry's law determinations for aqueous solutions of hydrogen peroxide, methylhydroperoxide, and peroxyacetic acid. *J. Geophys. Res.*, **91**, 7889-7895.

Lind, J. A. and Kok, G. L. (1994) Correction to "Henry's law determinations for aqueous solutions of hydrogen peroxide, methylhydroperoxide, and peroxyacetic acid." *J. Geophys. Res.*, **99**, 21119.

Lind, J. A., Lazrus, A. L. and Kok, G. L. (1987) Aqueous phase oxidation of sulfur(IV) by hydrogen peroxide, methylhydroperoxide and peroxyacetic acid. *J. Geophys. Res.*, **92**, 4171-4177.

Liu, S. C. and Trainer, M. (1988) Responses of the tropospheric ozone and odd hydrogen radicals to column ozone change. *J. Atmos. Chem.*, **6**, 221-233.

Maahs, H. G. (1983) Kinetics and mechanism of the oxidation of S(IV) by ozone in aqueous solution with particular reference to SO_2 conversion in nonurban tropospheric clouds. *J. Geophys. Res.*, **88**, 10721-10732.

MacDonald, A. M., Anlauf, K. G., Banic, C. M., Leaitch, W. R. and Wiebe, H. A. (1995) Airborne measurements of aqueous and gaseous hydorgen peroxide during spring and summer in Ontario, Canada. *J. Geophys. Res.*, **100**, 7253-7262.

Martens, C.S., Wesolowski, J.J., Harriss, R.C., and Kaifer, R. (1973) Chlorine Loss from Puerto Rican and San Francisco Bay Area Marine Aerosols. *J. Geophys. Res.*, **78**, 8778-8792.

Martin, L. R. and Damschen, D. E. (1981) Aqueous oxidation of sulfur dioxide by hydrogen peroxide at low pH. *Atmos. Env.*, **15**, 1615-1621.

McArdle, J. V. and Hoffman, M. R. (1983) Kinetics and mechanism of the oxidation of aquated sulfur dioxide by hydrogen peroxide at low pH. *J. Phys. Chem.*, **87**, 5425-5429.

McElroy, W. J. (1986) Sources of hydrogen peroxide in cloudwater. *Atmos. Env.*, **20**, 427-438.

Miller, M.S., Friedlander, S.K., and Hidy, G.M. (1972) A chemical element balance for the Pasadena aerosol. *J. Colloid Interface Sci.*, **39**, 165-175.

Mohnen, V.A. and Kadlecek, J.A. (1989) Cloud chemistry research at Whiteface Mountain. *Tellus*, **41B**, 79-91.

Mohnen, V.A. and Vong, R.J. (1993) A climatology of cloud Chemistry for the eastern United States cerived from the Mountain Cloud Chemistry Project. *Environ. Rev.*, **1**, 38-54.

Moore, D.S. and McCabe, G.P. (1993) Introduction to the Practice of Statistics, 2nd edition, W.H. Freeman and Company, New York.

Munger, J.W., Collett, J.L. Jr., Daube, B. Jr., and Hoffman, M.R. (1989) Chemical composition of coastal stratus clouds: dependence on droplet size and distance from coast. *Atm. Env.*, **23**, 2305-2320.

Noone, K.J., Charlson, R.J., Covert, D.S., Ogren, J.A. and Heintzenberg, J. (1988) Cloud droplets: solute concentration is size dependent. *J. Geophys. Res.*, **93**, D8, 9477-9482.

Noone, K. J., Ogren, J. A., Noone, K. B., Hallberg, A., Fuzzi, S. and Lind, J. A. (1991) Measurements of the partitioning of hydrogen peroxide in a stratiform cloud. *Tellus*, **43B**, 280-290.

Noone, K.J., Ogren, J.A., Hallberg, A., Hansson, H-C., Wiedensohler, A. and Swietlicki, E. (1992) A statistical examination of the chemical differences between interstitial and scavenged aerosol. *Tellus*, **44B**, 581-592.

Norusis, M. J. (1994) SPSS Professional Statistics 6.1. SPSS, Inc, U.S.

Ogren, J. A. and Rodhe, H. (1986) Measurements of the chemical composition of cloudwater at a clean air site in central Scandinavia. *Tellus*, **38B**, 190-196.

Ogren, J.A., Heintzenberg, J., Zuber, A., Noone, K.J. (1989) Measurements of the size-dependence of solute concentrations in cloud droplets. *Tellus*, **41B**, 24-31.

Ogren, J.A. and Charlson, R.J. (1992) Implications for models and measurements of chemical inhomogeneities among cloud droplets. *Tellus*, **44B**, 208-225.

Ogren, J. A., Noone, K. J., Hallberg, A., Heintzenberg, J., Schell, D., Berner, A., Solly, I., Kruisz, C., Reischle, G., Arends, B.G. and Wobrock, W. (1992) Measurements of the size dependence of the concentrations of non-volatile material in fog droplets. *Tellus*, **44B**, 570-580.

Okabe, H. (1978) Photochemistry of Small Molecules. John Wiley & Sons, Chicester.

Olszyna, K. J., Meagher, J. F. and Bailey, E. M. (1988) Gas-phase, cloud and rain-water measurements of hydrogen peroxide at a high-elevation site. *Atmos. Env.*, **22**, 1699-1706.

Pade, G., Covert, D. and Larson, T. (1987) Design and Calibration of a High Volume Fogwater Collector. *J. Atm. Oceanic Technol.*, **4**, 340-344.

Pandis, S. N., Seinfeld, J. H., and Pilinis, C. (1990) Chemical composition differences in fog and cloud droplets of different sizes. *Atm. Env.*, **24A**, 1957-1969.

Pandis, S. N. and Seinfeld, J. H. (1991) Should bulk cloudwater or fogwater samples obey Henry's Law? *J. Geophys. Res.*, **96**, 10791-10798.

Pedersen, T. (1995) Nighttime hydrogen peroxide production on sulfuric-acid-aerosols involving nitrate and sulfate radicals. *Geophys. Res. Letters*, **22**, 1497-1499.

Penkett, S. A., Jones, B. M. R., Brice, K. A. and Eggleton, A. E. J. (1979) The importance of atmospheric ozone and hydrogen peroxide in oxidizing sulphur dioxide in cloud and rainwater. *Atmos. Env.*, **13**, 123-137.

Prospero, J.M., Savoie, D.L., Nees, R.T., Duce, R.A. and Merrill, J. (1985) Particulate sulfate and nitrate in the boundary layer over the north Pacific Ocean. *J. Geophys. Res.*, **90**, D6, 10586-10596.

Pruppacher, H.R. and Klett, J.D. (1978) Microphysics of Clouds and Precipitation. D. Reidel Publishing Company, Dordrecht.

Quinn, P. K., Bates, T. S., Johnson, J. E., Covert, D. S. and Charlson, R. J. (1990) Interactions between the sulfur and reduced nitrogen cycles over the central Pacific Ocean. *J. Geophys. Res.*, **95**, 16405-16416.

Quinn, P. K., Kapustin, V. N., Bates, T. S. and Covert, D. S. (1996) Chemical and optical properties of marine boundary layer aerosol particles of the mid-Pacific in relation to sources and meteorological transport. *J. Geophys. Res.*, 6931-6951.

Quinn, P. K., Marshall, S. F., Bates, T. S., Covert, D. S. and Kapustin, V. N. (1995) Comparison of measured and calculated aerosol properties relevant to the direct radiative forcing of tropospheric sulfate aerosol on climate. *J. Geophys. Res.*, **100**, 9877-8992.

Roelofs, G. J. H. (1993) A cloud chemistry sensitivity study and comparison of explicit and bulk cloud model performance. *Atmos. Env.*, **27A**, 2255-2264.

Savoie, D.L., Prospero, J.M., Oltmans, S.J., Graustein, W.C., Turekian, K.K., Merrill, J.T. and Levy, H. (1992) Sources of Nitrate and Ozone in the Marine Boundary Layer of the Tropical North Atlantic. *J. Geophys. Res.*, **97**, D11, 11575-11589.

Sehested, K., Holcman, J., Bjerbakke, E. and Hart, E. J. (1984) A pulse radiolytic study of the reaction OH + O_3 in aqueous medium. *J. Phys. Chem.*, **88**, 4144-4147.

Seidl, W. (1989) Ionic concentrations and initial S(IV)-oxidation rates in droplets during the condensational stage of cloud. *Tellus*, **41B**, 32-50.

Seinfeld, J.H. (1986) Atmospheric Chemistry and Physics of Air Pollution. John Wiley and Sons, New York.

Siefert, R. L., Webb, S. M. and Hoffmann, M. R. (1996) Determination of photochemically available iron in ambient aerosols. *J. Geophys. Res.*, **101**, 14441-14449.

Sigg, A. and Neftel, A. (1991) Evidence for a 50% increase in H_2O_2 over the past 200 years from a Greenland ice core. *Nature*, **351**, 557-559.

Simonaitis, R., Olszyna, K. J. and Meagher, J. F. (1991) Production of hydrogen peroxide and organic peroxides in the gas phase reactions of ozone with natural alkenes. *Geophys. Res. Letters*, **18**, 9-12.

Soderlund, R. and Rosswall, T. (1982) *The Nitrogen Cycles*, in The Handbook of Environmental Chemistry, vol. 1, Part B, ed. by O. Hutzinger, Springer-Verlag, Berlin.

Staffelbach, T. A. and Kok, G. L. (1993) Henry's Law constants for aqueous solutions of hydrogen peroxide and hydroxymethyl hydroperoxide. *J. Geophys. Res.*, **98**, 12713-12717.

Talbot, R. W., Mosher, B. W., Heikes, B. G., Jacob, D. J., Munger, J. W., Daube, B. C., Keene, W. C., Maben, J. R. and Artz, R. S. (1995) Carboxylic acids in the rural atmosphere over the eastern United States during the Shenandoah Cloud and Photochemistry Experiment. *J. Geophys. Res.*, **100**, 9335-9343.

Thompson, A. M., Owens, M. A. and Stewart, R. W. (1989) Sensitivity of tropospheric hydrogen peroxide to global chemical and climate change. *Geophys. Res. Letters*, **16**, 53-56.

Thompson, A. M., Johnson, J. E., Torres, A. L., Bates, T. S., Kelly, K. C., Atlas, E., Greenberg, J. P., Donahue, N. M., Yvon, S. A., Saltzman, E. S., Heikes, B. G., Mosher, B. W., Shashkov, A. A. and Yegorov, V. I. (1993) Ozone observations and a model of marine boundary layer photochemistry during SAGA 3. *J. Geophys. Res.*, **98**, 16955-16968.

Tremmel, H. G., Junkermann, W. and Slemr, F. (1994) Distribution of organic hydroperoxides during aircraft measurements over the northeastern United States. *J. Geophys. Res.*, **99**, 5295-5307.

Twohy, C.H., Austin, P.H. and Charlson, R.J. (1989) Chemical consequences of the initial diffusional growth of cloud droplets: a clean marine case. *Tellus*, **41B**, 51-60.

Vong, R. J., Hansson, H.-C., Ross, H. B., Covert, D. S. and Charlson, R. J. (1988) Northeastern pacific submicrometer aerosol and rainwater composition: a multivariate analysis. *J. Geophys. Res.*, **93**, 1625-1637.

Vong, R.J. (1990) Mid-Latitude Northern Hemisphere Background Sulfate Concentration in Rainwater. *Atm. Env.*, **24A**, 1007-1018.

Vong, R.J., Baker, B.M., Brechtel, F.J., Collier, R.T., Harris, J.M., Kowalski, A.S., McDonald, N.C. and McInnes, L.M. (1997) Ionic and Trace Element Composition of Cloudwater Collected on the Olympic Peninsula of Washington State. *Atmos. Env.*, in press.

Watkins, B. A., Parrish, D. D., Buhr, S., Norton, R. B., Trainer, M., Yee, J. E. and Fehsenfeld, F. C. (1995) Factors influencing the concentration of gas phase hydrogen peroxide during the summer at Kinterbish, Alabama. *J. Geophys. Res.*, **100**, 22841-22851.

Weathers, K., Likens, G., Bormann, F., Bicknell, S., Bormann, B., Daube, B., Eaton, J., Galloway, J., Keene, W., Kimball, K., McDowell, W., Siccama, T., Smiley, D. and Tarrant, R. (1988) Cloudwater Chemistry from Ten Sites in North America. *Environ. Sci. Technol.*, **22**, 1018-1026.

Yuen, P.-F., Hegg, D. A. and Larson, T. V. (1994) The effects of in-cloud sulfate production on light-scattering properties of continental aerosol. *J. Appl. Meteor.*, **33**, 848-854.

Yuen, P.-F., Hegg, D. A. , Larson, T. V. and Barth, M. C. (1996) Parameterization of heterogeneous droplet chemistry for use in bulk cloud models. *J. Appl. Meteor.*, **35**, 679-689.

Zuo, Y. and Hoigne, J. (1993) Evidence for photochemical formation of H_2O_2 and oxidation of SO_2 in authentic fog water. *Science*, **260**, 71-73.

APPENDIX A - TRAJECTORIES FOR CAChE 3 CLOUD EVENTS

The cloud events were categorized by air mass origin into four classes using a classification scheme devised by the Charlson group (Tad Anderson, personal communication). These four classes were:

1. stagnant boundary layer
2. southerly boundary layer
3. modified marine boundary layer
4. marine boundary layer

Isentropic air mass back trajectories were calculated twice daily (0 GMT and 12 GMT) by Joyce Harris at NOAA CMDL using a model described previously (Harris and Kahl, 1994). The arrival point for the computed trajectories is at CPO at an elevation of 500 m above sea level. Each point reflects where the air mass came from at a given instant and does not reflect a time average.

The original classification contained six additional categories for continental and subsiding air masses. Subsiding and continental air are usually associated with cloudless skies so it is not surprising that none of the cloud events fell into these categories. The cloud events were classified based on visual inspection of the trajectories using a template and are therefore subject to user interpretation. All categories are based on the vector averages of the last two days of approach to CPO. A continental air mass approached Cheeka Peak from 330°-150°, whereas a southerly air mass approached from 150°-210° and a marine air mass approached from 210°-330°. (see Figure 1). An air mass was classified stagnant if it had a marine trajectory but had average wind speeds less than 4 m/s in its final two days of approach to Cheeka Peak. A modified marine parcel crossed land in its approach.

The trajectories for the twenty events during CAChE 3 are presented in Figures 2 - 17, ordered by julian day. Clearly, the cloud water samples were collected at various times of the day, not just 0 and 12 GMT. Matching the cloud event to within three hours

of a given back trajectory was considered acceptable and reaching the limits of uncertainty in the calculation of back trajectory. Some cloud events (> 8 hours) would span a few trajectories that invariably were classified as different types. In these cases, I represented the event as a coherent air mass type and chose the classification that described the beginning of the event. Classifying individual samples within a single event as having different origins exceeds the limit in uncertainty associated with the trajectory calculation and matching times that aren't 0 or 12 GMT.

It should be noted that back trajectory calculations are most accurate at the synoptic scale. These calculations may miss mesoscale events that affect local air quality. This problem is exacerbated at a coastal/continental interface such as Cheeka Peak because geography can cause local perturbations in the wind field that are undetectable by synoptic scale analyses.

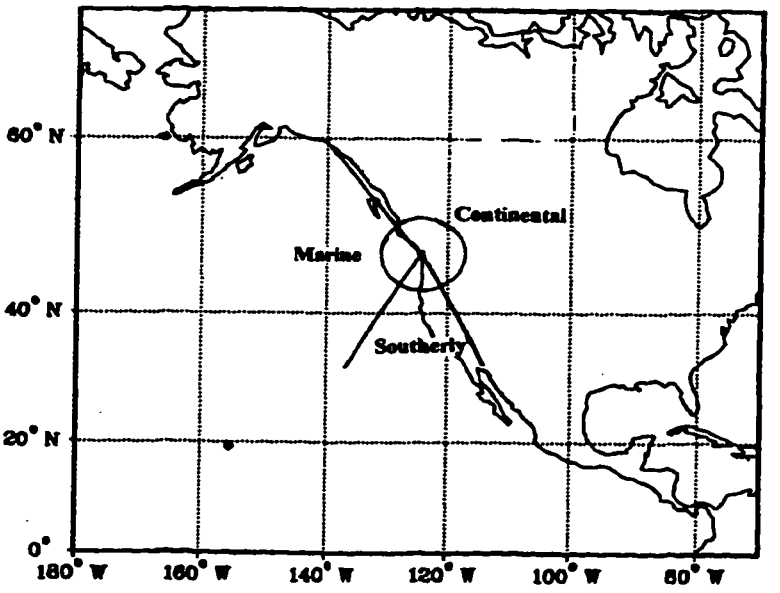

Figure 1. Template used for classifying trajectories. The outer circle represents the minimum distance traveled if the air mass was stagnant.

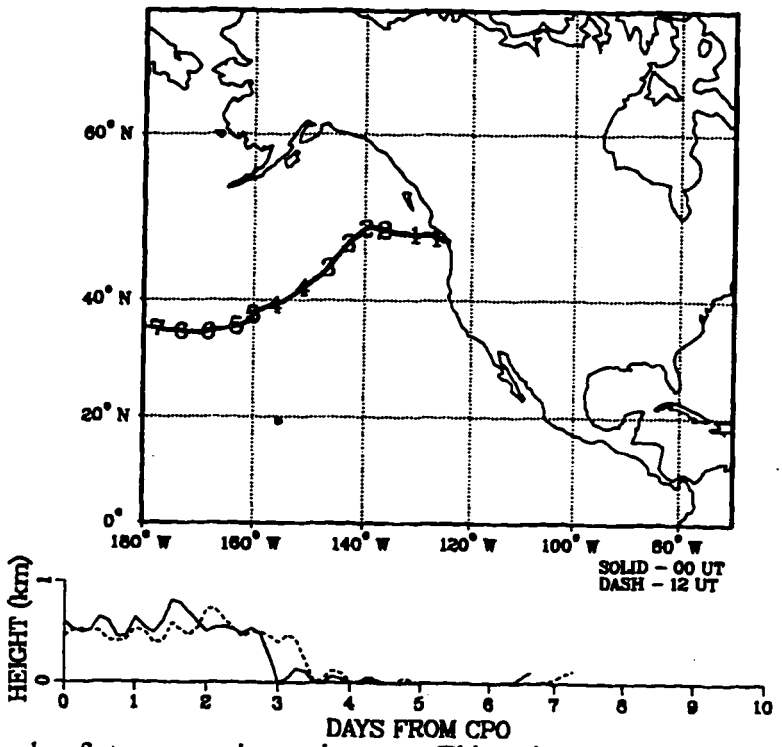

Figure 2. Example of strong marine trajectory. This trajectory is unusual because there is complete agreement between the 0 UT and 12 UT model runs.

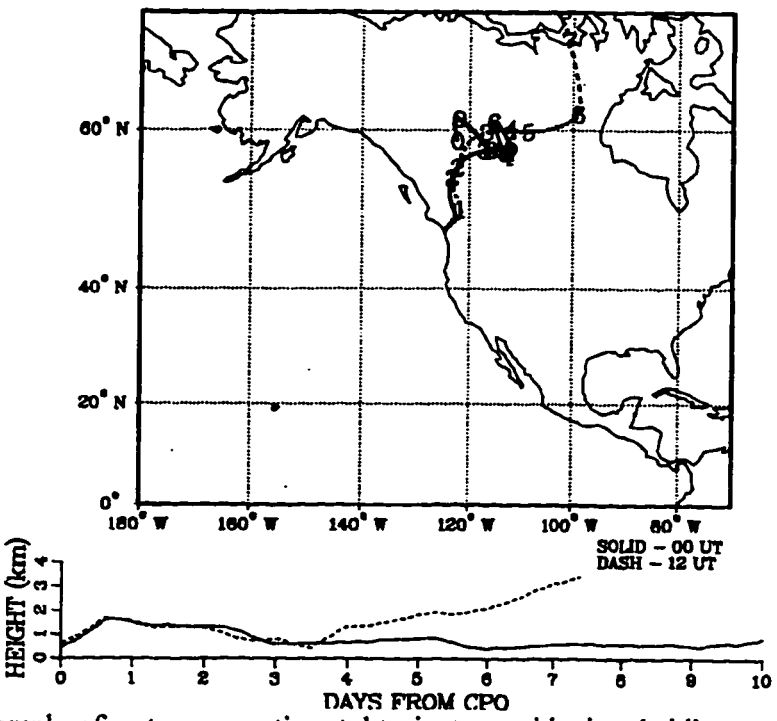

Figure 3. Example of a strong continental trajectory with air subsiding greater than 1km in final two days of approach.

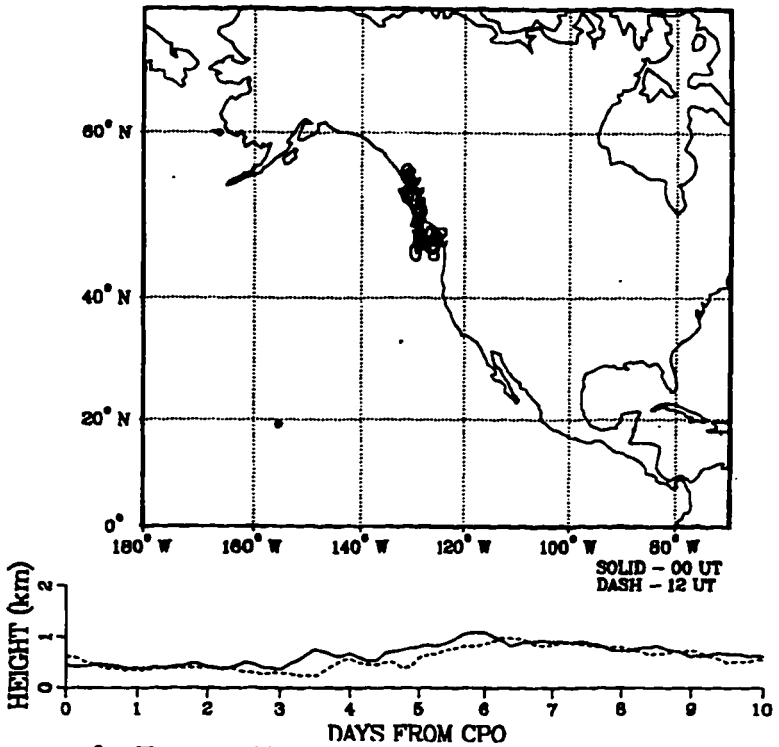

Figure 4. Trajectory for Event 1 (JD 224 13:55-18:22 UT) and Event 17 (JD 224 1:50-8:15 UT), both **stagnant boundary layer**

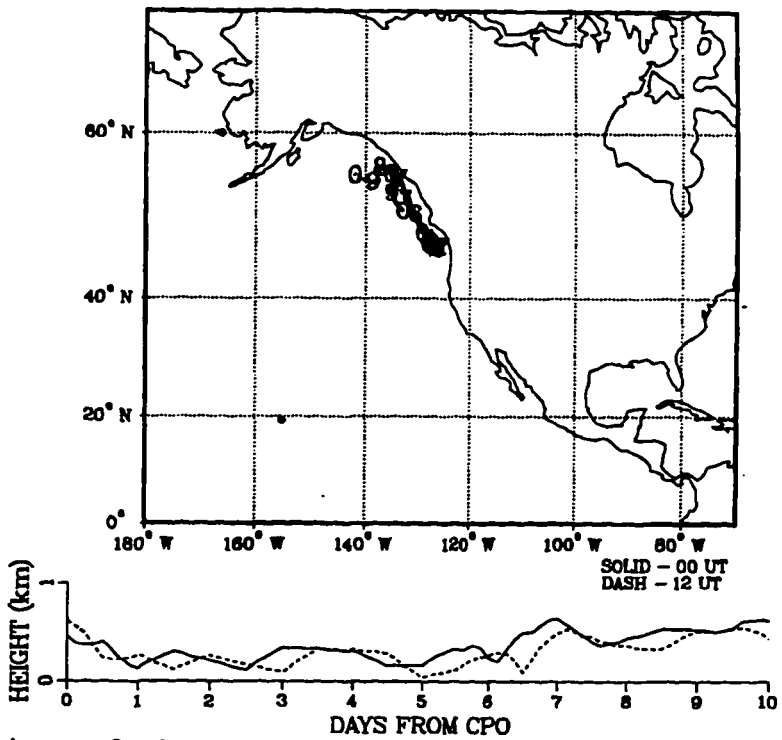

Figure 5. Trajectory for Event 2 (JD 226 13:50-19:50 UT); **stagnant boundary layer**

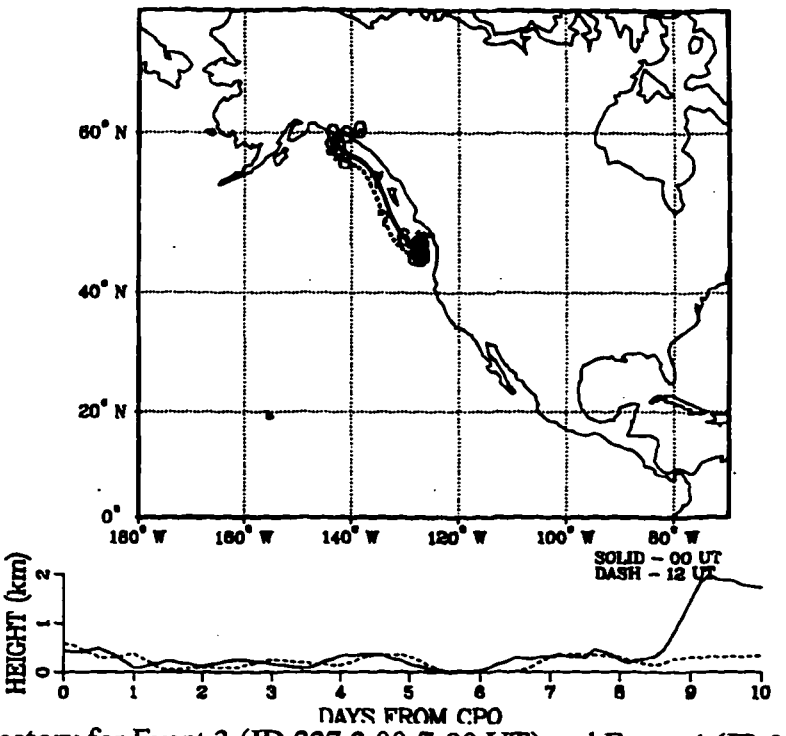

Figure 6. Trajectory for Event 3 (JD 227 2:00-7:00 UT) and Event 4 (JD 227 13:28-16:40 UT), both **stagnant boundary layer**

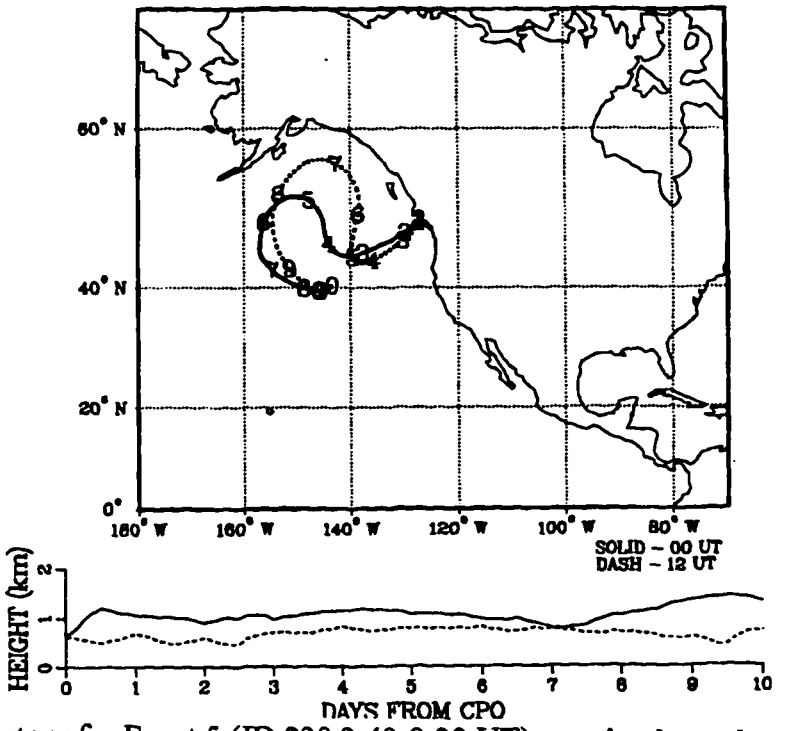

Figure 7. Trajectory for Event 5 (JD 230 3:40-9:23 UT), **marine boundary layer** and Event 6 (JD 230 13:46-18:38 UT), **stagnant boundary layer**

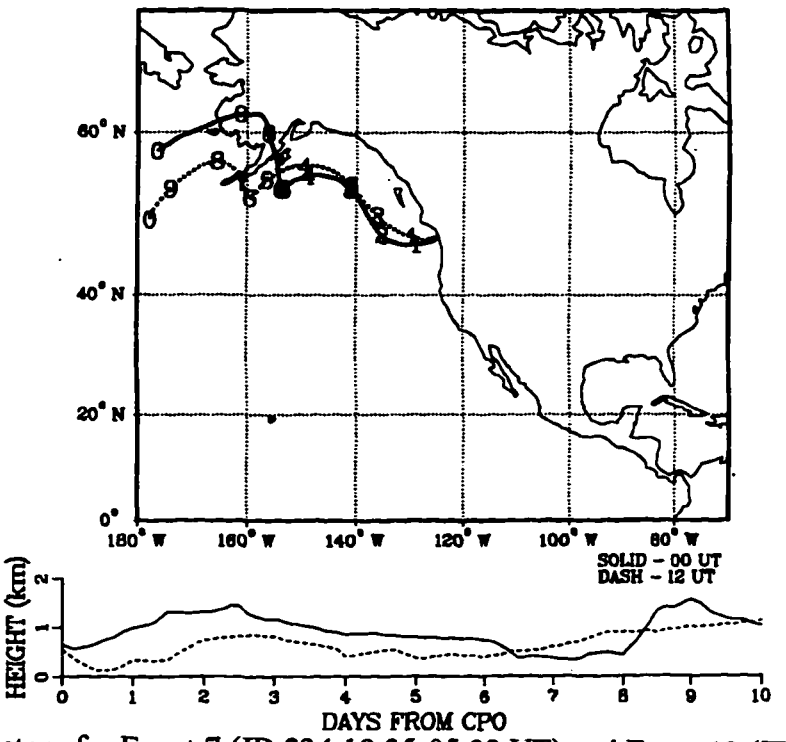

Figure 8. Trajectory for Event 7 (JD 234 19:35-05:22 UT) and Event 18 (JD 234 4:37-7:36 UT), both **marine boundary layer**

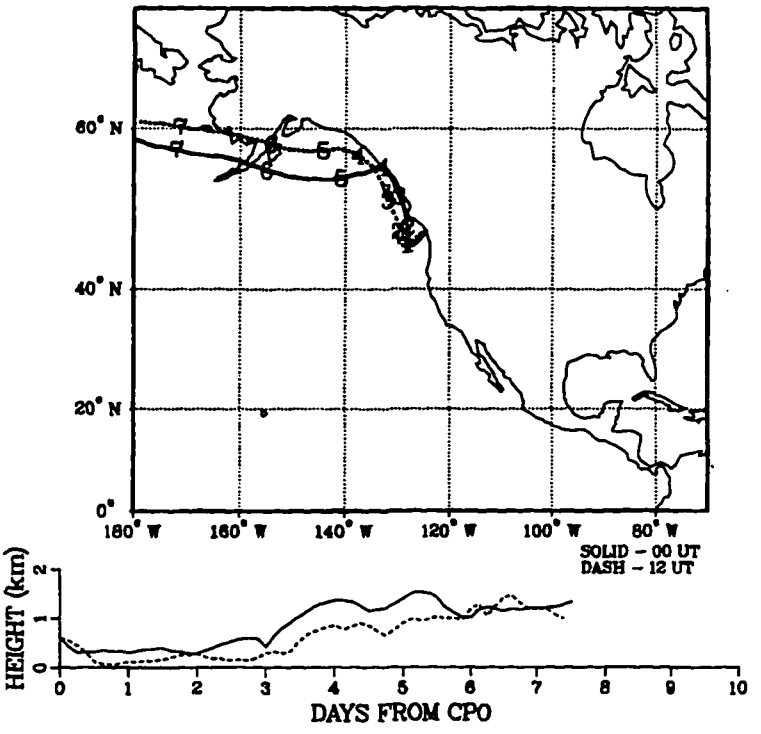

Figure 9. Trajectory for Event 8 (JD 241 13:35-16:35 UT), **marine boundary layer**

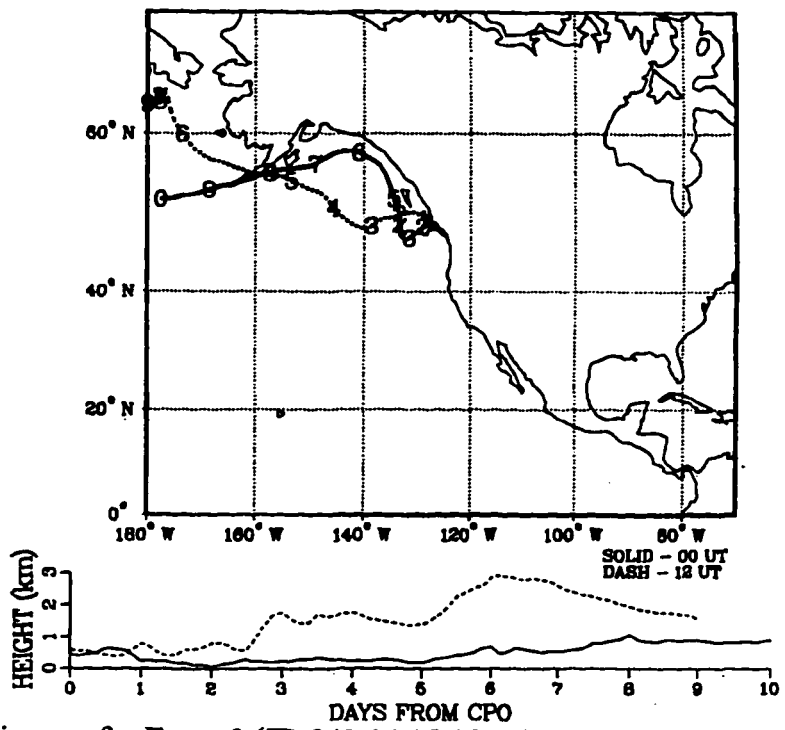

Figure 10. Trajectory for Event 9 (JD 243 14:15-23:25), **modified marine boundary layer**. O UT on JD244 was used because JD 243 was unavailable.

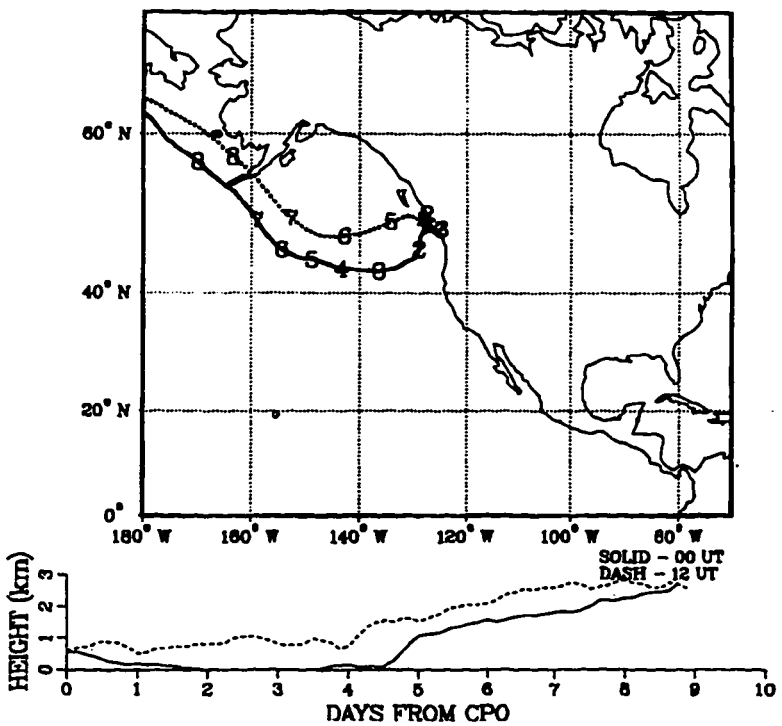

Figure 11. Trajectory for Event 10 (JD 247 3:20-7:15 UT), **modified marine boundary layer**

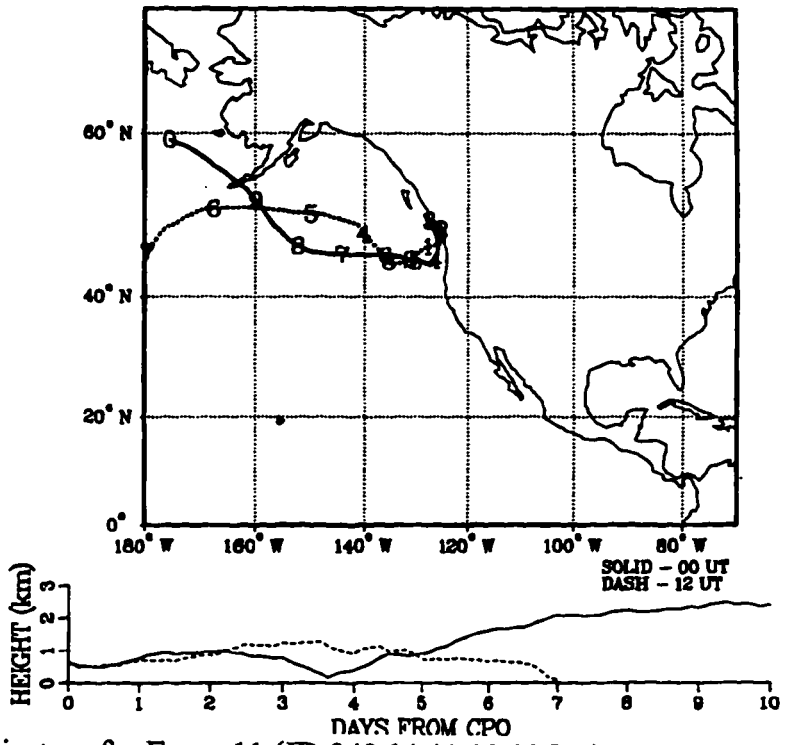

Figure 12. Trajectory for Event 11 (JD 249 14:44-19:10 UT), **marine boundary layer**

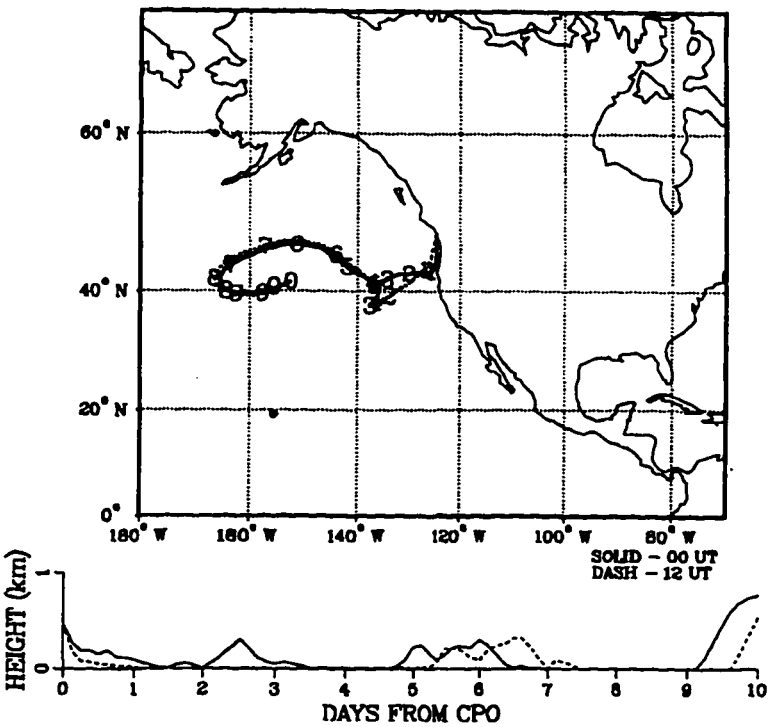

Figure 13. Trajectory for Event 12 (JD 251 3:52-5:32 UT) and Event 13 (JD 251 10:55-14:30), both **southerly boundary layer**

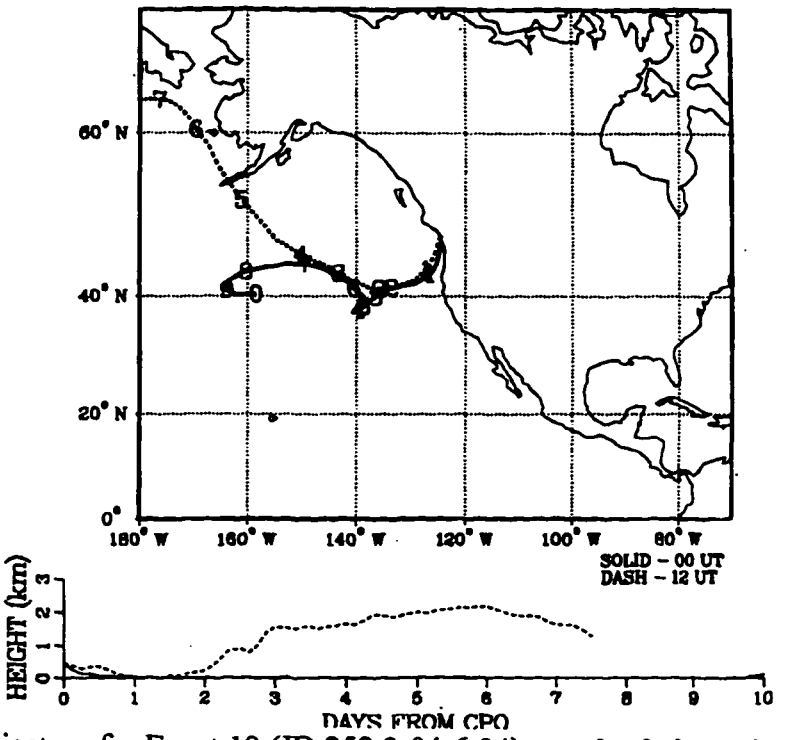

Figure 14. Trajectory for Event 19 (JD 252 3:04-6:04), **southerly boundary layer**

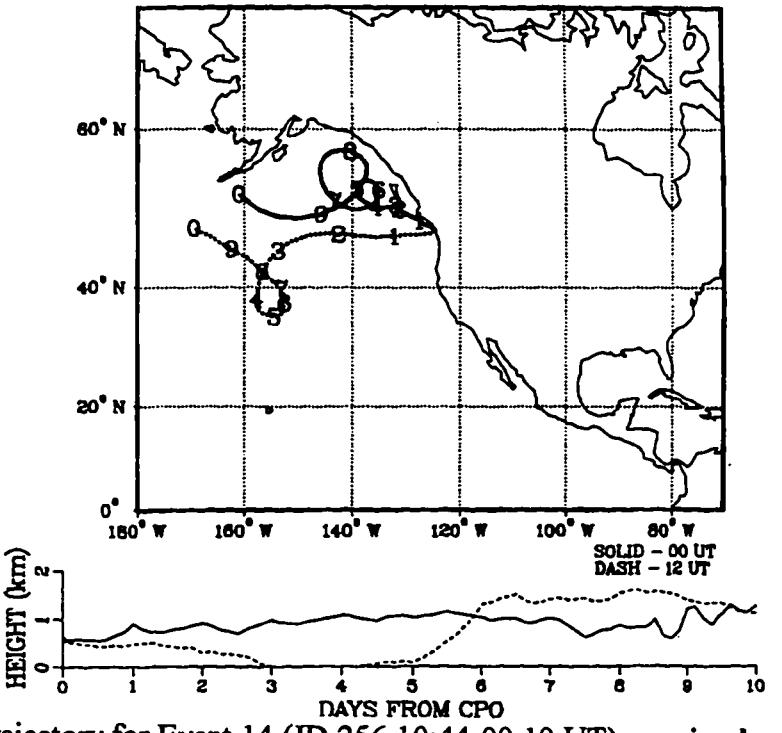

Figure 15. Trajectory for Event 14 (JD 256 10:44-00:10 UT), **marine boundary layer**

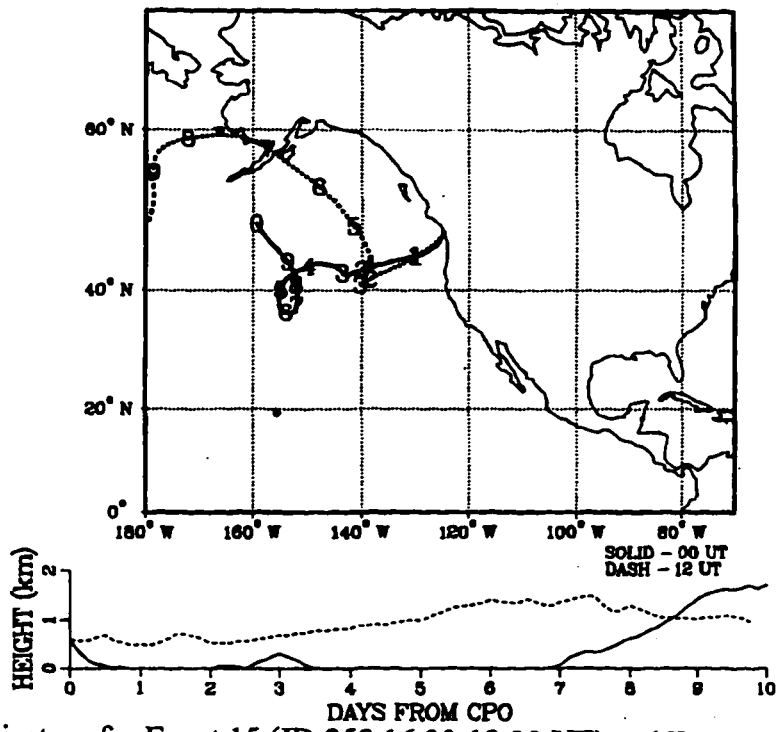

Figure 16. Trajectory for Event 15 (JD 258 16:30-18:20 UT) and Event 20 (JD 257 23:20-2:17 UT), both **marine boundary layer**

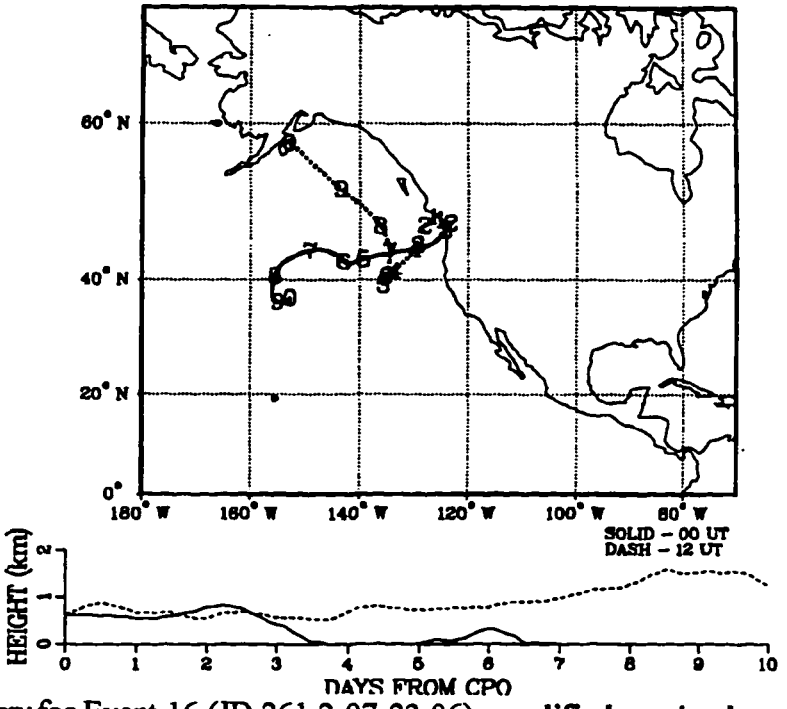

Figure 17. Trajectory for Event 16 (JD 261 2:07-23:06), **modified marine boundary layer**

APPENDIX B - CALIBRATION OF GAS PHASE PEROXIDE INSTRUMENT

Reproducible concentrations of H_2O_2 gas are generated by contacting humidified air with a solution of H_2O_2 of known concentration. Henry's Law equilibrium established for gases flowing through a cylindrical tube under laminar flow is well characterized (Lind and Kok, 1986, and references therein) and achieved under the setup described below .

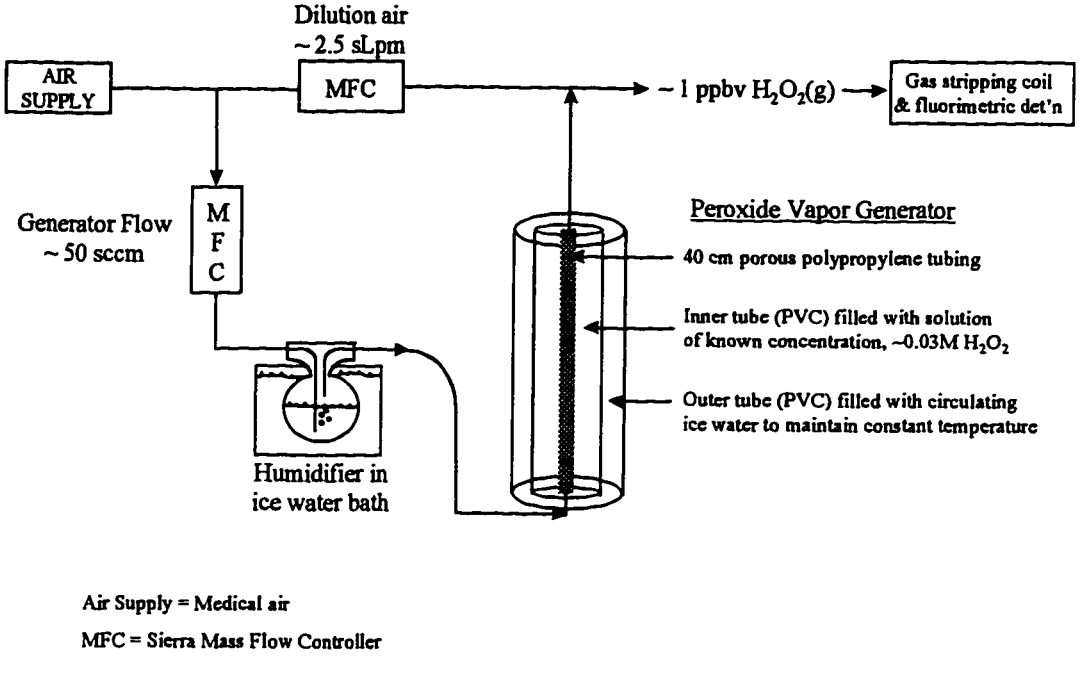

Figure B.1. Saturation system for generation of hydrogen peroxide gas standard.

The peroxide vapor generator is filled with a H_2O_2 solution of known concentration. Humidified air flows through the porous polypropylene tubing, allowing exchange of H_2O_2 between the solution and air stream. Equilibration inside the porous tubing typically takes about 10 minutes. Knowledge of dilution air flows and adherence to Henry's Law provides the basis for calculation. An example calculation is given below showing the results of a calibration made on September 5, 1994:

Generator Flow (at outlet of generator) = (0-2 SLpm MFC) 99.1 sccm

Dilution Flow (at outlet of MFC) = (0-5 SLpm MFC) 2.668 SLPM

Temperature of ice bath = 1.1 °C

Liquid phase standards run @ 7:00PM
$r^2 = 0.99985$
A = 0.1660
B = 5.776

Aliquot of generator-soaked H_2O_2, diluted by a factor of 1.00E-5 (8:00PM) = 1.63 V (zero = 0.726 V)

From calibration curve, diluted aliquot = 5.38 ppbm

Concentration of generator solution = 539 ppmm, 0.01584 M H_2O_2

Expected Henry's Law concentration from generator

K_H = exp((6338/274.1) - 9.74) = 648844 M atm^{-1}
Px = [X]/ K_H = 0.01584M/648844 M atm^{-1} = 2.44E-8 atm
2.44E-8 atm x (1 ppbv/1E-9atm) = 24.4 ppbv
With dilution, 24.4 ppbv x 99.1/(99.1+2668sccm) = **0.874 ppbv**

Voltage of generated H_2O_2 @ 7:00 PM = 1.50 ± 0.1 V (zero = 0.726 V)

Line check @ 7:30 PM = 1.45 ± 0.1 V (zero = 0.726 V)

From calibration curve, generated H_2O_2 = 4.636 ppbm

Conversion to ppbv:

$$ppbv = \frac{4.636ppbm \times 1mol\ H_2O_2/34.018\ g \times 22.4\ L/mol \times 0.6315\ ml/min}{2.133\ SLPM}$$

Generated H_2O_2 = **0.903 ppbv**

Percent difference = **3.3 %**

APPENDIX C - CLOUD WATER PEROXIDE CONCENTRATIONS

All concentrations are presented as μmol/L and are corrected for blank contribution. All peroxide present is assumed to be hydrogen peroxide (see Section 3.2b for justification). Samples are generally collected at one-hour intervals. Sample concentrations exceeded the blank level by greater than a factor of 30.

CAChE 2 (N=56)

Sample ID	Conc [uM]	PPT?		Sample ID	Conc [uM]	PPT?
April 23-24, 1994				*May 9, 1994*		
K50	12.35			M10	66.93	
K52	8.37			M12	44.25	
K54	8.46			M14	35.66	
April 26-27, 1994				M16	31.34	
K70	30.59			M18	32.05	
K72	28.06			M20	33.91	
K74	20.54			M22	72.48	
K76	20.27			M24	48.68	
K78	22.44			*May 11-12, 1994*		
K80	21.61	y		M32	45.42	
K82	26.12	y		M34	26.45	
K84	29.33	y		M36	18.10	
April 28, 1994				M38	32.92	
K88	50.01			M40	35.14	
K90	37.98			M42	37.43	
K92	32.84			M44	35.19	
K94	23.47			M46	31.76	
K96	24.54			M48	29.03	
K98	27.62			M50	29.06	
L00	33.23			M52	26.08	
L02	22.43			M54	25.15	
L04	19.57			M56	30.38	
April 28, 1994				M58	39.09	
L06	21.08			*May 17, 1994*		
L08	22.69			M76	52.06	
L10	24.10			M80	35.76	y
L12	23.67			M82	31.08	y
L14	31.39			M84	34.03	
L16	44.71			M86	44.31	
L20	46.14			M88	39.48	
				M90	38.57	

CAChE 3 (N=73; each row contains samples collected concurrently) Sample concentrations exceeded the blank level by at least a factor of 10.

d-50 (12um)		d-50 (5um)		
Sample ID	**Conc [uM]**	**Sample ID**	**Conc [uM]**	**PPT?**
August 31, 1994 (Event 9 - JD 243)				
V42	24.7	V43	26.4	
V44	10.2	V45	10.3	
V46	4.0	V47	4.5	
V48	9.2	V49	9.4	
V50	11.4	V51	12.0	
V52	12.7	V53	14.0	
V54	10.1	V55	12.5	
V56	13.0	V57	26.1	
		V59	35.0	
September 1-2, 1994				
		V63	66.0	
		V65	68.2	
		V67	79.4	
September 6, 1994 (Event 11 - JD 249)				
X16	2.8	X17	3.8	
X18	31.8	X19	57.5	
X20	81.6	X21	92.7	
X22	81.0	X23	84.9	
September 8, 1994 (Event 13 - JD 251)				
X30	16.9	X31	19.5	
		X33	27.9	
X34	25.8	X35	30.5	
rain	11.3			
September 13, 1994 (Event 14 - JD 256)				
X50	51.8	X51	61.2	
X52	40.1	X53	39.2	
X54	36.2	X55	40.6	
X56	42.3	X57	45.3	
X58	44.8	X59	49.6	y
X60	35.8	X61	38.8	y
X62	14.3	X63	15.2	y
		X65	19.5	y
		X67	6.7	y
		X69	10.1	y

CAChE 3 (continued)

d-50 (12um)		d-50 (5um)		
Sample ID	**Conc [uM]**	**Sample ID**	**Conc [uM]**	**PPT?**
September 17-18, 1994 (Event 16 - JD 261)				
Y04	27.7	small rods broken		
Y06	37.1			
Y08	23.6			
Y10	19.6			
Y12	23.4			y
Y14	21.6			y
Y16	16.4			y
Y18	9.0			y
Y20	3.9			y
Y22	4.0			y
Y24	1.4			y
Y26	2.0			y
Y28	1.4			y
Y30	1.8			y
Y32	1.1			y
Y34	2.6			y
Y36	3.0			
Y38	5.0			
Y40	6.4			
Y42	22.9			
Y44	32.3			

APPENDIX D - DATA USED FOR PRINCIPAL COMPONENTS ANALYSIS

CAChE 2 (n = 42)

SAMPLEID	Cl	NO3	nssSO4	Na	NH4	K	Mg	Ca
IK 72	416.92	12.36	17.84	355.62	1.58	7.90	79.75	15.13
IK 74	402.32	7.37	4.40	342.99	0.14	7.44	76.45	14.09
IK 76	444.90	8.71	11.15	379.42	1.57	8.67	85.25	15.50
IK 78	533.64	9.73	9.26	454.96	0.73	9.95	102.51	19.12
IK 80	681.59	11.47	11.16	582.41	1.31	13.03	131.09	25.63
IK 82	522.91	10.93	19.17	446.72	5.42	9.96	100.86	19.93
IK 88	208.43	26.23	31.47	177.30	2.35	3.99	40.75	8.42
IK 90	187.26	14.68	15.82	224.13	2.93	5.20	51.51	9.80
IK 92	185.56	16.02	27.04	164.37	0.20	3.87	37.80	7.33
IK 94	165.55	18.42	30.64	157.71	5.34	3.83	35.93	7.23
IK 96	173.33	13.76	24.36	155.68	9.26	3.54	35.90	6.30
IK 98	178.94	11.22	22.81	162.74	9.07	3.77	37.66	6.71
IL 00	197.67	9.69	20.04	175.37	16.26	3.81	40.92	9.69
IL 02	182.65	19.28	43.13	170.35	2.14	3.61	39.74	8.94
IL 04	231.98	10.38	21.68	211.39	0.96	4.62	48.75	11.31
IL 06	147.74	13.38	17.21	136.50	4.14	2.86	31.88	7.28
IL 08	151.69	13.83	16.66	155.00	5.79	3.31	35.47	7.85
IL 10	150.29	15.38	21.58	145.93	3.58	3.05	33.72	7.71
IL 12	231.46	25.06	35.21	195.85	6.97	4.09	45.80	10.73
IL 14	141.97	23.33	35.48	132.02	3.83	2.76	31.15	8.33
IL 16	68.10	13.17	23.90	61.33	2.18	1.30	14.37	3.99
IM 10	547.44	49.76	50.83	468.22	9.39	11.23	108.51	23.78
IM 12	418.47	42.03	60.50	356.89	9.89	7.86	80.90	16.77
IM 14	371.61	38.57	54.49	316.45	5.66	6.75	71.68	13.39
IM 16	291.14	35.37	34.83	266.15	4.67	5.51	61.36	11.67
IM 18	244.11	32.38	28.32	212.95	2.64	4.44	49.85	10.18
IM 20	204.70	43.82	25.41	187.37	2.05	3.90	43.34	9.05
IM 40	42.11	7.48	15.32	34.56	2.72	0.69	8.25	3.05
IM 42	100.50	8.83	23.24	81.13	1.75	1.70	18.11	4.77
IM 44	172.83	11.97	17.75	145.66	12.21	3.17	33.39	7.96
IM 46	179.99	9.61	15.30	162.07	13.35	3.24	37.31	8.68
IM 48	207.15	8.37	11.72	177.98	3.79	6.12	39.16	8.45
IM 50	224.62	7.14	10.01	190.44	2.09	4.16	43.30	8.60
IM 52	277.97	7.28	10.22	236.27	1.69	4.97	53.03	12.29
IM 54	254.64	4.41	6.32	216.45	1.28	4.51	48.41	10.12
IM 58	242.35	7.36	8.26	206.99	1.71	4.54	46.21	8.99
IM 76	350.49	18.66	25.25	299.92	9.87	7.24	70.54	14.94
IM 80	316.38	10.33	18.47	269.99	6.06	6.04	61.02	12.75
IM 82	533.20	12.57	10.32	455.70	16.72	10.77	103.24	22.37
IM 84	299.19	8.10	15.26	254.66	5.31	5.62	57.52	11.82
IM 86	275.08	8.34	16.54	234.32	5.12	5.25	52.52	12.58
IM 88	253.65	8.34	17.99	216.11	5.44	4.90	48.31	9.46

CAChE 2 (continued)

SAMPLEID	H	H2O2	O3	Radon	VMD	Nd	CPC1	WindDir
IK 72	58.88	12.32	35.70	1752	12.06	316.65	1297.50	266
IK 74	39.81	9.55	32.80	1548	11.91	361.85	853.87	271
IK 76	36.31	9.39	34.20	1355	13.64	234.72	687.67	266
IK 78	32.36	11.83	36.40	1211	14.42	238.50	551.78	241
IK 80	35.48	10.67	34.20	1220	13.90	243.27	555.38	247
IK 82	40.74	11.24	37.40	1196	13.55	210.84	535.53	257
IK 88	169.82	17.98	31.41	1420	9.95	394.45	901.33	273
IK 90	81.28	18.95	28.06	1507	12.20	361.22	758.98	269
IK 92	63.10	18.15	27.95	1607	13.11	338.92	450.48	268
IK 94	77.62	13.23	29.80	1479	12.42	415.66	846.43	271
IK 96	58.88	13.83	29.31	1627	13.16	345.74	706.63	270
IK 98	48.98	16.83	30.78	1695	13.94	323.06	492.33	269
IL 00	53.70	18.96	32.67	1579	13.66	317.17	395.92	264
IL 02	134.90	11.11	31.95	1554	12.25	367.05	452.23	262
IL 04	45.71	11.87	27.31	1424	14.76	270.25	290.11	263
IL 06	66.07	9.67	33.94	832	13.26	249.68	685.03	258
IL 08	69.18	10.09	34.41	741	13.31	235.48	307.37	245
IL 10	75.86	10.81	34.35	801	13.10	249.99	246.89	252
IL 12	91.20	12.04	35.34	729	13.02	307.70	246.41	255
IL 14	112.20	15.50	36.23	717	12.89	303.54	211.36	260
IL 16	112.20	17.15	35.88	783	11.84	260.43	177.81	259
IM 10	194.98	24.72	35.49	499	9.72	443.96	703.40	253
IM 12	199.53	19.53	36.07	465	10.32	500.10	907.10	252
IM 14	165.96	16.86	35.08	448	11.44	411.26	816.08	249
IM 16	100.00	16.20	34.96	438	12.64	346.30	895.75	242
IM 18	97.72	15.20	28.94	441	12.87	286.92	865.50	239
IM 20	141.25	13.52	27.30	523	10.26	429.28	1326.92	255
IM 40	36.31	18.72	30.38	339	15.70	186.92	555.38	276
IM 42	41.69	17.81	35.29	448	13.54	255.82	628.13	275
IM 44	41.69	17.64	35.46	450	14.64	211.24	1325.42	275
IM 46	36.31	16.19	31.35	453	15.16	195.91	682.36	274
IM 48	25.12	14.62	31.88	501	15.69	173.40	249.07	273
IM 50	22.39	12.96	36.23	660	15.37	153.14	261.42	275
IM 52	21.38	11.79	33.38	693	15.30	159.85	439.95	273
IM 54	14.45	10.53	35.18	638	16.48	112.87	247.38	274
IM 58	57.54	11.01	37.43	628	11.98	136.16	482.57	288
IM 76	141.25	14.52	33.04	549	9.39	281.50	850.92	279
IM 80	70.79	12.72	32.11	587	11.03	290.11	692.09	278
IM 82	50.12	12.68	33.16	638	12.77	232.75	543.18	275
IM 84	44.67	14.26	33.23	647	13.16	221.05	495.04	270
IM 86	53.70	16.66	30.99	752	12.32	225.55	521.05	265
IM 88	69.18	14.23	31.04	796	11.39	265.42	628.49	271

All cloud chem values, except H, are gas phase equivalent concentrations in neq/m3. H is ueq/L
H2O2 comes from p=[perox](LRT+1/H) assuming T=285K, units nmol/m3
O3 in ppbv, Radon in mBq

CAChE 3 (n = 28)

SAMPLEID	Cl	NO3	nssSO4	Na	NH4	K	Mg	Ca
VI 43	271.78	19.03	38.29	236.13	14.62	5.74	50.92	9.37
VI 45	149.38	14.11	46.43	132.06	12.71	3.80	29.13	6.99
VI 47	141.97	19.16	93.35	133.54	11.17	4.00	29.01	8.17
VI 49	138.29	14.33	54.21	124.14	6.73	3.53	26.83	8.03
VI 51	218.07	19.13	56.19	209.20	33.62	5.18	44.86	10.21
VI 53	359.04	31.29	70.58	342.34	11.83	8.19	72.85	15.86
VI 55	490.72	65.51	109.70	475.20	27.85	11.75	100.45	21.19
VI 57	353.27	55.61	65.88	329.86	16.16	7.74	70.19	13.85
XI 17	3.57	0.18	0.72	3.46	1.22	0.33	0.82	0.40
XI 19	18.19	2.48	5.90	16.34	5.58	0.83	3.75	1.46
XI 21	24.66	4.12	15.42	20.95	4.71	0.74	4.97	1.20
XI 23	21.47	4.04	10.09	20.99	6.26	0.56	4.69	0.96
XI 31	109.97	4.00	15.83	96.08	3.75	1.97	21.63	4.07
XI 33	81.65	10.65	11.76	71.58	8.76	2.15	15.70	3.03
XI 35	203.27	6.62	28.65	178.18	11.40	4.02	38.74	7.48
XI 39	370.07	10.94	22.05	338.02	7.78	7.41	83.01	14.86
XI 41	298.60	12.58	21.91	276.63	10.56	6.04	68.57	12.40
XI 43	166.67	9.09	14.91	163.36	10.63	3.41	36.57	7.40
XI 51	26.55	43.40	49.38	33.59	5.82	0.97	7.60	1.72
XI 53	19.09	47.93	56.77	19.88	8.42	0.77	3.99	1.24
XI 55	8.44	20.92	31.38	5.68	3.14	0.22	0.82	0.44
XI 57	13.53	23.01	31.72	16.24	8.03	0.53	3.19	0.91
XI 59	20.36	35.00	41.73	26.52	13.11	1.12	5.50	1.41
XI 61	7.56	19.24	31.88	11.10	14.88	0.83	2.07	0.75
XI 63	5.65	9.85	26.63	8.73	9.42	0.50	1.54	0.60
XI 65	6.54	7.49	21.91	10.15	1.48	0.44	2.07	0.63
XI 67	0.90	0.57	3.55	0.61	1.00	0.01	0.01	0.16
XI 69	0.46	0.32	2.18	0.65	1.91	0.03	0.00	0.16

All cloud chem values, except H, are gas phase equivalent concentrations in neq/m3. H is ueq/L
H2O2 comes from p=[perox](LRT+1/H) assuming T=285K, units nmol/m3
O3 in ppbv
Radon in mBq

CAChE 3 (continued)

SAMPLE ID	H	H2O2	O3	Radon	VMD	Nd	CPC1	WindDir	netrad
VI 43	66.07	15.77	25.80	282	16.15	233.25	601.25	249	26.15
VI 45	52.48	8.65	23.20	387	19.47	211.26	679.08	255	77.10
VI 47	100.00	3.71	21.79	331	16.66	323.72	860.60	258	174.31
VI 49	63.10	7.33	21.69	407	17.25	271.86	591.49	254	198.75
VI 51	93.33	7.52	22.83	417	14.53	342.34	799.21	253	225.49
VI 53	123.03	8.53	25.21	456	12.75	502.40	1132.48	258	233.38
VI 55	162.18	8.38	26.55	528	12.04	658.74	1405.24	266	184.88
VI 57	138.04	13.97	27.18	539	11.00	636.95	3634.70	267	225.17
XI 17	17.78	1.05	23.27	605	17.26	48.71	168.50	289	97.35
XI 19	40.74	17.20	23.07	420	14.46	107.19	144.29	285	180.20
XI 21	66.07	38.49	22.07	220	15.21	162.36	161.22	279	207.72
XI 23	77.62	23.80	21.30	188	11.59	100.11	217.82	259	233.52
XI 31	30.20	11.45	34.29	511	18.41	129.83	301.43	235	-4.35
XI 33	58.88	9.45	36.23	478	13.12	98.41	354.70	232	-12.16
XI 35	72.44	15.97	35.26	484	16.51	154.86	251.21	232	-3.27
XI 39	58.88	12.26	28.87	310	11.96	341.58	717.09	227	-2.11
XI 41	74.13	9.86	30.34	309	11.29	284.27	714.53	204	-5.53
XI 43	107.15	8.43	31.91	354	10.19	212.89	687.15	185	-8.18
XI 51	194.98	32.65	29.02	358	13.49	339.01	579.88	287	-0.31
XI 53	158.49	29.65	28.23	354	17.16	266.46	742.18	284	-0.15
XI 55	134.90	21.93	29.98	363	14.87	256.25	545.11	281	-0.33
XI 57	104.71	25.53	30.11	335	15.82	211.59	450.75	245	5.88
XI 59	134.90	28.13	28.10	360	14.51	297.84	429.14	224	46.06
XI 61	85.11	23.85	25.85	322	15.41	274.61	347.60	217	109.93
XI 63	66.07	8.87	28.63	380	15.20	271.13	250.58	207	143.23
XI 65	74.13	9.21	22.19	518	12.78	340.03	317.69	202	124.88
XI 67	8.51	4.40	24.37	929	19.13	163.03	142.74	217	55.79
XI 69	6.03	6.67	21.68	803	19.16	161.33	147.17	219	44.03

TRISTINE M. SAMBERG

17507 Eason Avenue
Bothell, WA 98011

(206) 488-3642
samberg@msn.com

EDUCATION

Ph.D. in Analytical Chemistry (June 1997) — University of Washington (UW), Seattle, WA
Research Advisors: Professor William Zoller
Professor Dean Hegg

B.S. in Chemistry (May 1989) — Florida State University (FSU), Tallahassee, FL
Summa Cum Laude, Phi Beta Kappa

HONORS AND ACTIVITIES

1991-1995	Department of Energy Global Change Fellow
1994-1996	Outreach Activities Co-Chair, Association for Women in Science
1991-present	Member, American Geophysical Union
1989-1990	Outstanding Teaching Assistant, UW Chemistry Department
1988-1989	President, Alpha Chi Sigma Professional Chemistry Fraternity

PROFESSIONAL EXPERIENCE

Coordinator, UW Science Service Learning Program (January 1996 – present)

Planning Commissioner, City of Bothell (1997 – 2001 term expiration)

Research Assistant, UW Department of Chemistry (September 1991 – December 1995)

Teaching Assistant, UW Department of Chemistry (September 1989 – August 1991)

PUBLICATIONS AND PRESENTATIONS

Hegg, D. A., Samberg, T. M. and Vong, R. J. (1997) A model-data intercomparison of heterogeneous cloud chemistry. *Tellus*, submitted.

Samberg, T., Hegg, D., Kok, G., Vong, R. and Zoller, W. (April 1995) Preliminary Field Measurements on the Sources of $SO_4^=$ in Maritime Cloud Water," Proceedings of the 209th ACS National Meeting - Symposium on Cloud and Aerosol Atmospheric Chemistry, Vol. 35, No. 1, Anaheim, CA.

Samberg, T., Wiegand, D. and Selfe, S. (1993) Course-specific Resource Manual for Chemistry Laboratory Courses" in The TA Experience: Preparing for Multiple Roles, K.G. Lewis, ed., New Forums Press, OK.